The senescence associated secretory phenotype coordinates with the immune system to modulate oncogene-induced senescence in murine models of lung cancer

Maria Milioara Manea

Dankort Lab

Department of Biology

McGill University

April 2025

A thesis submitted to McGill University in partial fulfillment of the requirements of the degree of

Master of Science

© Maria Milioara Manea 2025

Table of Contents

Table of Contents	. 2
Abstract	. 5
Résumé	. 6
Acknowledgments	. 8
Contribution to Original Knowledge	. 9
Contribution of Authors	. 9
List of Figures	10
List of Abbreviations	11
Chapter 1: Introduction & Literature Review	13
1.1 Introduction	13
1.2 Lung Cancer	14
1.2.1 The Mitogen-Activated Protein Kinase Pathway	15
1.2.2 BRAF	16
1.2.3 Tumor Suppressor Gene P53	18
1.3 Cellular Senescence	22
1.3.1 Senescence	22
1.3.2 Oncogene-Induced Senescence	24
1.3.3 MOB3A	26
1.3.4 SASP	31
1.3.5 The Immune System	34
1.3.6 The Tumor Microenvironment.	39
1.4 Animal Model	41
1.4.1 <i>Kras LA1-LA2</i> Model	41
1.4.2 LSL- <i>Kras</i> Model	42
1.4.3 Braf ^{CA} Model	42
1.4.5 Braf ^{FA} Model	
1.5 Thesis Objectives	
	45

Objective 2	46
Chapter 2: Materials and Methods	47
2.1 Cloning of pWZL-Hygro-myr:flag-MOB3A and pWZL-Hygro-myr:flag-EGFP	47
2.2 Cell Culture	47
2.3 Lentiviral and Retroviral Production	48
2.4 Infection of Cell Lines	48
2.5 Drug Selection	49
2.6 Cell Clone Isolation	49
2.7 Growth Curve	50
2.8 Crystal Violet	50
2.9 Western Blot	51
2.10 Hematoxylin and Eosin (H&E)	52
2.11 Immunofluorescence	52
2.12 Image Analysis	53
Chapter 3: Results	55
3.1 Development of a MOB3A BRER Cell Line Model for the Investigation of OIS	55
3.1.1 MOB3A-Expressing BRER Cells Fail to Proliferate and Exhibit Senescent Under 4OHT-Induced MAPK Signaling	
3.1.2 Drug Susceptibility Profiles of Parental HF E1T and IMR90 Fibroblast Cell I	
3.1.3 Selection of BRER Fibroblast Cell Lines and Evaluation of 4OHT Responsive	
3.1.4 Cloning of pWZL-myr:flag-Hygro-MOB3A and pWZL-myr:flag-Hygro-E	
3.1.5 Generation and Characterization of MOB3A/EGFP BRER Cell Lines	64
3.2 Characterizing Immune Infiltrates in Braf ^{FA} Mice	68
3.2.1 Sample Selection	68
3.2.2 Tissue Analysis	70
3.2.3 Quantification Analysis	72
Chapter 4: Discussion	76

	4.1 A MOB3A BRER Tissue Culture Model to Provide Insights into Senescence By	, 1
•••	4.2 Immune Profiles are Modulated by Tumor Density, Senescence and P53 Status	
	Appendix	83
	References	97

Abstract

The Mitogen-Activated Protein Kinase (MAPK) Pathway is conserved across most eukaryotic cells and plays a crucial role in cellular processes such as differentiation, migration and proliferation. Mutations in the RAS-RAF-MEK-ERK cascade are involved in developmental abnormalities and in many cancers. Expression of the constitutively active $BRAF^{V600E}$ allele initiates lung tumorigenesis and paradoxically induces a stable proliferative block to tumor progression termed Oncogene-Induced Senescence (OIS). This work explores the regulation of this barrier in both cell culture and animal models of BRAF-induced senescence, discussing the potential role of innate immune cells as modulators of senescence.

We examine the role of the kinase regulator MOB3A in OIS bypass. MOB3A was previously identified in a cell culture OIS bypass experiment and is known to modulate the Hippo pathway. In doing so, MOB3A facilitates the nuclear accumulation of non-phosphorylated YAP/TAZ, which promotes proliferation and survival despite sustained BRAF expression. To further analyze this mechanism, MOB3A BRER cell lines of human fibroblasts were developed through cell culture, confirmed by drug selection, growth curves and western blot.

Additionally, P53 was ablated in genetically engineered mouse models (GEMMs) 24 weeks after $BRAF^{V600E}$ induction, achieved through the administration of low and high adenoviral loads. We hypothesize that chemokines and cytokines associated with the Senescence-Associated Secretory Phenotype (SASP) distinctly recruit immune cell populations according to tumor burden and the expression of P53. This research employs tissue analysis methods such as hematoxylin and eosin staining and immunofluorescence to identify replicative, structural, and immune markers, which were quantified using computer-based analysis with Fiji ImageJ.

This study provides insight into the influence of the MAPK pathway on tumorigenesis, senescence, and immune dynamics, offering a deeper understanding of cell behavior and immune involvement in the context of senescence-associated lung tumorigenesis.

Résumé

La voie des protéines kinases activées par les mitogènes (MAPK) est conservée dans la majorité des cellules eucaryotes et joue un rôle crucial dans des processus cellulaires tels que la différenciation, la migration et la prolifération. Les mutations dans la cascade RAS-RAF-MEK-ERK sont impliquées dans des anomalies du développement et dans de nombreux cancers. L'expression de l'allèle constitutivement actif $BRAF^{V600E}$ initie la tumorigénèse pulmonaire et induit paradoxalement un arrêt prolifératif stable contre la progression tumorale appelé sénescence induite par l'oncogène (OIS). Ce travail explore la régulation de cette barrière dans des modèles de culture cellulaire et animaux de sénescence induite par BRAF, en discutant du rôle potentiel des cellules immunitaires innées en tant que modulateurs de la sénescence.

Nous examinons le rôle du régulateur de kinase MOB3A dans le contournement de l'OIS. MOB3A a été précédemment identifié dans une expérience de contournement de l'OIS en culture cellulaire et est connu pour moduler la voie Hippo. Ainsi, MOB3A facilite l'accumulation nucléaire de YAP/TAZ non phosphorylés, ce qui favorise la prolifération et la survie malgré l'expression soutenue de BRAF. Pour analyser davantage ce mécanisme, des lignées cellulaires MOB3A BRER de fibroblastes humains ont été développées en culture cellulaire, confirmées par sélection antibiotique, courbes de croissance et western blot.

De plus, le gène P53 a été inactivé dans des modèles murins génétiquement modifiés (GEMMs) 24 semaines après l'induction de $BRAF^{V600E}$, réalisée par l'administration de charges adénovirales faibles et élevées. Nous émettons l'hypothèse que les chimiokines et cytokines associées au phénotype sécrétoire lié à la sénescence (SASP) recrutent distinctement des populations de cellules immunitaires selon la charge tumorale et l'expression de P53. Cette

recherche utilise des méthodes d'analyse tissulaire telles que la coloration à l'hématoxyline-éosine et l'immunofluorescence pour identifier les marqueurs de réplicatifs, structurels et immunitaires, qui ont été quantifiés par analyse information à l'aide du logiciel Fiji ImageJ.

Cette étude fournit un aperçu de l'influence de la voie MAPK sur la tumorigenèse, la sénescence et la dynamique immunitaire, offrant une meilleure compréhension du comportement cellulaire et de l'implication immunitaire dans le contexte de la tumorigenèse pulmonaire associée à la sénescence.

Acknowledgments

I would like to express my gratitude to my supervisor, Dr. David Dankort, for providing me with the opportunity to work in his laboratory and explore a topic that has always deeply fascinated me. This thesis is not solely the product of my efforts but rather the result of the collective contributions of many wonderful individuals who have supported me throughout this journey. I extend my sincere thanks to my supervisory committee members, Dr. Frieder Schöck and Dr. Arnold Hayer.

Everyday felt engaging in the presence of my wonderful lab mates Mary Nicoll and Timea Papp. Timea provided me with unwavering mental support during difficult times, delighted me with her delicious cooking and made everyday an enjoyable experience. Mary, our lovely doctorate candidate, was indispensable to my progress. She answered my countless questions concerning experiments, taught us the basics of the lab, and I thoroughly enjoyed our conversations about books and our shared love for the Harry Potter series.

The second floor of Bellini was a hub of vibrant student life, where I had the pleasure of meeting many brilliant and kind individuals who made each day enjoyable and fun. I immensely appreciated the few, yet truly delightful, outings shared with my friends. I am extremely grateful to two exceptional PhD students who were always generous in lending reagents when we needed them and selflessly assisted me with parts of my image analysis. Both are remarkable individuals, and I wish them all the best in their future endeavors.

Finally, I am grateful to my parents for their unyielding support and love, my boyfriend for his awesome knowledge in information technology and my grandmother's weekly calls, who greatly helped lift my morale.

Contribution to Original Knowledge

This thesis builds on the work of Dr. Samantha Garnett and Dr. Kendall Dutchak. Mouse model experiments were conducted using Dr. Garnett's paraffin-embedded blocks, and cell line generation was further developed based on the previous work of Dr. Dutchak.

Contribution of Authors

This thesis was written by Maria Milioara Manea under the direction of Dr. David Dankort. Experimental design was a collaboration between both student and principal investigator, with the occasional input from the supervisory committee and laboratory members. All experiments and analysis illustrated below are products of this thesis, unless stated otherwise.

List of Figures

Figure 1-1 The MAPK pathway (p.16)

Figure 1-2 The Hippo pathway. (p.26)

Figure 1-3 Schematic representation of \triangle BRAF:ER. (p.30)

Figure 1-4 Conditional activation of *Braf*^{V600E} and P53 deletion in mouse models. (p.44)

Figure 3-1 Initial model of MOB3A-expressing BRER cells under 4OHT-induced MAPK signaling appear to drift. (p.57)

Figure 3-2 Drug susceptibility profiles of HF E1T and IMR90 cell lines. (p.59)

Figure 3-3 Growth curves for control and BRER-infected populations of HF E1T and IMR90 fibroblast cell lines exposed to 100 4OHT or EtOH. (p.61)

Figure 3-4 Excision of the neomycin resistance gene with hygromycin resistance in pWZL-myr:flag-MOB3A and pWZL-myr:flag-EGFP plasmids. (p.63)

Figure 3-5 Characterization of MOB3A/EGFP BRER cell lines. (p.67)

Figure 3-6 Experimental timeline for $Braf^{V600E}$ induction and p53 deletion in mouse models. (p.69)

Figure 3-7 Histological and immunofluorescence staining of tumors 24-weeks post *Braf*^{V600E} induction. (p.71)

Figure 3-8 Immune Infiltrates Quantification and Characterization in Sparse or Dense *p53* WT or Null Tumors. (p.74)

List of Abbreviations

4OHT 4-hydroxytamoxifen
AAH adenomatous hyperplasia
AdenoCre adenoviral particles

AdFlp adenoviral flp

ALK anaplastic lymphoma kinase
APC antigen-presenting cell
ATM ataxia-telangiectasia mutated
ATP adenosine triphosphate
BCL2 B-cell lymphoma 2

BRD4 bromodomain-containing protein 4

CCL2 chemokine ligand 2

CDKN1A cyclin dependent kinase inhibitor 1A CEBPβ CCAAT/enhancer-binding protein beta

CHK checkpoint kinase CRD cysteine-rich domain

CTLA4 cytotoxic T-lymphocyte associated protein

DC dendritic cell

DMEM Dulbecco's modified eagle's medium

DNA deoxyribonucleic acid

EGFP enhanced green fluorescent protein EGFR epidermal growth factor receptor

ER estrogen receptor

ETS E26 transformation-specific

FBS fetal bovine serum

FRT Flp recombination target

GEMM genetically engineered mouse model

GM-CSF granulocyte-macrophage colony-stimulating factor

HBD hormone-binding domain
H-EBC HF E1T EGFP BRER cells
H-MBC HF E1T MOB3A BRER cells
I-EBC IMR90 EGFP BRER cells

IFN-γ interferon gamma

IGFBP7 insulin-like growth factor (IGF)-binding protein

IL interleukin

I-MBC MOB3A BRER IMR90 cells KIBRA kidney and brain expressed protein

LSL lox-stop-lox

LUAD lung adenocarcinoma

MAPK mitogen-activated protein kinase MHC major histocompatibility complex MDM2 mouse double minute 2 homolog

MMP matrix metalloproteinase
MOB MPS-one binder co-activator

MST mammalian sterile-twenty-like

NDR nuclear dbf2-related

NET neutrophil extracellular trap

NF1 neurofibromin 1

NF-κB nuclear factor kappa-light-chain-enhancer of activated B cells

NK natural killer

NSCLC non-small cell lung cancer
OIS oncogene-induced senescence

PAMP pathogen-associated molecular pattern

PCNA proliferating cell nuclear antigen PD-1 programmed cell death protein 1

PFU plaque forming unit PP1 protein phosphatase 1

PTEN phosphatase and tensin homolog

RB retinoblastoma
RBD ras binding domain
ROI region of interest
ROS reactive oxygen species
RTK receptor tyrosine kinase

SASP senescence-associated secretory phenotype

SCLC small cell lung cancer

SHP src homology region 2 domain-containing phosphatase

STAT signal transducer and activator of transcription STRIPAK striatin interacting phosphatase and kinase

TAM tumor-associated macrophages

TAZ transcriptional coactivator with PDZ-binding motif

TCR T cell receptor

TGF-β transforming growth factor beta

Th Thelper

TLR toll-like receptor

TME tumor microenvironment TNF-α tumor necrosis factor alpha

Treg regulatory T cell

VEGF vascular endothelial growth factor

YAP yes-associated protein

Chapter 1: Introduction & Literature Review

1.1 Introduction

Cancer has surpassed cardiovascular issues as the leading cause of death in Canada, with an expectation that one in two Canadians will be diagnosed with the disease. This condition is characterized by a complex accumulation of mutations, with each variant posing unique challenges for treatment. Consequently, understanding the underlying mechanisms of each cancer subtype becomes essential.

The mitogen-activated protein kinase (MAPK) pathway plays a crucial role in driving uncontrolled cell proliferation, particularly when key effectors like RAS and RAF become mutated, leading to inappropriate survival signals and tumorigenesis. Tumor suppressor mechanisms can detect these aberrant signals and respond by engaging oncogene-induced senescence (OIS), which acts as a barrier to proliferation and alters the cell's behavior and secretory phenotype.

A screen to uncover kinases that can mediate bypass of OIS was conducted by Dutchak *et al*. (Dutchak et al., 2022). Here, it was discovered that the MPS-one binder co-activator (MOB) 3A protein allowed senescence bypass through the altered signaling of the Hippo pathway. Since OIS is considered an impenetrable barrier to excessive proliferation, developing an in vitro cell model will be advantageous for future research, providing opportunities to better characterize the pathways involved in senescence bypass.

This thesis also aims to evaluate and quantify the recruitment of immune cells to tumor sites using a live murine model and immunofluorescence. Senescent cells interact distinctly with their

environment, often recruiting specific subsets of immune cells to the site of inflammation. Given that the immune system is a natural antagonist to tumor growth, a deeper understanding of how the senescent secretory phenotype influences immune cell behavior in the tumor microenvironment (TME) could provide valuable insights to support the development of immune-enhancing therapies.

1.2 Lung Cancer

Cancer is the leading cause of mortality in Canada. According to a recent study by Brenner *et al.* (Brennet et al., 2024), lung cancer was projected to be the most diagnosed cancer in 2024 and continues to be the foremost cause of cancer-related deaths among both men and women. While lung, breast, prostate and colorectal cancers collectively account for nearly half of all cancer cases, lung cancer alone is responsible for more fatalities than the other three types combined, totaling one-quarter of all cancer deaths despite constituting less than 15% of cancer diagnoses (Lee, 2020).

Lung cancer can be histologically characterized as small cell lung cancer (SCLC) or non-small cell lung cancer (NSCLC), with the latter accounting for 85% of cases (Molina et al., 2009). SCLC is an aggressive subtype originating from the bronchi or airways, predominantly caused by tobacco smoking (National Cancer Institute, 2019; Ciupka, 2020). It is known for rapidly metastasizing to the lymph nodes and other parts of the body (National Cancer Institute, 2019). SCLC can be further classified into two subtypes based on cellular morphology: small cell carcinoma and combined small cell carcinoma (Ciupka, 2020).

NSCLC is the most common form of lung cancer and progresses slower than SCLC (National Cancer Institute, 2023). It is often diagnosed at a late stage because it remains asymptomatic in its early phases. As a result, the five-year survival rate for NSCLC remains under 20% (Lee, 2020;

Ciupka, 2020). NSCLC encompasses three primary subtypes: large-cell undifferentiated carcinoma, squamous cell carcinoma, and lung adenocarcinoma (LUAD), with adenocarcinoma being the most prevalent, accounting for nearly one-third of all lung cancer cases (Ciupka, 2020).

1.2.1 The Mitogen-Activated Protein Kinase Pathway

Over 75% of lung adenocarcinoma cases exhibit recurrent aberrations in the RTK/RAS/RAF pathway resulting in the constitutive activation of the MAPK signaling cascade, a critical regulator of cellular processes such as replication, differentiation, stress response, and apoptosis (Devarakonda et al., 2015; Collison et al., 2014; Cargnello and Roux, 2011). This pro-proliferative cascade is typically initiated by external stimuli such as the activation of the epidermal growth factor receptor (EGFR) or phosphorylation events triggered by protein kinases like Ras, Raf, MEK, and ERK, downstream of cell surface receptors (Cargnello and Roux, 2011; McCain, 2013; Stefani et al., 2021). Additionally, G protein-coupled receptors can trigger the pathway in response to extracellular signals like growth factors and stress (McCain, 2013). However, receptor tyrosine kinases (RTKs) are more common activators of the MAPK pathway. Upon ligand binding, RTKs undergo dimerization and auto-phosphorylation, which, with the help of adaptor proteins, activates the RAS GTPase. RAS then activates RAF, which subsequently phosphorylates the dualspecificity kinases MEK1/2, leading to the activation of ERK1/2. ERK1/2 regulates transcription factor activity and promotes cell proliferation in the nucleus (Cargnello and Roux, 2011; McCain, 2013).

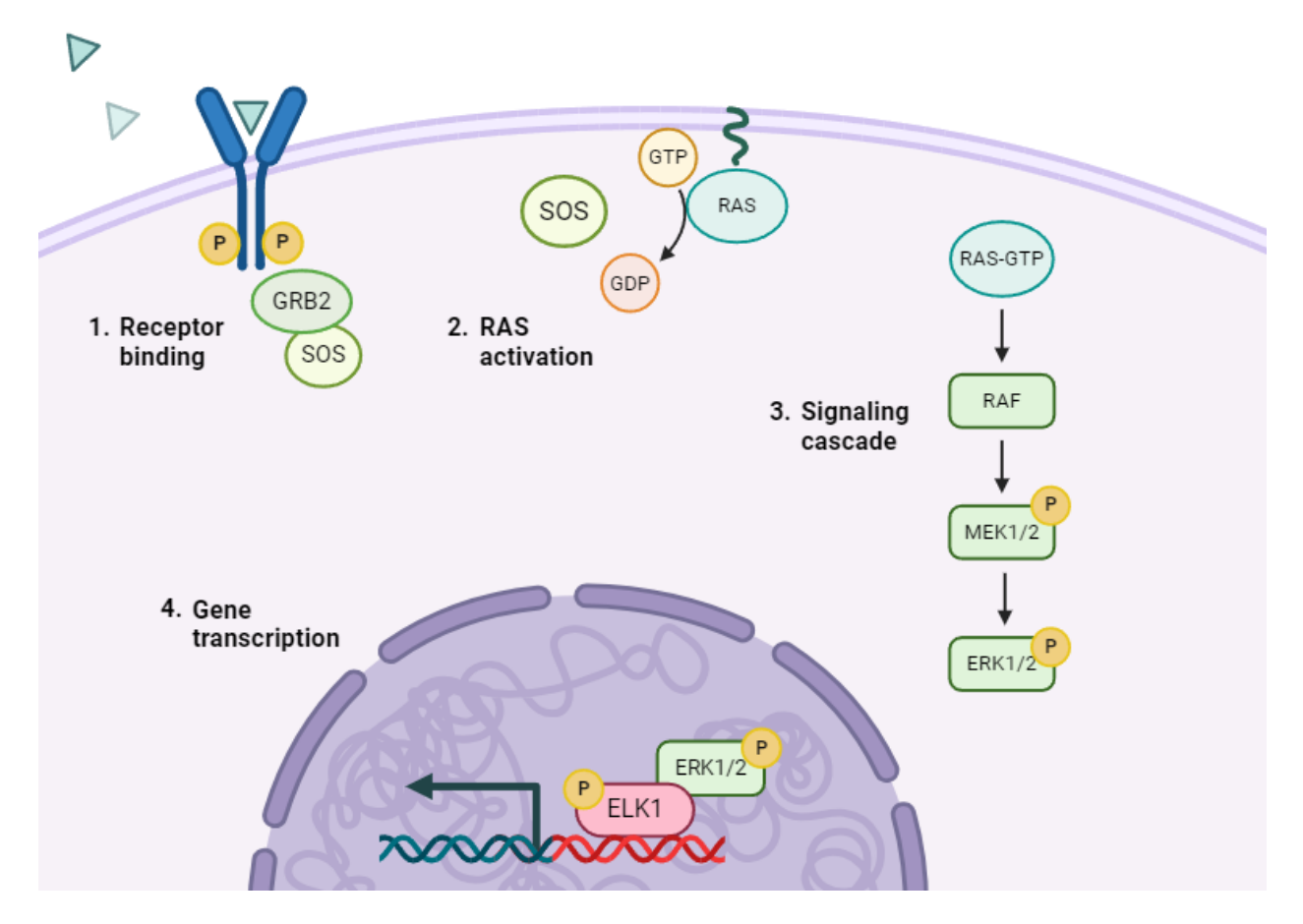


Figure 1-1. The MAPK pathway. Upon receptor binding and phosphorylation, adaptor proteins GRB2 and SOS facilitate the activation of RAS by promoting the exchange of GDP for GTP. Activated RAS initiates a signaling cascade through RAF, MEK1/2, and ERK1/2, leading to phosphorylation events. Phosphorylated ERK1/2 translocates to the nucleus, where it activates transcription factors, driving gene expression and cellular responses such as proliferation, differentiation, and survival. Created with BioRender.com.

1.2.2 BRAF

Oncogenes play a crucial role in the development of cancer. Five mutually exclusive oncogenes are active in over 50% of LUAD cases, involving somatic alterations in *KRAS*, *EGFR*, *ALK*, *ERBB2*, and *BRAF* (Greulich, 2010). While all these mutations typically lead to abnormal

cell proliferation and malignant behavior, this thesis will focus specifically on *BRAF* (Gutschner and Diederichs, 2012).

RAF is a serine-threonine kinase characterized by three conserved regions: CR1, CR2, and CR3. The RAF amino-terminal CR1 contains a zinc-finger-like domain and the RAS binding domain, both essential for RAF activation (Matallanas et al., 2011). CR2, a serine-rich regulatory domain, primarily functions as a hinge connecting CR1 and CR3. The carboxy-terminal CR3 contains the catalytic kinase domain, including the adenosine triphosphate (ATP)-binding pocket and the phosphate binding loop (Matallanas et al., 2011). In its inactive state, CR1 and CR3 interact through this loop to maintain RAF in an autoinhibited conformation. Upon RAS binding, this interaction is disrupted, leading to the phosphorylation of residues T599 and S602 within the CR3 region, which activates the kinase by dimerization (Garnett and Marais, 2004; Hmitou et al., 2007).

Three RAF isoforms exist: ARAF, BRAF, and CRAF. BRAF is the most catalytically active but also the most mutated form of the protein (Matallanas et al., 2011). All RAF isoforms share the three conserved regions (CR1, CR2 and CR3) but differ in terms of co-activators, ability to homo or hetero-dimerize and affinity to downstream MEK proteins (Matallanas et al., 2011).

Three distinct classes of *BRAF* mutations have been identified. Class I *BRAF* mutations are RAS-independent, exhibiting elevated kinase activity and functioning effectively even in their monomeric form. Point mutations in codon 600 of exon 15 (*BRAF*^{V600}) fall into this class, with the V600E mutation, where valine is substituted by glutamate, being the most common (Riudavets et al., 2022). This V600E missense mutation is particularly significant in tumor initiation, especially in melanoma and to some extent in NSCLC. It causes constitutive activation of the BRAF protein by destabilizing its autoinhibitory conformation, thereby increasing kinase activity (Wan et al.,

2004). Although BRAF typically functions as a dimer, the mutated form can function independently (Matallanas et al., 2011).

Class II and Class III BRAF mutations occur either in the glycine-rich G-loop of exon 11 or in the activation segment of exon 15 (Wooster et al., 2006). The G-loop, located in the CR3 region, is critical for kinase function. While BRAF mutations are common somatic alterations in cancer, they can also occur in the germline, leading to developmental disorders known as RASopathies (Therrien and Lavoie, 2015). Ultimately, the $BRAF^{V600E}$ mutation is associated with poor prognoses due to its role in promoting increased cell migration, proliferation and resistance to apoptosis (Matallanas et al., 2011, Ascierto et al., 2012).

1.2.3 Tumor Suppressor Gene P53

P53 is arguably the most critical tumor suppressor gene in the mammalian genome, earning it the title of "guardian of the genome" (Lane, 1992). In response to cellular stress, P53 functions as a master regulator by transactivating a wide array of target genes that are involved in cell cycle arrest, apoptosis, deoxyribonucleic acid (DNA) repair, senescence, and other essential processes. It regulates the expression of over 3600 genes, and its activity is finely tuned through extensive post-translational modifications (Zhang et al., 2014; Fujita, 2019).

P53 is subject to a wide range of post-translational modifications, which are crucial for its function and regulation. These modifications are triggered by various stress signals, including DNA damage, hypoxia, nitric oxide, and oncogene activation (Harris and Levine, 2005). Different types of stress activate specific enzymes that modify P53 at distinct amino acid residues. For example, DNA damage caused by gamma irradiation, base alkylation, and oxidative free radicals each activate unique detection mechanisms and repair pathways, leading to diverse modifications

of P53 (Harris and Levine, 2005). These modifications include phosphorylation, acetylation, methylation, ubiquitination, and sumoylation (Appella and Anderson, 2001). The specific combination and location of these post-translational modifications communicate the nature of the stress signal to P53, enabling it to adjust its activity accordingly (Colman et al., 2000). These modifications not only enhance P53's ability to bind specific genes but also extend its half-life from a few minutes to several hours. Notably, phosphorylation of P53 at Ser15 and Ser20 stabilizes the protein by preventing its interaction with mouse double minute 2 homolog (MDM2), which normally targets P53 for degradation (Kruse and Gu, 2009). Enzymes such as ataxia-telangiectasia mutated (ATM), checkpoint kinases (CHK) 1 and 2 are responsible for phosphorylating P53 in this manner (Appella and Anderson, 2001).

As previously discussed, when a cell enters senescence due to critically shortened telomeres, the disruption of the shelterin protein complex triggers a DNA damage response. Serine/threonine kinase transducers, such as ATM become activated upon recognizing double-stranded breaks. ATM then phosphorylates downstream effectors, initiating the DNA damage response cascade. Specifically, ATM activates CHK2, which in turn phosphorylates P53 on Ser20, thereby inhibiting MDM2 from sequestering P53 and disrupting the P53-MDM2 interaction (Shiloh, 2003). This results in the accumulation of the tumor-suppressive transcription factor P53, which proceeds to initiate the transcription of target genes (Fujita, 2019). Additionally, ATM phosphorylates P53 on Ser15, further enhancing its activity, and phosphorylates MDM2 on Ser395, preventing the nuclear export of the P53-MDM2 complex and protecting P53 from degradation (Shiloh, 2003).

MDM2's functions extend beyond P53 degradation. As a nuclear protein, MDM2 can shuttle to the cytoplasm to mediate the degradation of its targets via the proteasome (Shi and Gu, 2012). However, its primary role is to regulate P53 levels within the cell. Interestingly, MDM2 itself is a

target gene of P53, meaning that as P53 levels increase, P53 activates the MDM2 promoter. The resulting MDM2 protein then targets P53 for ubiquitination and subsequent proteasomal degradation (Shi and Gu, 2012). This tight regulation between P53 and MDM2 is crucial, as excessive P53 activity can induce cell death in otherwise healthy cells, while insufficient P53 levels can lead to cellular transformation (Shi and Gu, 2012; Nag et al., 2013; Fujita, 2019).

Downstream targets of P53 are specific DNA sequences known as P53-responsive elements, which P53 binds in the form of a homo-tetramer to initiate a transcriptional program tailored to the stress signal received. In the case of DNA damage, cell cycle arrest is promoted by the P53 activation of cyclin dependent kinase inhibitor 1A (CDKN1A) family of cyclin-dependent kinase inhibitors (Fujita, 2019). During P53-mediated G1 arrest, cyclin-dependent kinase inhibitors such as P21^{WAFI/CIP1} inhibit cyclin E-CDK2, a kinase responsible for activating E2F1 by releasing it from its sequestering protein, retinoblastoma (RB) (Harris and Levine, 2005). Additionally, P53 can mediate G2 arrest by upregulating the transcription of 14-3-3, a protein that prevents the nuclear transport of the CDC25C phosphatase (Malumbres and Barbacid, 2005). CDC25C normally activates the cyclin B-CDC2 complex by dephosphorylating the Thr14 and Tyr15 sites (Malumbres and Barbacid, 2005). Sequestering the phosphatase to the cytoplasm thus prevents the cell cycle transition from G2 to the M phase. P53-mediated senescence has also been observed in primary cell cultures following expression of oncogenic *RAS*, leading to the transcription of P19 and p14^{ARF} and reinforcing its role as a key regulator of the cell cycle (Bates et al., 1998).

Since P53 functions as a tetramer, one wild-type allele can be insufficient to restore the protein's full activity in the case of mutations, particularly in dominant-negative mutations where the mutant impairs the function of the wild-type allele (Higashimoto et al., 2006). Mutant P53 subunits can bind to wild-type subunits, forming mixed tetramers that compromise the tumor-

suppressive function of P53 and in some cases, leads to a gain of function activity (Dittmer et al., 1993) able to promote cancer progression independently from wild-type P53 (Yue et al., 2017b). This gain of function allows P53 to interact with other transcription factors such as E26 transformation-specific (ETS)1/2, nuclear factor kappa-light-chain-enhancer of activated B cells (NF-κB), and SMADs and thereby regulate the transcription of their target genes (Pfitster and Prives, 2017). In contrast to wild-type P53, mutant P53 activates cyclins such as cyclin A, CDK1 and the CDC25C phosphatase to promote cell cycle progression (Di Agostino et al., 2006). Besides enabling metastasis, genomic instability and metabolic reprogramming (Zhang et al., 2020), gain of function mutant P53 has also been reported to promote resistance against chemotherapies (Chin et al., 1992).

Oncogenes too are considered a form of cellular stress, leading to the activation of cell cycle arrest mediated by P53 and the DNA damage response. Di Micco *et al.* observed that cells undergoing OIS exhibited clear signs of an active DNA damage response through the presence of senescence-associated DNA-damage foci bound with activated ATM (Di Micco et al., 2006). They also noted the activation of CHK1 and CHK2, phosphorylation of P53 at Ser15, and an increase in the cyclin-dependent kinase inhibitors P21^{WAF1/CIP1} and P16^{INK4A} (Di Micco et al., 2006). Their study demonstrated that successful OIS is dependent on an efficient DNA damage response, as the proliferation of damaged cells becomes possible in its absence. Given that P53 is a key mediator of the DNA damage response, these findings suggest that senescence could be bypassed were the tumor suppressor absent or mutated (Serrano et al., 1997; Di Micco et al., 2006). However, it is important to note that OIS is not always mediated by P53. Other pathways, such as the P16^{INK4A}/RB pathway, can also induce senescence independently of P53, however this area remains under active investigation (Larsson, 2011).

1.3 Cellular Senescence

1.3.1 Senescence

Replicative cellular senescence was first identified by Hayflick and Moorhead in 1961 when they observed that human fibroblast cells, while remaining alive and viable, ceased to divide after 40 to 60 passages in culture (Hayflick and Moorhead, 1961). This phenomenon, now known as the Hayflick limit, marks a critical threshold where cells undergo significant changes in morphology and gene expression, resulting in a stable yet altered phenotype (van Deursen, 2014). Cellular senescence is a state of stable cell cycle arrest and is primarily triggered by telomere shortening, a consequence of the inability of DNA polymerases to fully replicate the telomere's lagging strand during cell division (Harley et al., 1990). The role of telomere length in limiting cellular replication was illustrated by studies showing that ectopic expression of telomerase can bypass senescence (Bodnar et al., 1998). Senescence is initiated when the loss of telomere repeats disrupts the shelterin protein complex, which normally binds the exposed ends of chromosomes (Griffith et al., 1999). This prompts the cell's DNA repair machinery to recognize the exposed telomere ends as double-stranded breaks, triggering a DNA damage response (Victorelli and Passos, 2017). Indeed, a model by Di Micco et al. suggests that senescent cells stall in S phase due to a DNA damage response caused by excessive replication (Di Micco et al., 2006). They reported an increased number of active replicons and replication fork progression defects (Di Micco et al., 2006; Courtois-Cox et al., 2008).

Cellular senescence can also occur prematurely in response to various stressors to prevent the proliferation of damaged cells. This process can be triggered by a range of factors, depending on the cell type and the nature of the stressor. Key inducers of senescence include oxidative stress,

oncogene activation, DNA damage, overexpression of cell cycle inhibitors, and telomere erosion, among others (Chen et al., 2007).

Although senescent cells no longer proliferate, they remain metabolically active (Fujita, 2019). The behavior and secretory phenotype of these cells can vary significantly, adapting in a context-specific manner. Senescent cells often exhibit distinct phenotypical changes, such as an enlarged morphology and alterations in plasma membrane composition (Kumari and Jat, 2021). The nucleus may also appear enlarged. These cells are unresponsive to mitogens and frequently exhibit resistance to apoptosis. Gene expression is profoundly altered, likely due to chromatin remodeling (Kumari and Jat, 2021). Additionally, senescent cells typically show an increased DNA damage response, heightened lysosomal activity, and the development of an altered secretory phenotype through specific signaling cascades (Kumari and Jat, 2021).

The cell cycle arrest of senescent cells is controlled by two key tumor suppressor pathways: the P53-P21^{WAF1/CIP1} pathway and the P16^{INK4A}-RB pathway (Borgdorff et al., 2010; Kumari and Jat, 2021). These pathways can function independently or in conjunction with each other to enforce senescence. Both P53 and RB are potent transcription factors that regulate gene expression and cell cycle control. In the P53 pathway, p21^{WAF1/CIP1} acts downstream of P53 to mediate the senescence response, while in the p16^{INK4A} pathway, p16^{INK4A} functions upstream of RB (Kumari and Jat, 2021). The sustained expression of these inhibitors enforces cellular senescence, preventing the proliferation of damaged cells.

Senescent cells are integral to a variety of physiological processes, including tissue homeostasis, repair, embryonic development, inflammation, wound healing, and insulin secretion (Fujita, 2019). Beyond these roles, senescent cells serve as a critical barrier to tumor progression

by halting the replication of damaged or transformed cells and their presence can be beneficial in maintaining tissue integrity and preventing malignancy.

1.3.2 Oncogene-Induced Senescence

Oncogenes are well-established drivers of tumorigenesis, as their expression can lead to uncontrolled cell proliferation. The $BRAF^{V600E}$ mutation, for instance, is constitutively active, resulting in the persistent activation of the MAPK pathway, which can eventually contribute to cancer development. However, cells can counteract this sustained oncogenic signaling by initiating an irreversible growth arrest, a phenomenon known as OIS (Chandeck and Mooi, 2010). OIS is not the same as replicative senescence, as it occurs independently from telomere shortening (Deng et al., 2008).

This mechanism is observed in the overexpression of oncogenic *RAS*, which triggers premature growth arrest in human primary lung fibroblasts (Liu et al., 2018). Beyond *BRAF* and *RAS*, other oncogenes such as *AKT*, *E2F1*, and *cyclin E* are also capable of promoting OIS (Courtois-Cox et al., 2008). Additionally, the suppression of tumor suppressor genes like *P53*, *phosphatase and tensin homolog (PTEN)*, and *neurofibromin 1 (NF1)* can further induce OIS (Liu et al., 2018).

Cells that have undergone OIS display classical markers of cellular senescence, such as increased beta-galactosidase activity and the presence of a senescence-associated secretory phenotype (SASP) (Bieging et al., 2014). The regulation of OIS is largely governed by tumor suppressor pathways involving P53, RB, P16^{INK4A} and P21^{WAF1/CIP1} (Bieging et al., 2014). Notably, cells undergoing OIS typically accumulate P53, which plays a crucial role in maintaining the senescent state. For instance, studies in mice have shown that expression of oncogenic *RAS*^{G12D}

leads to the formation of benign, senescent adenomas when P53 is present. However, in the absence of P53, these adenomas can progress to malignant adenocarcinomas, highlighting the protective role of P53 in preventing tumor progression (Dankort et al., 2007; Bieging et al., 2014).

Cellular senescence is increasingly recognized as a powerful mechanism for suppressing tumor growth by halting the proliferation of damaged or transformed cells (Chandeck and Mooi, 2010). One of the key strengths of OIS is its ability to influence tumor development through the secretion of senescence-associated factors such as transforming growth factor beta (TGF-β) and chemokine ligand 2 (CCL2) (Liu et al., 2018). These factors can propagate oncogenic stress to neighboring cells and the surrounding microenvironment, recruiting immune cells and effectively curbing tumor progression. This growth arrest is often regarded as a potent barrier to malignant transformation, serving as a critical tumor-suppressive mechanism (Liu et al., 2018; Fujita, 2019).

Despite its significance, the underlying mechanisms of cellular senescence are not yet fully understood, highlighting the importance of continued research in this field. A deeper understanding of cellular senescence could unveil novel therapeutic approaches for combating the persistent threat of cancer.

1.3.3 MOB3A

1.3.3.1 The Hippo Pathway 2. MST1/2 recruits MOB1 and activates MST1/2 MST1/2 NF2 LATS1/2 1.NF2 recruits and scaffolds MST1/2 and SAV1 **STRIPAK** 3. LATS1/2 phosphorylates YAP/TAZ MOB1 LATS1/2 14-3-3 4B. Degradation 4A. Cytoplasmic YAP/TAZ YAP/TAZ Retention YAP/TAZ TEAD1-4 Gene expression OFF ON Hippo Pathway ON- OFF

Figure 1-2. The Hippo Pathway. MST1/2 activates LATS1/2 with the assistance of MOB1. Activated LATS1/2 phosphorylates YAP/TAZ, leading to cytoplasmic retention by 14-3-3 binding or ubiquitin-mediated degradation. In the absence or inhibition of the pathway by the STRIPAK complex, YAP/TAZ translocate to the nucleus to drive gene expression. Created with BioRender.com.

The Hippo pathway is an evolutionarily conserved signal transduction pathway first identified in *Drosophila*. It defines the molecular mechanisms underlying organ growth during development or regeneration (Pan, 2010). The four main components of the Hippo pathway were discovered in genetic screening of tumor suppressor genes and include the nuclear dbf2-related (NDR) family protein kinase Warts (LATS1/2 in mammalians), the Salvador adaptor protein (SAV1), the Ste20-like protein kinase Hippo (MST1/2) and the adaptor protein Mats (MOB1) (Justice et al., 1995; Tapon et al., 2002; Wu et al., 2003; Lai et al., 2005). Loss of function of any of these four genes causes increased proliferation and a reduction in apoptosis resulting in severe tissue overgrowth (Pan, 2010).

The Hippo pathway is activated by various upstream signals responsible for cell size and density, often conveyed by membrane proteins such as kidney and brain expressed protein (KIBRA) and NF2 (Xiao et al., 2011; Hong et al., 2020). MST1/2 becomes active once phosphorylated by TAO kinases on residues Thr183 and Thr180 of its activation loop (Boggiano et al., 2011). It is bound to SAV1, an adaptor protein that enhances phosphorylation and activation of LATS1/2 by MST1/2 (Tapon et al., 2002). LATS1/2 is recruited by NF2 to the plasma membrane, where it will be phosphorylated by the MST1/2-SAV1 complex (Yin et al., 2013). MOB1 is recruited by MST1/2 and forms a complex with LATS1/2, acting first as a scaffold, then as an adaptor to enhance MST1/2's kinase activation (Hergovich et al., 2006). The LATS1/2-MOB1 complex will then phosphorylate yes-associated protein (YAP)/ transcriptional coactivator with PDZ-binding motif (TAZ), creating a 14-3-3 binding site, leading to its sequestration it in the cytoplasm (Zhao et al., 2007), preventing it from activating cell proliferative genes and inhibiting apoptosis (Pan, 2010; Boopathy and Hong, 2019) (Figure 1-2).

1.3.3.2 The MOB Protein Kinase Family

The MOB protein family is involved in a variety of cellular processes such as cell division, tissue growth, morphogenesis, intracellular signaling and homeostasis (Duhart and Raftery, 2020). The human genome encodes seven MOB proteins: MOB1A, MOB1B, MOB2, MOB3A, MOB3B, MOB3C, MOB4 (Meng et al., 2016). MOB1 is an adaptor and scaffolding protein devoid of any specific functional domain highly conserved in eukaryotes (Hergovich, 2016).

In the Hippo pathway, MOB1A and MOB1B function as scaffold proteins that facilitate the interaction between MST1/2 and LATS1/2. While MOB1 itself does not have enzymatic activity, it is a crucial regulatory subunit that modulates the activity of kinases. MST2 autophosphorylates to create a docking site for MOB1 recruitment (Ni et al., 2015). The binding of MOB1 to MST2 induces a conformational change in MOB1, enabling LATS to associate with the MOB1-MST2 complex (Wei et al., 2007). This ternary complex promotes the phosphorylation of MOB1 at residues T35 and T12, while MST2 activates LATS1 by phosphorylating its hydrophobic motif T1079 (Ni et al., 2015). The phosphorylation of MOB1 subsequently triggers the dissociation of the MOB1-LATS1 complex from MST2 (Ni et al., 2015). MOB1 then facilitates the autophosphorylation of LATS1 at its activation loop, further enhancing its activity (Meng et al., 2016). Because of its critical function in the Hippo pathway, MOB1 is considered a potent tumor suppressor in a multitude of human cancers, ranging from colorectal cancer, glioblastoma and NSCLC (Ando et al., 2020).

MOB2 is less involved in the Hippo pathway compared to MOB1, as it primarily interacts with serine/threonine kinase proteins that play roles in broader signaling pathways crucial for regulating various cellular processes such as cell cycle control, cell polarity, and apoptosis (Duhart

and Raftery, 2020). Additionally, MOB2 is known to inhibit the function of NDR1/2 kinases, which are important for regulating cytoskeletal dynamics (Bichsel et al., 2004; Kohler et al., 2010).

MOB3 plays a role in the STRIPAK complex, a critical regulator of the Hippo signaling pathway. The STRIPAK complex attenuates Hippo pathway signaling by dephosphorylating key components such as MST1/2 and YAP/TAZ, primarily through the action of protein phosphatases PP1 and PP2A (Couzens et al., 2013). MOB3 interacts with striatin, a central scaffolding protein within the STRIPAK complex, and is believed to modulate the activity of the associated kinases and phosphatases (Couzens et al., 2013; Duhart and Raftery, 2020).

1.3.3.4 The Role of MOB3A in OIS Bypass

The oncogene-driven RAF-MEK-ERK MAPK pathway plays a crucial role in the development of many cancers, with the *BRAF*^{V600E} mutation being particularly prevalent in certain malignant forms of melanoma, thyroid, colorectal cancers, and NSCLCs (Bamford et al., 2004). Interestingly, while the *BRAF*^{V600E} mutation is present in up to 85% of early melanocytic nevi, it occurs at a much lower frequency in melanomas, where it is found in approximately 50% of cases (Davies et al., 2002; Pollock et al., 2003, Damsky et al., 2015). Studies in both human and mouse models have shed light on this discrepancy, showing that tumors driven by oncogenic BRAF expression are often restrained by OIS (Michaloglou et al., 2005; Pritchard et al., 2007; Wellbrock et al., 2008; Dankort et al., 2009). The reduced frequency of *BRAF*^{V600E} mutations in melanoma suggests that additional mutations, such as those in P53 and CDKN2A, are required to bypass OIS and allow progression from a benign nevus to a malignant melanoma (Damsky et al., 2015). This drives the search for genes able to promote proliferation despite sustained oncogenic signaling.

Dutchak *et al.* pursued this search by conducting an activated kinase OIS bypass screen using a previously established library (Boehm et al., 2007) in cells expressing a conditionally active form

of BRAF (Garnett et al., 2021). To generate these cells, the wild-type BRAF kinase domain (CR3 region) was fused to a modified hormone-binding (HBD) domain of the human estrogen receptor (ER), while the CR1 and CR2 regulatory regions were excluded (Figure 1-3) (Pritchard et al., 1995). This ΔBRAF:ER (BRER) mutant was introduced into human lung fibroblasts immortalized with hTERT (HF E1T cells) via lentiviral transduction (Dutchak et al., 2022), allowing for controlled induction of MAPK signaling. Upon treatment with 4-hydroxytamoxifen, the ΔBRAF:ER construct is activated and produces a stable protein that led to subsequent ERK phosphorylation. Cells treated with the drug exhibited several hallmarks of senescence, including reduced DNA synthesis, induction of negative cell cycle regulators, increased senescence-associated β-galactosidase activity, and proliferation arrest (Garnett et al., 2021; Dutchak et al., 2022).

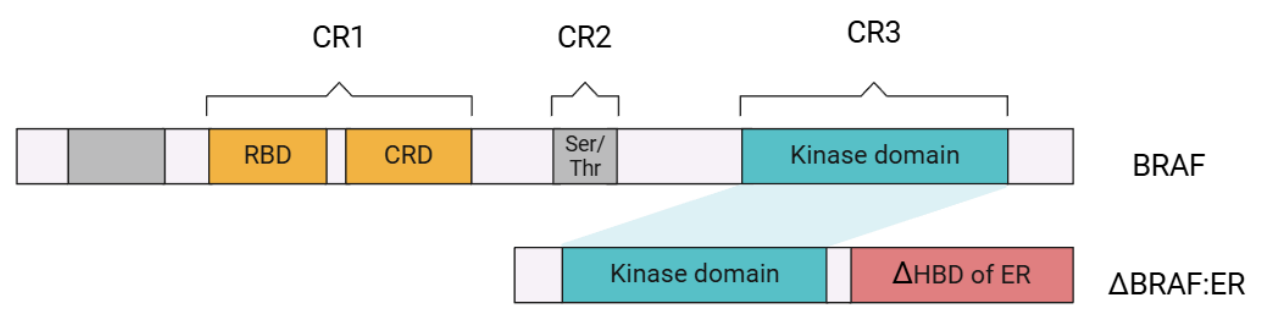


Figure 1-3. Schematic representation of ΔBRAF:ER. The BRAF protein consists of three conserved regions: CR1, CR2, and CR3. CR1 contains the RAS binding domain (RBD) and the cysteine-rich domain (CRD), which regulate membrane localization and RAS-mediated activation. In the ΔBRAF:ER fusion protein, the CR1 and CR2 regions are removed, leaving only the CR3 kinase domain fused to a modified HBD of the ER. This construct enables controlled conditional activation of the BRAF kinase domain using 4OHT. Created with BioRender.com.

To identify kinases capable of inducing OIS bypass, BRER cells were transduced with individual retroviral vectors encoding myristoylated kinases and kinase regulatory molecules from

the library. Dutchak *et al.* identified a population of cells that continued to proliferate under constitutive BRAF activation. The retroviral vector associated with this population encoded MOB3A, a kinase regulator involved in the negative regulation of the Hippo pathway (Dutchak et al., 2022). The specific role of certain MOB proteins, including MOB3A, in cell cycle regulation and senescence bypass is not fully understood. Given that MOB3A is part of the STRIPAK complex, it is plausible that MOB3A could influence OIS bypass by inhibiting Hippo signaling, thereby promoting cell proliferation and survival. This occurs through the accumulation of non-phosphorylated YAP/TAZ in the nucleus, leading to the transcription of proliferative genes and the avoidance of apoptosis.

While the data was consistent with a role for Hippo inhibition leading to OIS bypass, a subsequent genetic screen to identify kinases required for OIS bypass failed to identify MST or LATS family members suggesting additional research is needed to fully elucidate the mechanism behind MOB3A-mediated bypass of senescence. Unfortunately, the cell model created by Dutchak *et al.* was found to 'drift'. It is possible that this is due to accumulated mutations or epigenetic changes resulting in modifications of cell behaviour. Recreating the BRER MOB3A cell model in an alternative cell line would provide a valuable platform for further study of MOB3A's role in senescence bypass.

1.3.4 **SASP**

In the absence of additional mutations or dysfunctions in regulatory mechanisms, OIS results in irreversible and premature cell cycle arrest (Braig et al., 2005; Braig and Schmitt, 2006). OIS serves as a critical barrier to tumorigenesis by maintaining cells in a premalignant state (Braig et al., 2005; Braig and Schmitt, 2006). Although OIS can be triggered by over 50 different oncogenes, the most well-known and extensively studied models, both *in vivo* and *in vitro*, involve effectors

of the MAPK pathway, such as *RAS* and *RAF* (Lin et al., 1998; Michaloglou et al., 2005; Dankort et al., 2007). OIS leads to an increase in senescence-associated beta-galactosidase activity and the formation of senescence-associated heterochromatic foci, characterized by the condensation of individual chromosomes into heterochromatic bodies (Narita et al., 2003). Despite being in a state of cell cycle arrest, senescent cells remain metabolically active and significantly influence the surrounding microenvironment through the secretion of a complex mixture of molecules, collectively known as the SASP (Cristofalo and Pignolo, 1996; Krtolica et al., 2001; Coppé et al., 2008).

The SASP encompasses a collection of pro-inflammatory and growth-stimulating proteins, lipids, excreted vesicles and non-coding nucleic acids (Schmitt et al., 2022). These components can reinforce senescence in the surrounding environment and play both pro- and anti-tumorigenic roles (Kuilman et al., 2008). The SASP facilitates the release of both pro- and anti-inflammatory molecules, including interleukins (IL), chemoattractants, macrophage inflammatory proteins, growth factors and proteases, with the full repertoire varying according to specific circumstances (Pérez-Mancera et al., 2014). For instance, in response to BRAF^{V600E}, human fibroblasts express insulin-like growth factor (IGF)-binding protein 7 (IGFBP7), IL-6, and CXCR2, which are essential for OIS modulation (Wajapeyee et al., 2008; Kuilman et al., 2008).

The secretion of senescence-associated chemokines and cytokines is tightly related but not exclusive to P53 expression (Coppé et al., 2010). ATM kinase, a crucial P53 activator, also promotes SASP by stimulating GATA-4 during senescence (Kumari and Jat, 2021). In turn, GATA-4 activates the transcription factor NF-κB, leading to the release of senescence-associated factors (Kang et al., 2015). Another critical transcription factor involved in regulating SASP proteins is CCAAT/enhancer-binding protein beta (CEBPβ), which promotes the expression of the SASP

master regulator IL-1α and pro-inflammatory cytokines IL-6 and IL-8 (Kuilman et al., 2008; Orjalo et al., 2009; Chien et al., 2011). Once initiated, the signaling cascade is amplified in a feed-forward loop by factors such as IL-1α, IL-6 and IL-8, which further enhance NF-κb and CEBPβ activity (Tasdemir et al., 2016; Kumari and Jat, 2021).

This regulatory process can also be influenced by epigenetic regulators like bromodomain-containing protein 4 (BRD4), leading to the induction of remodeling proteins and fibrolytic factors that play key roles in wound healing (Demaria et al., 2014; Hernandez-Segura et al., 2017; Basisty et al., 2020; Chen et al., 2023). In fact, OIS has been shown to be quite dependent on BRD4, which is required for downstream signaling following its recruitment to super-enhancers located near key SASP genes (Tasdemir et al., 2016).

P53 plays an active role in inhibiting the SASP, suggesting a possible mechanism by which P53 suppresses tumorigenesis (Coppé et al., 2010). This mechanism involves preventing the formation of a tissue microenvironment that promotes tumor growth and inflammation, as this may also contribute to tumorigenesis. When P53 activity is compromised in senescent or damaged fibroblasts, there is a marked increase in both the SASP and its stimulatory impact on malignant epithelial cells (Coppé et al., 2010).

Many of the factors mentioned above are involved in the local recruitment of the immune cells. For example, granulocyte-macrophage colony-stimulating factor (GM-CSF), recruited by signal transducer and activator of transcription (STAT) 3, supports myeloid cell maturation and dendritic cell (DC) differentiation (Egea et al., 2010). STAT3 itself is an essential signal transducer for the maturation of lymphocytes such as T cells and B cells, which are potent actors in the adaptive immune system (Hu et al., 2024).

CXCR2, a chemokine receptor, aids the infiltration of pro-tumorigenic leukocytes into tumors and facilitates inflammation (Jamieson et al., 2012). It also acts as a chemoattractant for neutrophils and other monocytes (Barnes and Rennard, 2009). IL-6, primarily a pro-inflammatory cytokine, is pivotal in host defenses, regulating secretion and amplify signaling within the inflammatory network (Liu et al., 2018). Expressed by macrophages and DCs recruited to injury sites, IL-6 is also an effector in T cell development (Tanaka et al., 2014; Aliyu et al., 2022). Similarly, IL-8 is a pro-inflammatory cytokine involved in recruiting neutrophils to sites of infection or tissue damage. It is expressed by a variety of immune cells, including macrophages, neutrophils, eosinophils and T cells (Zhang and An, 2007). IL-8 also plays an important role in oxidative stress responses initiated by stressed epithelial cells (Qazi et al., 2011).

Most factors secreted by senescent cells function through paracrine and autocrine signaling. For instance, the SASP-associated cytokine TGF-β propagates senescence by generating reactive oxygen species (ROS) and DNA damage, ensuring immune recruitment to sites of inflammation to clear senescent cells and limit tissue fibrosis (Hubackova et al., 2012).

1.3.5 The Immune System

The microscopic world is filled with pathogenic and toxic entities that constantly threaten host functions. The immune system acts as a protective barrier, defending the body against pathogens (viruses, bacteria, fungi, parasites), toxins, and cancer cells that evolve to replicate and spread (Aristizábal and González, 2013). To prevent damage to host tissues, the immune system has developed complex mechanisms to distinguish self from non-self-based on the structure of these threats (Chaplin, 2010). These defenses are divided into two systems: the innate immune response, which is non-specific and immediate, and the adaptive immune response, which is powerful, long-lasting, antigen-specific and resulting in memory (Marshall et al., 2018).

1.3.5.1 Innate Immunity

The innate immune system serves as the first line of defense, a non-specific and evolutionarily ancient mechanism shared across all multicellular organisms (Aristizábal and González, 2013). It includes physical barriers such as the skin, mucosa, and secretions, which provide a formidable defense against potential invaders (Aristizábal and González, 2013). On a macroscopic level, this barrier is reinforced by tight junctions within the skin layers and the lining of the gut (Assimakopoulos et al., 2018). Non-specific phagocytic cells, such as neutrophils and macrophages, patrol the blood vessels and tissues, identifying and eliminating foreign material while presenting antigens to the adaptive immune system. Additionally, secreted proteins contribute to a robust innate immune response, including inflammatory serum proteins like the complement system, C-reactive protein, lectins, and antimicrobial granules (Aristizábal and González, 2013). Toll-like receptors (TLRs), a conserved subtype of pattern recognition receptors on plasma membranes, play a crucial role in recognizing pathogens by binding to pathogenassociated molecular patterns (PAMPs) in the extracellular matrix (Botos et al., 2011). This binding triggers an intracellular signaling cascade, leading to transcriptional activation that drives various immune responses, including inflammation, cytokine processing, phagocytosis, and even apoptosis (McClure and Massari, 2014; Brubaker et al., 2016).

A. Macrophages

Macrophages are widely present in tissues throughout the body, where they contribute to wound healing, tissue formation, inflammation, and coagulation (Koh and DiPietro, 2011). In the context of cancer, macrophages are particularly abundant in the TME, sometimes constituting up to 50% of the tumor mass (Vitale et al., 2019). These tumor-associated macrophages (TAMs) play a complex and often dual role in cancer progression.

Normally, macrophages can differentiate into two main subtypes: the pro-inflammatory M1 subtype, which is known for killing pathogens and limiting cell proliferation through the secretion of reactive oxygen and nitrogen species, and the M2 subtype, which is involved in tissue repair and the production of anti-inflammatory cytokines (Vitale et al., 2019; Lei et al., 2020). The TME influences macrophage dynamics by either suppressing the M1 subtype or promoting differentiation toward the M2 subtype, which is associated with immune suppression, angiogenesis, and matrix remodeling (Hinshaw and Shevde, 2019).

In cancer, macrophages are recruited from the bone marrow in response to chemokines (such as those from the CCL and CXCL families) and are influenced by surrounding cells, including tumor cells, osteoblasts, and epithelial cells, to differentiate (Biswas et al., 2013). The TME, through factors like IL-4 secretion, tends to favor the development of M2 macrophages, which contribute to cancer progression by suppressing immunosurveillance and promoting tumor growth (Hinshaw and Shevde, 2019; Lei et al., 2020).

B. Dendritic Cells

For efficient activation of the adaptive immune system, DCs must capture antigens, upregulate co-stimulatory molecules, release inflammatory cytokines, and migrate to secondary lymphoid organs to present antigens to T cells (Hinshaw and Shevde, 2019). DCs transport antigens from pathogens or cancer cells to lymph nodes, where they mediate T-cell activation and immunity (Fanale et al., 2022).

In the TME, DC maturation is inhibited by soluble factors such as vascular endothelial growth factor (VEGF), IL-10, and TGF-β, which impair their ability to prime T cells. Instead, these immature DCs promote immune tolerance within the TME by encouraging regulatory immune responses (Hinshaw and Shevde, 2019). However, if DCs reach maturity before encountering the

tumor, they can enhance immune activation and recruitment, leading to a more robust anti-tumor response (Lei et al., 2020).

C. Natural Killer Cells

Natural killer (NK) cells are an essential component of the innate immune system, serving as the body's first line of defense against infections and tumor cells. Unlike other immune cells, NK cells can recognize and kill virally infected or cancerous cells without prior sensitization or specific antigen recognition (Brandstadter and Yang, 2011). They are activated by cytokines secreted from macrophages, DCs, and T cells, enabling them to carry out their cytotoxic functions (Paul and Lal, 2017). NK cells contribute to immune defense through cytotoxicity, upregulation of the Fas death ligand, and secretion of cytokines like interferon gamma (IFN-γ), tumor necrosis factor alpha (TNF-α), and GM-CSF (Paul and Lal, 2017).

1.3.5.2 Adaptive Immunity

Adaptive immunity represents a highly specialized and evolved aspect of the immune system, designed to mount a specific, targeted, and sustained defense against invading pathogens (Marshall et al., 2018). Unlike the rapid but non-specific innate immune response, the adaptive immune response is slower to develop but offers long-lasting protection. The sophisticated memory system enables to "remember" foreign antigens, allowing a swift response upon re-exposure (Bonilla and Oettgen, 2010).

The adaptive immune response is not only highly specific but also extremely potent. This potency requires a precise distinction between self and non-self, which is a critical process during the development of lymphocytes (Marshall et al, 2018). Proper differentiation ensures that the immune system targets only foreign invaders, minimizing the risk of autoimmunity.

Central to the adaptive immune system are T cells and B cells, which are activated in response to specific antigens presented by antigen-presenting cells (APCs) (Chaplin, 2010). These lymphocytes orchestrate the immune response through two main pathways: cell-mediated immunity and humoral immunity (Bonilla and Oettgen, 2010). T cells are primarily involved in cell-mediated responses. They either attack infected, foreign or neoantigen-presenting cells through cytotoxic actions or signal neighboring phagocytes to eliminate the threat (Marshall et al., 2018; Xie et al., 2023). B cells contribute to humoral immunity by producing antibodies. Once antibodies bind to their specific targets, they mark the intruders for destruction by phagocytic cells (Chaplin, 2010). Additionally, antibodies can neutralize viruses and toxins by blocking their ability to bind to cell receptors (Alberts et al., 2002; Marshall et al., 2018).

A. T cells

T cells, the primary effectors of the adaptive immune response, are generated in the thymus and mediate cell-based immunity. They recognize antigens presented by APCs through the major histocompatibility complex (MHC). Three signals are required to fully prime a T cell: T cell receptor (TCR) recognition of the antigen, co-stimulatory molecules expressed by the APC, and cytokines, which may originate from either the APC or the surrounding environment (Sun et al., 2023).

T cells exist in various subtypes and are divided into two main categories: CD4+ T helper (Th) cells and CD8+ cytotoxic T cells. CD4+ T cells recognize antigens presented by MHC class II molecules, while CD8+ T cells interact with MHC class I molecules (Teh et al., 1988). CD4+ T cells can further differentiate into several Th subtypes, including Th1, Th2, and regulatory T cells (Treg) (Cenerenti et al., 2022). Th1 cells combat intracellular bacteria and viruses by secreting the pro-inflammatory cytokine IFN-γ (Bradley et al., 1996). In contrast, Th2 cells produce anti-

inflammatory cytokines like GATA-3 and IL-4, contributing to tissue repair (Walker and McKenzie, 2018). The functions of Th1 and Th2 cells are opposing, with the cytokines from one subtype inhibiting the other. For example, IFN- γ from Th1 cells suppresses Th2 activity, while GATA-3 expressed by Th2 cells inhibits Th1 development by silencing Th1-related genes (Dobrzanski, 2013; Spinner and Lazarevic, 2021). Treg cells specialize in maintaining immune tolerance by suppressing excessive immune responses through inhibitory cytokines like IL-10 and TGF- β (Plitas and Rudensky, 2016).

Cytotoxic CD8+ T cells are crucial in defending against pathogens and tumor cells by inducing apoptosis through the presentation of the Fas ligand on their surface, which binds to the Fas receptor on target cells, and by secreting perforin and granzymes to trigger cell death (Kaech and Wherry, 2007). CD8+ T cells can also differentiate into long-lived memory cells that retain the same TCR as the effector CD8+ T cells that initially responded to the antigen (Sun et al., 2023). This enables them to rapidly mount an adaptive immune response upon re-exposure to the antigen, through both cytokine release and rapid proliferation (Tanel et al., 2010).

1.3.6 The Tumor Microenvironment

The TME is the extracellular niche that supports tumor growth, composed of angiogenic blood vessels, immune cells, the extracellular matrix, and connective tissue (Fanale et al., 2022). The TME plays a crucial role in tumor development, influencing survival, metastasis, and immune resistance. It exerts both pro- and anti-tumorigenic effects, with the subtype of tumor-infiltrating lymphocytes often being a key determinant of tumor progression (Anderson and Simon, 2020; Fanale et al., 2022).

The ratio of cytotoxic CD8+ T cells to CD4+ T cells is critical for patient outcomes, with higher CD8+ T cell levels generally leading to better prognoses (Oh and Fong, 2022). Macrophages also play a major role. Pro-inflammatory M1 macrophages are associated with favorable outcomes, while immune-suppressive M2 macrophages promote tumor progression. M2 macrophages secrete IL-4, which downregulates Th1 helper cells and enhances Th2 helper cell activity (Muraille et al., 2014). This supports tumor growth by promoting metastasis, increasing TGF-β expression, which drives malignant transformation, and encouraging M2 macrophage differentiation (Pixley and Stanley, 2010; Hinshaw and Shevde, 2019; Le et al., 2021).

In contrast, Th1 helper cells recruit CD8+ T cells and NK cells to the tumor site by expressing adhesion molecules that facilitate immune cell migration (Nishimura et al., 1999). NK cells are particularly potent in eliminating malignant cells through mechanisms such as death receptor-mediated apoptosis, and the release of perforin and granzymes. They are guided to the tumor by chemokine-expressing DCs and secrete pro-inflammatory cytokines (e.g., IFN-γ, TNF, IL-6) to combat the tumor (Lei et al., 2020). A low NK cell count has been correlated with increased cancer risk (Hinshaw and Shevde, 2019). However, tumors evade NK cell detection by coating themselves with collagen and platelets to inhibit recognition from NK cell receptors (Hinshaw and Shevde, 2019; Lei et al., 2020).

The TME creates a range of barriers that hinder the effectiveness of tumor-infiltrating lymphocytes. For example, the overexpression of the programmed cell death protein 1 (PD-1) ligand on cancer cells inhibits T cells by binding to the PD-1 receptor, which regulates antigen response thresholds. Once bound, PD-1 translocates to the TCR, impairing key T cell functions such as proliferation, activation, cytokine production, cytotoxic activity, and survival (Zitvogel

and Kroemer, 2012; Ai et al., 2020; Fanale et al., 2022). There is a strong inverse correlation between CD8+ T cell levels and PD-L1 expression on cancer cells (Chardin and Leary, 2021).

In addition to PD-L1 and CD80/86 expression, the TME employs other immune evasion mechanisms, such as overexpression of the anti-apoptotic protein B-cell lymphoma 2 (BCL2) and the Fas ligand, which induces apoptosis in immune cells (Fanale et al., 2022).

1.4 Animal Model

1.4.1 Kras LA1-LA2 Model

Mousel models have been pivotal in studying LUAD, particularly the role of KRAS, an oncogene mutated in approximately 25% of human tumors (Drosten et al., 2018). In 2001, Tyler Jacks' team generated a mouse strain carrying a targeted insertion allele of Kras in cultured embryonic stem cells and allowed excision to occur in vivo by spontaneous recombination to better mimic human tumorigenesis while avoiding supraphysiological levels of expression that would accompany traditional transgenic expression of oncogenes in all cells of the target tissue (Johnson et al., 2001). Using a "hit-and-run" gene targeting strategy, they introduced latent oncogenic Kras alleles (Kras LA1 and Kras LA2) into embryonic stem cells for blastocyst injection and germline transmission. These alleles were designed to activate upon recombination: Kras LA1 could produce either a mutant (G12D) or wild-type allele, while Kras LA2 exclusively generated the mutant form. This model successfully replicated the histological progression of human NSCLC with tumors expressing markers of alveolar type II cells (Johnson et al., 2001). Crossing the Kras LA1 strain with a p53-deficient model revealed that p53 mutations enhanced tumor malignancy, broadened the tumor spectrum and featured animals with a lower lifespan, highlighting its role in lung cancer progression (Johnson et al., 2001).

1.4.2 LSL-Kras Model

To improve on their previous model, the researchers developed a conditional mouse model that enabled spatial and temporal control of endogenous Kras^{G12D} expression via Cre-mediated recombination. This Lox-Stop-Lox (LSL) Kras conditional strain utilized floxed transcriptional termination ("Stop") elements to express WT KRAS until excision, therein KRAS^{G12D} expression would occur (Jackson et al., 2001). Following intranasal instillation of adenoviral particles (AdenoCre), the Stop codon was removed, allowing tissue-specific mutant Kras transcription. The researchers administered 5×10⁸ plaque-forming units (PFUs) of AdenoCre coprecipitated with calcium phosphate to enhance epithelial infection (Jackson et al., 2001). Histological analysis revealed that atypical adenomatous hyperplasia (AAH), confirmed by SPC positivity and CCA negativity, originated from alveolar type II cells. To regulate tumor multiplicity, a dose-response study demonstrated a direct correlation between the viral dose and the number of lung lesions, with higher doses producing diffuse hyperplasia and lower doses yielding well-isolated lesions (Jackson et al., 2001). Time-course studies using 5×10^5 and 5×10^6 PFUs tracked progression from AAH to adenomas and adenocarcinomas, with AAH lesions becoming indistinguishable from adenomas by 12 weeks post-infection and adenocarcinomas evident by 16 weeks (Jackson et al., 2001). This model improved on the Kras LA1-LA2 model by allowing precise control over tumor initiation and burden, providing a powerful tool to study LUAD progression.

1.4.3 Braf^{CA} Model

Oncogenic *RAS* can transform immortal cell lines on its own, but primary cells require additional oncogenic alterations, such as loss of *P53* or *P16* and overexpression of *c-MYC* or D-type cyclins, to achieve transformation (Serrano et al., 1997). In murine primary fibroblasts, loss of either *p53* or *p16* alone is sufficient for *Ras*-induced transformation (Tanaka et al., 1994; Serrano

et al., 1996). This has been validated *in vivo*, as p53-deficient mice develop normally but show a higher susceptibility to tumors (Jacks et al., 1994). Collado *et al.* demonstrated that in premalignant tumors induced by oncogenic $Kras^{V12}$ in mice, OIS restricts tumor progression. Using markers like p16INK4A and senescence-associated β -galactosidase, they showed that senescence occurs in adenomas but not in malignant adenocarcinomas, where OIS effectors like p16INK4A or p53 are lost (Collado et al., 2005). This suggests that OIS serves as a tumor-suppressive mechanism that prevents malignant progression in $Kras^{V12}$ -driven models.

Building on these findings, Dankort *et al.* developed the $Braf^{CA}$ mouse model to study $BRAF^{V600E}$ -driven tumorigenesis. In this model, the wild-type Braf allele is replaced by the V600E mutant upon Cre-mediated recombination following adenoviral delivery of Cre recombinase. Similar to the $Kras^{V12}$ model, $BRAF^{V600E}$ expression initiated benign adenomas with rare progression to adenocarcinomas. These tumors displayed senescence markers early on but showed decreased Ki67 expression over time, indicative of growth arrest (Dankort et al., 2007). Crossing homozygous floxed p53 alleles into $Braf^{CA}$ mice revealed that p53 loss accelerated tumor progression, leading to increased proliferation and more malignant tumor features, underscoring the role of tumor suppressors in constraining $BRAF^{V600E}$ -driven malignancies (Dankort et al., 2007).

1.4.5 Braf^{FA} Model

To address limitations of the $Braf^{CA}$ model, particularly its inability to decouple oncogene activation from tumor suppressor loss, the Dankort lab developed the $Braf^{FA}$ mouse model. In this system, $BRAF^{V600E}$ expression is driven by Flp recombinase instead of Cre, allowing for independent and temporally controlled activation of $BRAF^{V600E}$ (Garnett et al., 2017). This dual-recombinase strategy enables $BRAF^{V600E}$ activation via Flp while preserving Cre for targeted p53

deletion, achieving precise temporal and independent separation of these events (Garnett et al., 2017). This allows the bypass of OIS, which prevents the progression of lung adenomas to adenocarcinomas in the $Braf^{CA}$ model. Adenoviral FLP (AdFlp) is administered intranasally, enabling controlled induction of $BRAF^{V600E}$ in lung epithelial cells. The resulting tumors are morphologically similar to those produced in $Braf^{CA}$ mice, displaying similar density, numbers and proliferation rates. (Garnett et al., 2017). Adenomas expressing BRAF^{V600E} continue to proliferate actively until 16 weeks after the oncogene is activated. The period thereafter is referred to as 'late' time points and the period before, is referred to as 'early'. The $Braf^{EA}$ model demonstrated that the timing of p53 ablation significantly impacts OIS bypass, with early p53 loss driving the progression of more aggressive tumors, including high-grade adenocarcinomas, whereas late p53 loss fails to influence tumor advancement (Garnett et al., 2017).

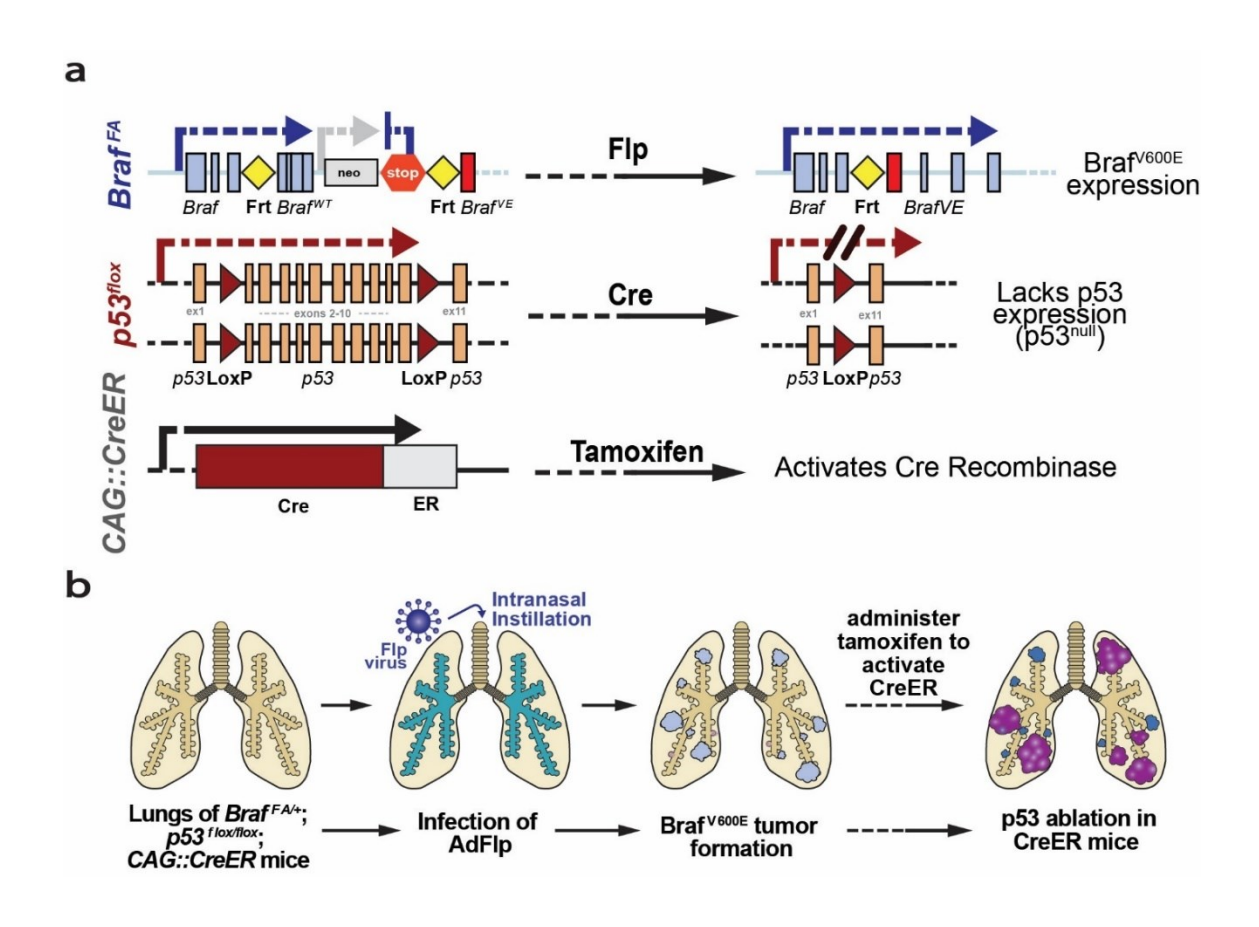


Figure 1-4. Conditional activation of *BRAF*^{V600E} and *P53* deletion in mouse models. (a) The *Braf*^{FA} allele contains wild-type *Braf* exons flanked by Flp recombinase target (Frt) sites, followed by mutant *Braf* exons encoding the V600E substitution. Upon Flp recombinase activation, the stop cassette is excised, resulting in BRAF^{V600E} expression. The *P53* LoxP allele contains exons 2–10 of the *P53* gene flanked by LoxP sites. Cre recombinase-mediated excision of these exons generates a null P53 allele resulting in the loss of P53 expression. A tamoxifen-inducible Cre recombinase (CAG::CreER) enables temporal control of P53. (b) *Braf*^{EA/+}; *P53*^{flox/flox}; CAG::CreER mice were infected intranasally with AdFlp virus to induce BRAF^{V600E} expression in lung epithelial cells, leading to the formation of BRAF^{V600E}-driven tumors. At 24 weeks post-infection, tamoxifen was administered to activate CreER and P53 ablation in tumor cells. Figures taken from Garnett *et al.*, 2017.

1.5 Thesis Objectives

Objective 1

MOB3A, a kinase regulator identified by Dutchak *et al.*, has been involved in OIS bypass through modulation of the Hippo pathway (Dutchak et al., 2022). Specifically, MOB3A facilitates the nuclear accumulation of non-phosphorylated YAP/TAZ, thereby driving cell proliferation and survival despite sustained BRAF signaling. To further investigate this mechanism, human fibroblast cell lines co-expressing BRAF and MOB3A were developed. Initial cell lines exhibited improper responses to experimental settings, requiring their redesign to ensure reliable functionality. The newly established cell lines were validated through drug selection, growth curves, and western blot analysis, providing a robust in vitro model for elucidating MOB3A's role

in senescence bypass and advancing our understanding of Hippo pathway regulation in the context of OIS.

Objective 2

One of Dr. Garnett's pivotal findings was the effect of tumor density on progression. High density tumors, induced by higher viral titers, predominantly formed low-grade adenomas with minimal progression. In contrast, low-density tumors, resulting from lower titers, displayed aggressive growth and a higher incidence of adenocarcinoma. This density-dependent outcome raised critical questions about the role of the TME and immune system in modulating tumor behavior.

Density differences may also influence immune responses, as OIS and the SASP can affect the proliferation profiles of tumors induced by both low and high viral titers (Garnett, 2019). While the SASP can reinforce OIS, elevated secretion of pro-inflammatory molecules enhances the recruitment of immune cells, such as macrophages, which play a critical role in determining tumor size (Garnett, 2019). Notably, lung fibrosis becomes evident at later time points, suggesting that higher viral titers may infect more macrophages, leading to their accumulation in the lung. These activated macrophages can secrete factors such as $TGF-\beta$, which promote fibroblast activation and collagen deposition, contributing to fibrosis (Saito et al., 2018). Similar observations were reported in the *Kras*-LSL mouse model infected with Ad5-CMV-Cre, where spleen removal resulted in macrophage depletion and reduced tumor size (Cortez-Retamozo et al., 2012). Therefore, characterizing immune profiles in high- and low titer samples, both in *p53* WT and *p53* null backgrounds, is essential to better understand the mechanisms of inflammation driving fibrosis, tumor progression and the interplay with senescence factors.

Chapter 2: Materials and Methods

2.1 Cloning of pWZL-Hygro-myr:flag-MOB3A and pWZL-Hygro-myr:flag-EGFP

A restriction digest was performed using SphI, HindIII, and NheI enzymes on the pWZL-Neomyr, pWZL-Neomyr (Dutchak et al., 2022), and pWZL-Hygro (from David Dankort, Addgene #18750 and #18749) plasmids. The 7376-base pair HindIII—NheI fragment containing the vector backbone from the pWZL-Neo-myr plasmid, the 7568-base pair HindIII—NheI fragment containing the vector backbone from the pWZL-Neo-myr plasmid, and the 1475-base pair HindIII—NheI insert from the pWZL-Hygro plasmid were isolated via gel extraction using the Bio Basic EZ-10 Spin Column DNA Gel Extraction Minipreps Kit (BS354-100 Preps). Both vectors were individually ligated to the insert, and the resulting plasmids were transformed into DH5α *Escherichia coli* competent cells. Colonies were selected on LB agar plates containing 100 mg/mL ampicillin, diluted 1:1000 (171 mM NaCl, 10 g/L tryptone, 5 g/L yeast extract, 15 g/L agar), and DNA was isolated using standard mini-prep procedures. The same digest was repeated to confirm successful transformation. A large-scale plasmid preparation was then carried out using standard methods.

2.2 Cell Culture

Human fibroblast cell lines HF E1T (Garnett et al., 2017) and IMR90, a gift from Gerardo Febeyre (Malette et al., 2007), were cultured at 37°C in 5% CO₂ and 21% O₂. Cells were grown in Dulbecco's Modified Eagle's Medium (DMEM 1X) (Wisent Inc., Catalog No. 319-005-CL) supplemented with 10% fetal bovine serum (FBS) (Wisent Inc., Catalog No. 080450) and 1%

penicillin/streptomycin (Wisent Inc., Catalog No. 450-201-E), hereafter referred to as regular media.

2.3 Lentiviral and Retroviral Production

On day 0, 3.5×10^6 293T cells were seeded into 10 cm dishes using regular media. On day 1, a transfection mixture was prepared by vortexing 550 μ L of Opti-MEM with 5.2 μ g of the PAX2 packaging plasmid, 2.8 μ g of the PCi VSVg packaging plasmid, and 8 μ g of the vector. Next, 42.5 μ L of PEI (1 mg/mL) was added dropwise, and the mixture was gently shaken. After a 10-minute incubation period, during which the media was replaced with fresh media, the transfection mixture was added dropwise to the plate, followed by gentle shaking. On day 2, the media was replaced again. On day 3, the media containing the virus was collected, filtered through a 0.22 μ m filter (FroggaBio, Catalog No. SF0.22PES) into a 15 mL Falcon tube, and either stored at -80°C or used fresh.

The same procedure was followed for retroviral vector production, except the pHit60 Gag Pol packaging plasmid was used in place of PAX2, along with the appropriate retroviral vector (Geiling et al., 2013).

2.4 Infection of Cell Lines

2 × 10⁵ IMR90 and HF E1T human fibroblasts were seeded into each well of a 6-well plate. The next day, the media was replaced with 1 mL of 1 nM polybrene media (10% FBS, 1% penicillin/streptomycin) and 1 mL of viral suspension per well. On day 2, the media was replaced with regular media. On day 3, the cells were transferred to a 10 cm dish. Drug selection was initiated on day 4 by adding the appropriate drugs at the following concentrations: blasticidin at

12.5 μg/mL (stock: 5 mg/mL), G418 (neomycin equivalent) at 500 μg/mL (stock: 200 mg/mL), and hygromycin at 100 μg/mL (stock: 50 mg/mL).

Cells were infected with the pLEG-ΔBRAF-ERiBlast lentivirus to promote ΔBRAF-ER expression in response to 100 nM 4OHT (Sigma, H6278) administered in the media. Subsequently, the pWZL-Neo-myr plasmid was introduced into HF E1T cells, and pWZL-Hygro-myr was introduced into IMR90 cells. pWZL-Neo-myr and pWZL-Hygro-myr were used as controls in HF E1T and IMR90 cells, respectively.

2.5 Drug Selection

Both human fibroblast cell lines, HF E1T and IMR90, were subjected to drug treatment to confirm susceptibility and resistance prior to infection. In each well of a 12-well plate, 15,000 cells were seeded. The following day, the media was replaced with increasing concentrations of the respective drugs. Cells were treated with blasticidin at 12.5, 25, and 37.5 μ g/mL for 3 days; puromycin at 1, 2, and 4 μ g/mL for 14 days; G418 at 200, 400, and 800 μ g/mL for 14 days; or hygromycin at 125, 250, and 500 μ g/mL for 14 days.

Selection for lentiviral integration was performed using 12.5 μ g/mL of blasticidin for 3 days. Similarly, 400 μ g/mL of G418 or 125 μ g/mL of hygromycin, maintained for 14 days, was used for selection of retroviral integration in BRER HF E1T and BRER IMR90 cell lines, respectively.

2.6 Cell Clone Isolation

HF E1T and IMR90 populations were assessed for responsiveness to 4OHT. Naïve populations that demonstrated 4OHT-induced growth arrest were plated at 5,000, 500, and 50 cells per 100 mm tissue culture dish without drug selection. Once isolated colonies emerged, twelve clones per

population were picked and seeded into triplicate wells of 24-well plates. Clones were screened for 4OHT responsiveness at 100 nM 4OHT relative to ethanol treatment, as assessed by crystal violet staining. The clones demonstrating the largest difference in growth between ethanol and 4OHT treatments were used for subsequent infections with MOB3A/EGFP-encoding retroviruses.

After successful infection with pLEG-ΔBRAF-ERiBlast and either pWZL-Neo-myr or pWZL-Hygro-myr, and maintaining the cells in hygromycin and G418 for 14 days, clones were selected again to prepare for growth curves. This step ensured minimal drift and provided a pure pool of identical cells.

2.7 Growth Curve

Growth curves for BRER HF E1T and BRER IMR90 cells were performed in 12-well plates, with wild-type HF E1T and wild-type IMR90 cells as controls. A total of 15,000 cells were seeded per well. In triplicate, cells were exposed to either 100 nM 4OHT or 17.4 M ethanol (as a control). The drug was maintained in the media for up to seven days, with cell counts taken on days 0, 3, 5, and 7.

Following the second round of infection, growth curves were repeated, comparing MOB3A BRER HF E1T and IMR90 cells to EGFP BRER HF E1T and IMR90 cells. Crystal violet staining was used to confirm the results.

2.8 Crystal Violet

Cells were washed with PBS and fixed with 1 mL of zinc-formalin per well, incubating overnight. Each plate was then thoroughly rinsed with dH₂O and allowed to dry. Subsequently, 0.5 mL of 0.1% crystal violet solution (Amresco, 0528-100G) diluted in dH₂O was added to each well and

incubated at room temperature on a rotor shaker for 30 minutes. The crystal violet solution was disposed of according to safety guidelines, and the plates were rinsed thoroughly with dH₂O and dried. To elute the dye, 1 mL of 10% acetic acid was added to each well. After a 30-minute incubation at room temperature on the rotor shaker, 100 µL from each well was transferred to a flat-bottom clear 96-well plate in triplicate, with three control wells containing 10% acetic acid. The plate was read at 592 nm using a plate reader.

2.9 Western Blot

To confirm the presence of MOB3A in the cells, protein extraction and immunoblotting were performed. Cells at 70% confluency were trypsinized, washed with PBS, and lysed in 100 μL of modified PLCγ lysis buffer (50 mM HEPES pH 7.5, 150 mM NaCl, 10% glycerol, 1% Triton X-100, 1 mM EGTA, 1.5 mM MgCl₂, 10 mM NaF, 10 mM Na₄P₇O₂) for 30 minutes on a rotor at 4°C. Samples were centrifuged at 16,000 RCF for 15 minutes, and the supernatant was subjected to the Pierce BCA Protein Assay Kit (ThermoScientific, REF 23227) to quantify protein levels and standardize them for SDS-PAGE. Samples were diluted in lysis buffer and 4x Laemmli buffer (50 mM Tris-HCl pH 7, 12.5 mM EDTA, 2% SDS, 10% glycerol, 1% 2-mercaptoethanol, 0.02% bromophenol blue) and boiled at 100°C for 5 minutes.

The samples were loaded into the wells of a 4% stacking gel (distilled water, 4x upper Tris, 30% acrylamide [Bio-Rad, 1610154], 3.55 mM TEMED [Bio-Rad, 1610801]) and electrophoresed for 15 minutes at 80 volts until reaching the 10% separation gel (distilled water, 30% acrylamide [Bio-Rad, 1610154], 4x lower Tris, 4.24 mM TEMED). Electrophoresis was continued at 150 volts until the dye front ran out. The gel was transferred onto an activated PVDF membrane (Bio-Rad, Catalog No. 1620177) using semi-dry transfer for 40 minutes at 15 volts. The membrane was

briefly soaked in 100% ethanol before being blocked in 5% (w/v) milk in TBS-T and incubated overnight at 4°C with the Flag-Tag primary antibody in 5% milk in TBS-T.

Following TBS-T washes, the membranes were incubated with the secondary antibody for 1 hour at room temperature (see Table 1 for antibody details). Each membrane was treated with 1 mL of enhanced chemiluminescence reagent (Amersham ECL Start Western Blotting Detection Reagent, RPN2209) and developed. The same membrane was stripped with mild stripping buffer (0.2 M glycine, 3.47 mM SDS, 1% v/v Tween-20, dH₂O) and reprobed for MOBKL2A, ERα, and α-tubulin.

2.10 Hematoxylin and Eosin (H&E)

Slides were deparaffinized and rehydrated through sequential soaking in xylene, followed by 100% and 95% ethanol, using the Varistain™ Gemini ES Automated Slide Stainer. Nuclei were stained using 100% Fisherbrand Harris hematoxylin (Catalog No. 245-678), followed by rinsing with distilled water (dH₂O). Tissues were then counterstained with a 25% solution of Sigma-Aldrich Eosin Y (Catalog No. HT110180), diluted in 70% ethanol. The slides were dehydrated through increasing concentrations of ethanol and xylene and finally mounted using Leica Surgipath Acrytol mounting medium (REF 3801720).

2.11 Immunofluorescence

Slides were deparaffinized and rehydrated by sequential soaking in xylene and decreasing concentrations of ethanol (100%, 95%, 70%) using the Varistain[™] Gemini ES Automated Slide Stainer. Antigen retrieval was performed by immersing the slides in 10 mM sodium citrate solution (pH 6) for 10 minutes under high pressure, using a Cuisinart electric pressure cooker (CPC-600C).

Slides were washed with distilled water and 1x Tris Buffered Saline (20 mM Tris base, 150 mM NaCl, pH 7.6), and the sections were circled with a PAP pen.

Each section was permeabilized with a 0.5% permeabilization solution (137 mM NaCl, 2.7 mM KCl, 10 mM Na₂HPO₄, 1.8 mM KH₂PO₄, 8.27 mM Triton X-100) for 15 minutes at room temperature, followed by treatment with a freshly prepared 0.3 M glycine solution for 20 minutes at room temperature to attenuate autofluorescence. After a second round of TBS washes, blocking was carried out using 2% BSA in 1x Tris Buffered Saline for 30 minutes before adding the primary antibody (**Table 1**). Slides were incubated at 4°C, washed in 1x Tris Buffered Saline, and then the secondary antibody was applied (**Table 1**).

Primary antibodies were detected by one of two methods: either via a fluorescent-conjugated secondary antibody or a biotin-conjugated secondary antibody followed by streptavidin Alexa 488. DAPI (Sigma-Aldrich, D9542-1MG, 1:1000) was added alongside the fluorophores. Finally, the slides were mounted with Invitrogen ProLong Gold Antifade Reagent (REF: P36934) and coverslipped.

2.12 Image Analysis

Images were captured using a Leica DM4000B Automated Upright Microscope System equipped with an Olympus DP73 camera and a Chroma filter system, which included the ET DAPI (C132204), ET GFP (C132205), and ET – mCherry/Texas Red (C202845) filters. These filters were used to visualize fluorophores with excitation wavelengths of 358 nm, 488 nm, and 555 nm, respectively. The same exposure times were maintained per fluorophore as follows: 250 ms for DAPI (358 nm), 333 ms for CD45 and F4/80 (488 nm), and 400 ms for SPC and Ki67 (555 nm).

All images were captured using a 20x objective lens. Ten tumors were randomly selected per sample, for a total of 30 tumors per group.

Images were processed in Fiji with ImageJ, with the following channel settings: for the blue channel, the minimum was set to 190 and the maximum to 255; for the green channel, the minimum was set to 50 and the maximum to 120; for the red channel, the minimum was set to 0 and the maximum to 175.

For individual channel analysis, the number of nuclei per tumor was quantified using the Trainable Weka Segmentation plugin in Fiji with ImageJ. The red and green channels were individually processed by applying a mask to the tumor area, converting to 16-bit grayscale, and thresholding based on intensity to remove background noise. A median filter (2 pixels) was applied to eliminate small artifacts from noise. Obvious fused regions of interest (ROIs) were manually split using the Edit > Clear command. Particles were counted using the Analyze Particles command. To quantify the overlap between channels, each channel was assigned a different color using the Merge Channels feature, and overlapping spots were manually counted.

Chapter 3: Results

3.1 Development of a MOB3A BRER Cell Line Model for the Investigation of OIS

3.1.1 MOB3A-Expressing BRER Cells Fail to Proliferate and Exhibit Senescent Drift Under 4OHT-Induced MAPK Signaling

To confirm that MOB3A allows senescence bypass under elevated MAPK signaling, BRER cells expressing myr-MOB3A were treated with 4OHT to activate the Δ BRAF:ER construct, which mimics the effect of oncogenic BRAF^{V600E} and hyperactivates the MAPK pathway. This is perceived as an oncogenic stress by the cell, and OIS is established as a response. MOB3A can rescue this cell cycle arrest by modulating the Hippo pathway. Western blot analyses confirmed MOB3A expression and ER α stabilisation in the presence of 4OHT, validating the activation of BRAF and MAPK signaling (**Figure 3-1a**). In contrast, ER α was absent in EtOH-treated cells, indicating that the construct's expression is specifically induced by 4OHT.

Despite the confirmed expression of MOB3A, growth curve analyses revealed an unexpected phenotype. In comparison to Dutchak *et al.*'s model, when seeded at an initial density of 15,000 cells per well, both MOB3A-expressing and control cells failed to proliferate under 4OHT treatment (Figure 3-1b). Morphological changes consistent with senescence, such as bright cellular edges and flattened shapes, were observed in 4OHT-treated cells, regardless of MOB3A expression (Figure 3-1c). This suggests that MOB3A expression alone is insufficient to prevent the senescent phenotype induced by MAPK hyperactivation. To further explore this observation, a washout experiment was performed. Cells were exposed to 4OHT for 24, 48, or 72 hours,

followed by removal of the drug. However, no recovery or proliferation was observed in either group, confirming that the senescent phenotype was irreversible under these conditions (**Figure 3-1d**).

Together, these findings demonstrate that while MOB3A is expressed and MAPK signaling is activated in BRER cells, MOB3A fails to bypass senescence under high MAPK activity. These results highlight potential cellular drift in MOB3A BRER cells.

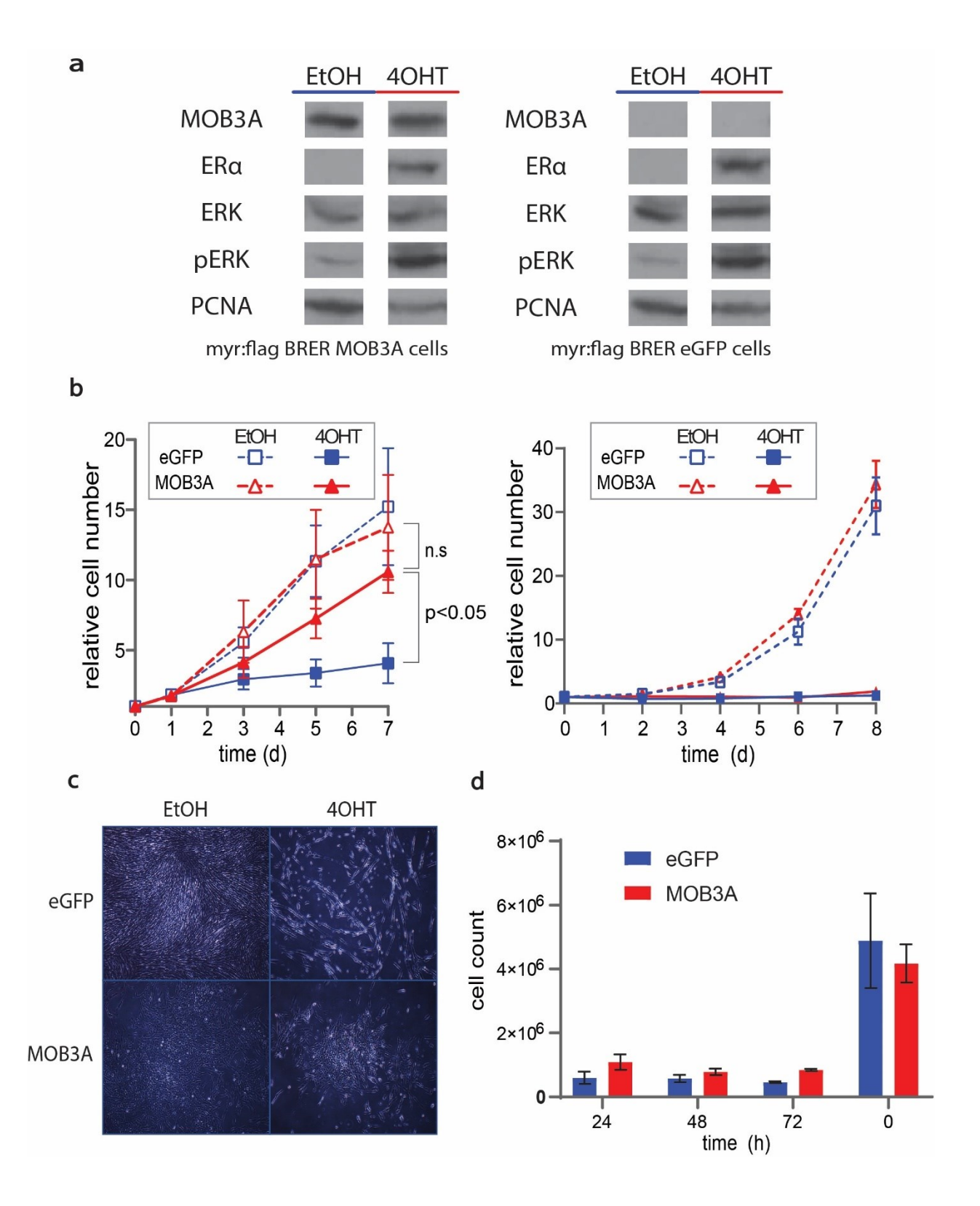


Figure 3-1. Initial model of MOB3A-expressing BRER cells under 4OHT-induced MAPK signaling appear to drift.

(a) Western blot analysis of MOB3A and EGFP BRER cells treated with 4OHT or EtOH. ERα and pERK levels confirmed activation of ΔBRAF:ER and MAPK signaling in the presence of 4OHT. (b) Growth curves of MOB3A-expressing (red) and EGFP-expressing control (blue) BRER cells treated with 100 nM 4OHT or EtOH (control) over 7 days. MOB3A cells now exhibit similar proliferation rates as EtOH-treated cells under 4OHT. (c) Images of MOB3A and EGFP BRER cells after 7 days of treatment with 4OHT or EtOH. (d) Washout experiment showing cell counts after exposure to 4OHT for 24, 48, or 72 hours, followed by drug removal. No recovery or proliferation was observed in either group.

3.1.2 Drug Susceptibility Profiles of Parental HF E1T and IMR90 Fibroblast Cell Lines

To establish a robust BRER MOB3A cell model, drug susceptibility of the parental fibroblast cell lines HF E1T and IMR90 was assessed over a two-week period. Cells treated with increasing concentrations of puromycin, the neomycin equivalent G418, and hygromycin to evaluate their respective resistance profiles. As shown in **Figure 3-2**, HF E1T cells exhibited resistance to hygromycin but were susceptible to both G418 and puromycin. In contrast, IMR90 cells demonstrated an innate resistance to G418 while remaining susceptible to puromycin and hygromycin.

These findings indicate that HF E1T cells are suitable for selection with G418 or puromycin, while IMR90 cells can be selected using puromycin or hygromycin. This drug susceptibility data informed the selection strategy for generating the BRER MOB3A cell lines.

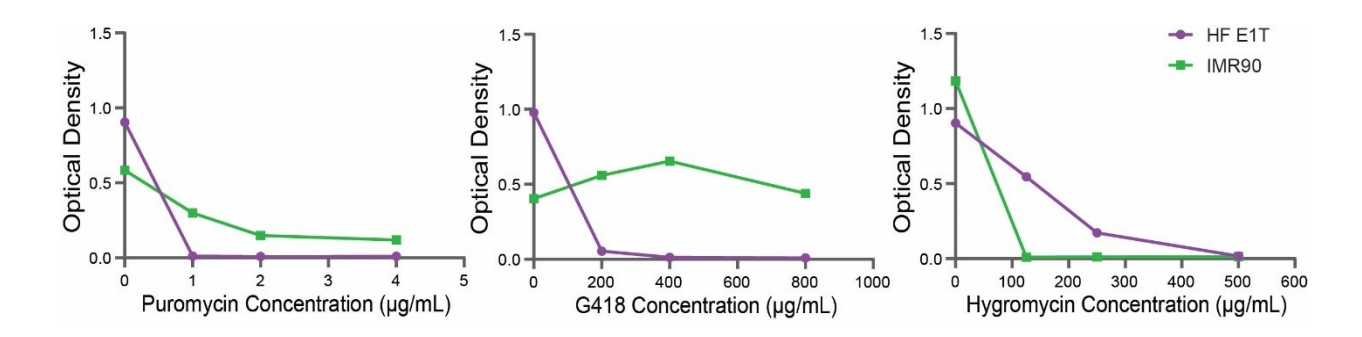


Figure 3-2. Drug susceptibility profiles of HF E1T and IMR90 cell lines. HF E1T (purple) and IMR90 (green) cells were treated with increasing concentrations of puromycin (none, 1 ug/mL, 2 ug/mL, 4 ug/mL), G418 (none, 200 ug/ml, 400 ug/ml and 800 ug/ml) and hygromycin (none, 125 ug/ml, 250 ug/ml and 500 ug/ml) over two weeks. Cells were fixed, stained and optical density measurements were taken to assess proliferation. HF E1T cells were found to be susceptible to G418 and puromycin but resistant to hygromycin, whereas IMR90 cells were susceptible to puromycin and hygromycin but resistant to G418.

3.1.3 Selection of BRER Fibroblast Cell Lines and Evaluation of 4OHT Responsiveness

HF E1T and IMR90 parental fibroblast cell lines were infected with the pLEG-ΔBRAF-ERiBlast lentivirus to induce ΔBRAF:ER expression under 4OHT conditions. Following infection, the cells were selected using blasticidin (12.5 μg/mL). The surviving populations were expanded and tested for their responsiveness to 4OHT. The ΔBRAF:ER construct is prompted by 4OHT to activate the kinase and hyperactivate the MAPK pathway. Since this hyperactivation leads to excessive signaling, OIS is triggered as a stress response and induces cell cycle arrest. Thus, a decrease in proliferation is expected in BRER cells exposed to 4OHT.

Growth curves were performed for six populations of BRER-infected cells per cell line. Each cell line was seeded at 15 000 cells/well in 12-well plates, alongside uninfected control cells. The

next day, half of the wells were treated with 100 nM 4OHT to activate ΔBRAF:ER, while the other half were treated with 100 nM EtOH as a vehicle control. Cell counts were recorded on days 0, 3 and 7.

Uninfected control cells displayed the same proliferation rates in both 4OHT and EtOH media, consistent with the absence of Δ BRAF:ER expression and thus present no susceptibility to 4OHT (**Figure 3-3**). In contrast, BRER cells demonstrated a marked decrease in proliferation under 4OHT treatment, confirming the activation of Δ BRAF:ER and MAPK signaling, leading to cell cycle arrest.

BRER IMPR90 populations exhibited a more polarized response compared to BRER HF E1T cells. While all HF E1T populations showed a sustained decrease in proliferation under 4OHT treatment, some replicative activity persisted. In contrast, IMR90 cells demonstrated a strong suppression of proliferation under 4OHT, and minimal growth observed by day 7 compared to the control. This suggests that IMR90 cells may be more responsive to MAPK pathway activation and subsequent growth arrest than HF E1T cells. Of the six populations tested, populations 2 and 3 of the BRER HF E1T cell line and populations 2 and 4 of the BRER IMR90 cell line were selected for subsequent MOB3A infection and clonal screening. These populations displayed the most robust responses to 4OHT, making them proper candidates for further investigation of MOB3A-mediated senescence bypass.

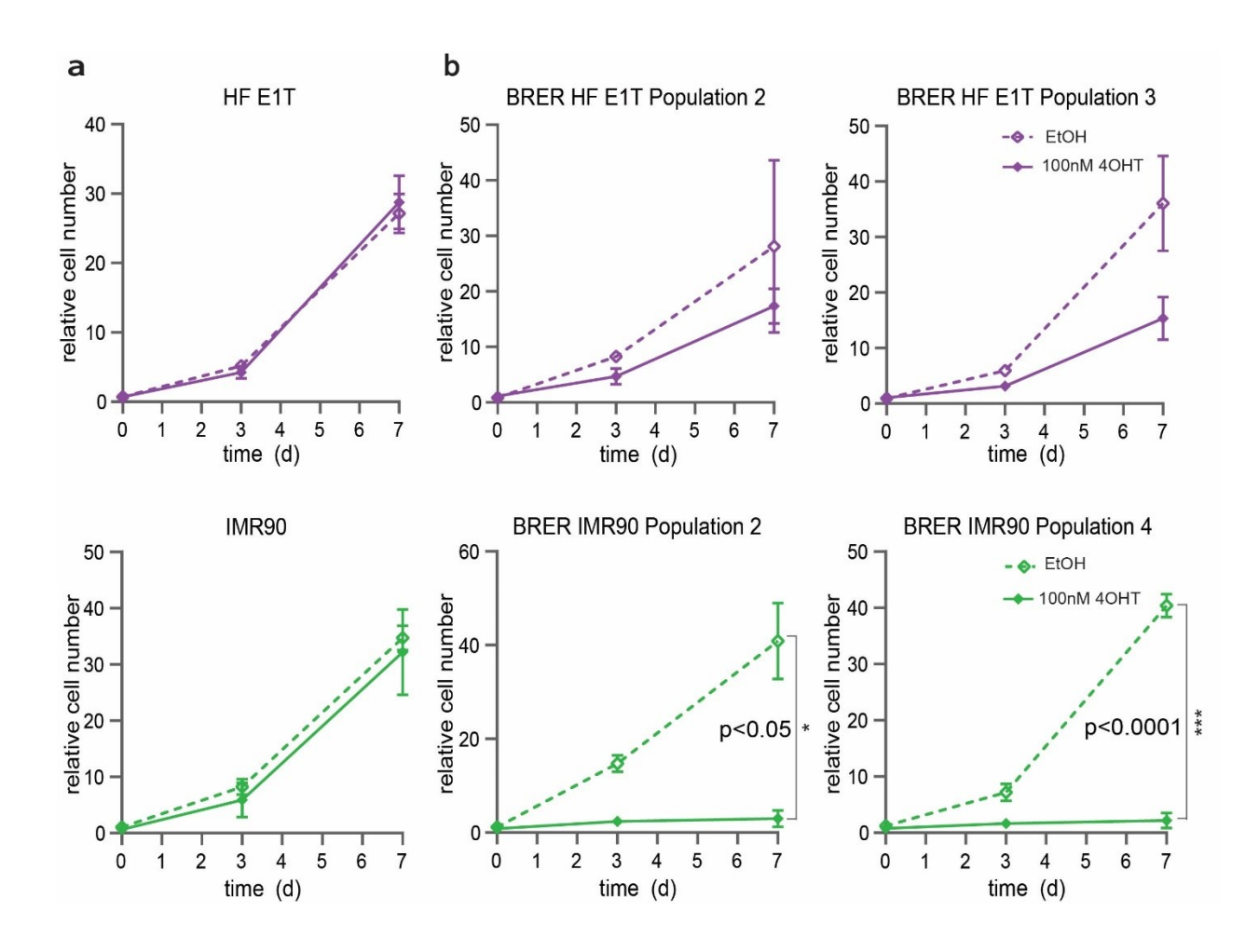


Figure 3-3. Growth curves for control and BRER-infected populations of HF E1T and IMR90 fibroblast cell lines exposed to 100 4OHT or EtOH. Cells were seeded at an initial density of 15,000 cells/well, and counted on days 0, 3, and 7. (a) HF E1T and IMR90 control cells showed no significant proliferative differences between 4OHT and EtOH treatments. (b) BRER-infected populations displayed reduced proliferation in the presence of 4OHT. IMR90 populations 2 and 4 demonstrated the most polarized response to 4OHT compared to HF E1T populations.

3.1.4 Cloning of pWZL-myr:flag-Hygro-MOB3A and pWZL-myr:flag-Hygro-EGFP

Given the inherent resistance of IMR90 cells to G418, we aimed to modify the pWZL-myr:flag-Neo-MOB3A and pWZL-myr:flag-Neo-EGFP vectors by replacing the neomycin resistance gene with a hygromycin resistance gene. Since IMR90 cells demonstrated susceptibility to hygromycin, this modification would allow for effective selection following viral transduction.

To achieve this, the Neo-MOB3A and Neo-EGFP plasmids were digested overnight with HindIII, NheI, and SphI to excise the neomycin resistance gene. In parallel, pWZL-Hygro was digested with HindIII and NheI, allowing the excised hygromycin resistance gene to be used as an insert for ligation into the vector backbone (Figure 3-4a). These enzymes were chosen because the resistance gene sequences in the vector are flanked by HindIII and NheI, while SphI cuts within the sequence (Figure 3-4b).

Following digestion, The DNA fragments corresponding to the vector backbones and insert genes were extracted and purified. A T4 ligation reaction was performed to integrate the hygromycin resistance gene into the MOB3A and EGFP vectors, and the resulting plasmids were transformed into *DH5a Escherichia coli*. Sixteen bacterial colonies were selected for mini-prep plasmid extraction.

To confirm successful insertion, the mini-prepped plasmids were digested with HindIII, NheI, and SphI simultaneously, and the resulting fragments were analyzed by gel electrophoresis alongside control plasmids of pWZL-myr:flag-Neo-MOB3A, pWZL-myr:flag-Neo-EGFP and pWZL-Hygro (Figure 3-4c). Backbone validation was performed using XmaI digestion, which

distinguishes between MOB3A and EGFP constructs based on their unique restriction patterns.

The digestion profiles matched expectations, confirming proper backbone integrity.

To generate a high-yield stock of plasmid DNA for transduction, the selected colonies underwent a second bacterial transformation followed by maxi-prep purification. A final round of confirmation digests was performed to ensure the plasmids retained the correct sequence before proceeding to cell infection.

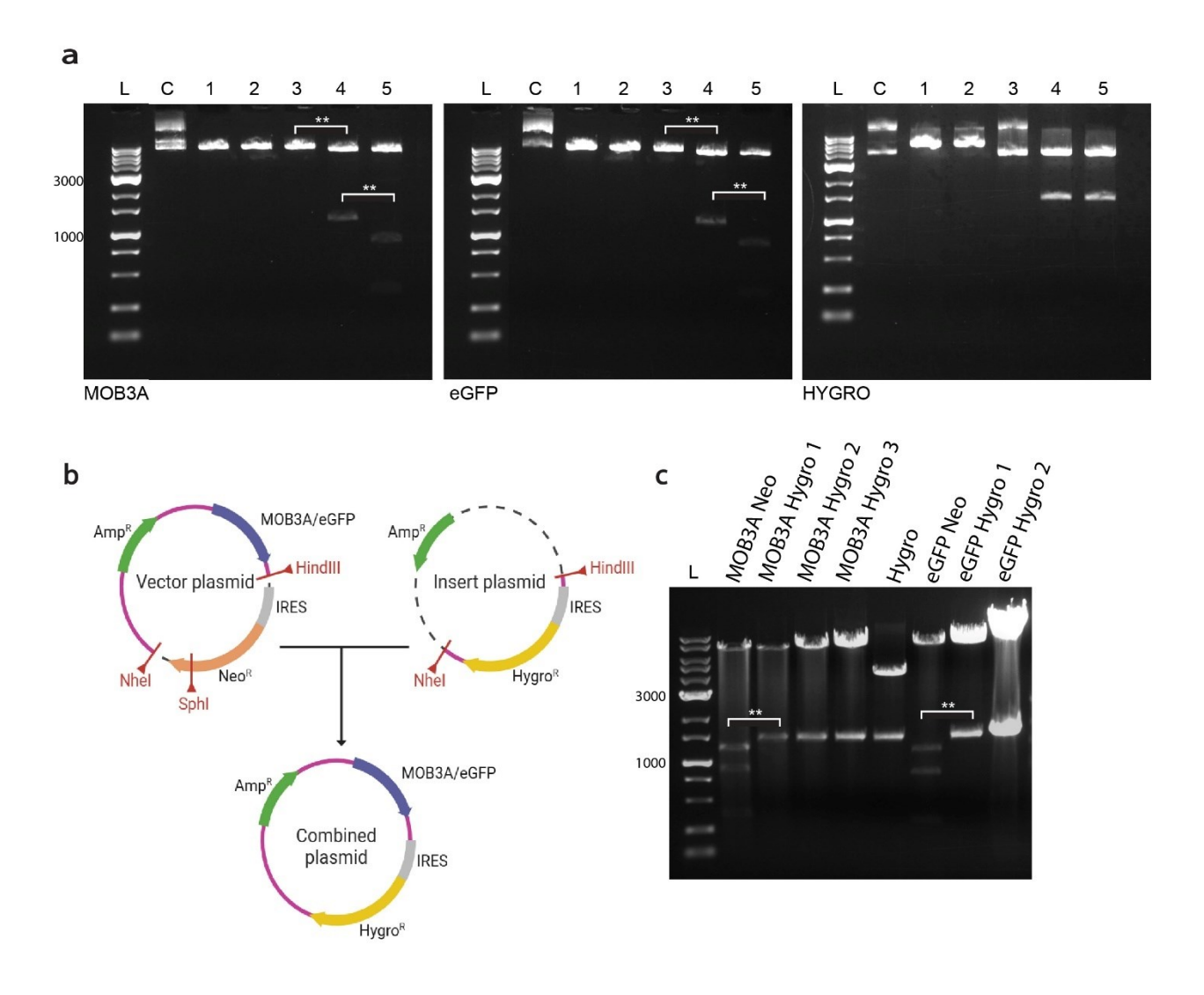


Figure 3-4. Excision of the neomycin resistance gene and ligation with hygromycin resistance in pWZL-myr:flag-MOB3A and pWZL-myr:flag-EGFP plasmids. (a) Vector plasmids were

digested using HindIII, NheI, and SphI to excise and isolate respective backbones. L represents the molecular weight marker, C corresponds to uncut pWZL-myr:flag-MOB3A, pWZL-myr:flag-EGFP, or pWZL-Hygro plasmids. Lanes correspond to restriction digest conducted with the enzymes as follows: HindIII (1), NheI (2), SphI (3), HindIII and NheI (4), HindIII, NheI and SphI (5). (b) Schematic representation of the cloning strategy illustrating the excision of the neomycin resistance gene from pWZL-myr:flag-MOB3A and pWZL-myr:flag-EGFP and the hygromycin resistance gene from pWZL-Hygro using HindIII and NheI followed by the ligation of the insert into the vector. Created with BioRender.com. (c) Ligated, transformed and maxi-prepped plasmids were digested with HindIII, NheI, and SphI simultaneously and compared against uncut controls to validate insertion.

3.1.5 Generation and Characterization of MOB3A/EGFP BRER Cell Lines

To introduce the pWZL-myr:flag-Hygro-MOB3A and pWZL-myr:flag-Hygro-EGFP constructs into cells, viral particles were first generated using 293T cells transfected with the retroviral packaging plasmids pHit60 Gag-Pol and PCi-VSVg, along with either DNA vector. Virus-containing supernatant was harvested, stored at -80°C, and subjected to freezing cycles to eliminate unstable viral units.

For infection, BRER HF E1T (population 2, clone 12; population 3, clone 8) and BRER IMR90 (population 2, clone 11; population 4, clone 5) were seeded at a density of 2.5×10^5 cells per well in a 6-well plate. The following day, viral supernatant was added to the media. In BRER HF E1T clones, three wells were infected with pWZL-myr:flag-Neo-MOB3A, and three wells with pWZL-myr:flag-Neo-EGFP. The same approach was used for BRER IMR90 clones, using the newly produced pWZL-myr:flag-Hygro-EGFP and pWZL-myr:flag-Hygro-MOB3A plasmids.

Following infection, cells were expanded into 10 cm dishes and subjected to drug selection. G418 (400 μg/mL) was used for BRER HF E1T (MOB3A/EGFP), while hygromycin (125 μg/mL) was applied to BRER IMR90 (MOB3A/EGFP). Drug selection was maintained for 14 days, after which up to six clones per population were isolated and expanded in 24-well plates. As colonies reached confluency, they were sequentially expanded into 12-well plates, 6-well plates, and finally 10 cm dishes. Throughout the process, EGFP-expressing cells were monitored via fluorescence microscopy to confirm successful integration of the plasmid.

To assess whether MOB3A expression rescues the senescent phenotype observed in **Figure 3-3**, growth curves of selected clones were performed under conditions identical to previous experiments. As seen in **Figure 3-5a**, MOB3A-expressing BRER cells exhibit a significant escape from senescence in response to 4OHT, in contrast to control cells, which maintain growth arrest. This suggests that MOB3A may play a role in bypassing OIS, potentially by interfering with MAPK pathway-mediated stress responses.

Western blotting further validated MOB3A, EGFP, and ER α expression under 4OHT treatment (**Figure 3-5b**). Since the Δ BRAF:ER construct consists of the CR3 domain of BRAF fused to ER α , its stabilization and subsequent detection are only expected upon 4OHT treatment, as the ligand-binding domain requires 4OHT for activation.

Finally, fluorescence microscopy confirmed EGFP-positive cells, demonstrating successful integration of the BRER EGFP construct (**Figure 3-5c**). This indicates that the transduction and selection process was efficient, with EGFP expression serving as a marker for successfully infected cells.

Together, these findings provide strong evidence that MOB3A expression enables BRER cells to override 4OHT-induced growth arrest, reinforcing its potential role in senescence evasion mechanisms.



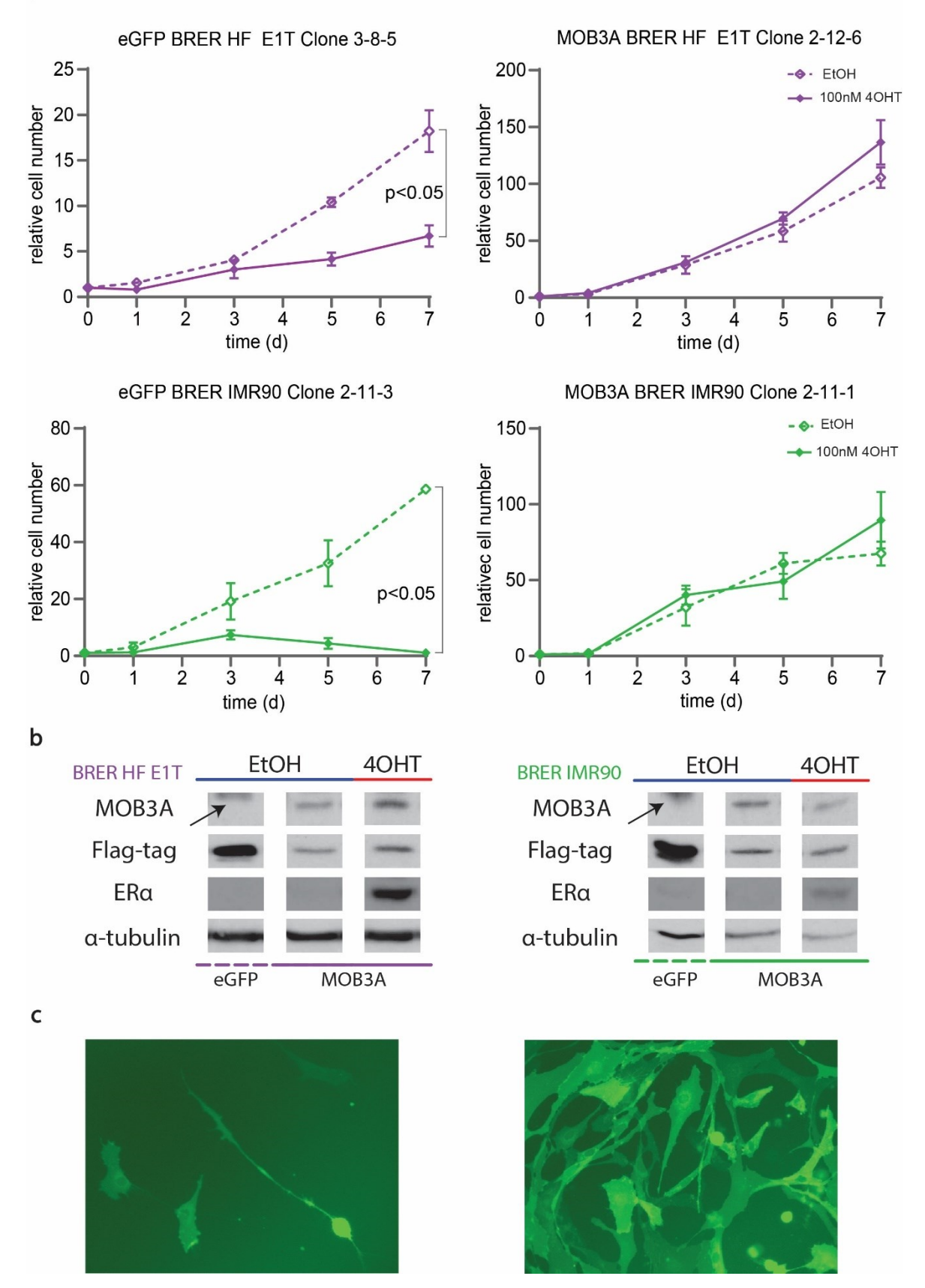


Figure 3-5. Characterization of MOB3A/EGFP BRER cell lines. (a) Growth curves of MOB3A and EGFP BRER HF E1T and BRER IMR90 clones in the presence or absence of 100 nM 4OHT. 4OHT Treatment of EGFP BRER resulted in a significant reduction in proliferation (p < 0.05) while MOB3A-expressing BRER cells continued to proliferate despite 4OHT exposure. (b) Western blot detection of MOB3A, Flag-tag (EGFP) and ERα expression in BRER HF E1T and BRER IMR90 clones under EtOH (control) and 4OHT. α-Tubulin serves as a loading control. Arrow represents unspecific background bands. (c) Fluorescence microscopy of BRER EGFP clones, confirming stable EGFP expression in HF E1T and IMR90 cells.

3.2 Characterizing Immune Infiltrates in Braf^{FA} Mice

3.2.1 Sample Selection

Building upon the work of Samantha Garnett, mice lungs from the 24-week timepoint (experimental groups EXP 6, 7, and 32) were selected for histological and immunofluorescence analyses. To investigate the impact of tumor density on progression and immune recruitment, BRAF V600E was activated using two viral titers: low titer (5×10^5 PFUs) and high titer (5×10^6 PFUs). Within each titer condition, half of the mice were WT for p53, while the other half underwent CreER-mediated p53 ablation (p53 null) at 24 weeks using tamoxifen. Previous studies (Garnett, 2019) demonstrated that tumor density plays a crucial role in tumor progression. Low titer infections produce fewer, more isolated tumors, which are more likely to escape OIS, alter the SASP and orient the TME towards a pro-tumorigenic phenotype leading to aggressive adenocarcinoma progression (Garnett et al., 2017). High titer infections generate dense, well-confined tumors that primarily remain low-grade adenomas. These tumors may be subject to enhanced senescence signaling and increased immune infiltration, which can act as barriers to

progression. Additionally, adenomas exhibit a functional SASP, which recruits immune cells, including macrophages, to clear senescent tumor cells and reinforce growth suppression. This experimental setup allows for a direct comparison between low and high tumor densities, focusing on their effects on OIS, immune infiltration, and the TME. Distinct phenotypic differences are hypothesized to reflect variations in SASP composition, immune cell recruitment, and tumor progression.

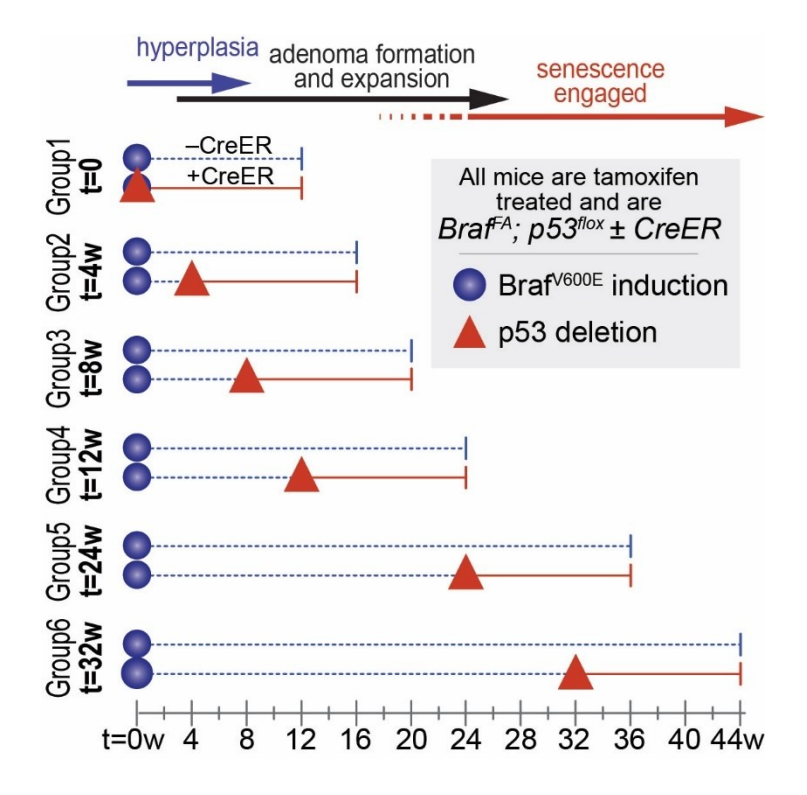


Figure 3-6. Experimental timeline for $Braf^{V600E}$ induction and p53 deletion in mouse models. $Braf^{V600E}$ expression (blue circles) was induced at t = 0 weeks via AdFlp infection, leading to hyperplasia, adenoma formation, and subsequent senescence engagement. p53 deletion (red triangles) was triggered at different time points (4, 8, 12, 24, and 32 weeks) using tamoxifen administration in CreER+ mice.

3.2.2 Tissue Analysis

To assess tumor proliferation, morphology, and immune infiltration, paraffin-embedded lung tissues from the 24-week experimental timepoint were analyzed (**Figure 3-7**). $Braf^{V600E}$ induction was initiated at week 0, followed by p53 deletion at 24 weeks. The intended endpoint for mice lung extraction was 12 weeks post-p53 ablation but was not attainable for many mice due to excessive tumor burden. The mice were stratified into four groups: Low titer ($5x10^5$ PFUs), p53 WT; High titer ($5x10^6$ PFUs), p53 null; High titer ($5x10^6$ PFUs), p53 null.

H&E staining was used to evaluate tumor architecture and cellular composition across experimental conditions. Representative images illustrate differences in tumor morphology, reflecting variations in proliferation, structural organization, and malignant progression (Figure 3-7a). Immunofluorescence was performed to identify proliferative cells by staining for Ki67 (red, Alexa Fluor 555), while F4/80 (green, Alexa Fluor 488) was used to detect macrophage infiltration (Figure 3-7b). Regions of co-localization (yellow) indicate proliferating macrophages.

CD45 (green, Alexa Fluor 488), a pan-leukocyte marker, was detected in parallel with surfactant protein C (red, Alexa Fluor 555), an alveolar type II epithelial marker (**Figure 3-7c**). This combination provides insights into immune infiltration within tumor-associated alveolar structures. The low titer *p53* WT tumor exhibits the most structured and uniform morphology, with relatively low nuclear density and well-defined architecture, consistent with an adenoma constrained by OIS. In contrast, the low titer *p53* null tumor shows markedly disorganized growth, loss of glandular architecture, and increased nuclear pleomorphism, indicative of an aggressive adenocarcinoma. The high titer *p53* WT tumor remains relatively structured with a glandular pattern, but increased nuclear density and localized disorganization suggest early signs of tumor

progression. Similarly, the high titer p53 null tumor retains some structural organization but exhibits regions of nuclear crowding and architectural disruption, suggesting a potential early transition toward adenocarcinoma. These findings support the hypothesis that tumor density and p53 status influence tumor progression, with low titer p53-null tumors exhibiting the most aggressive phenotype.

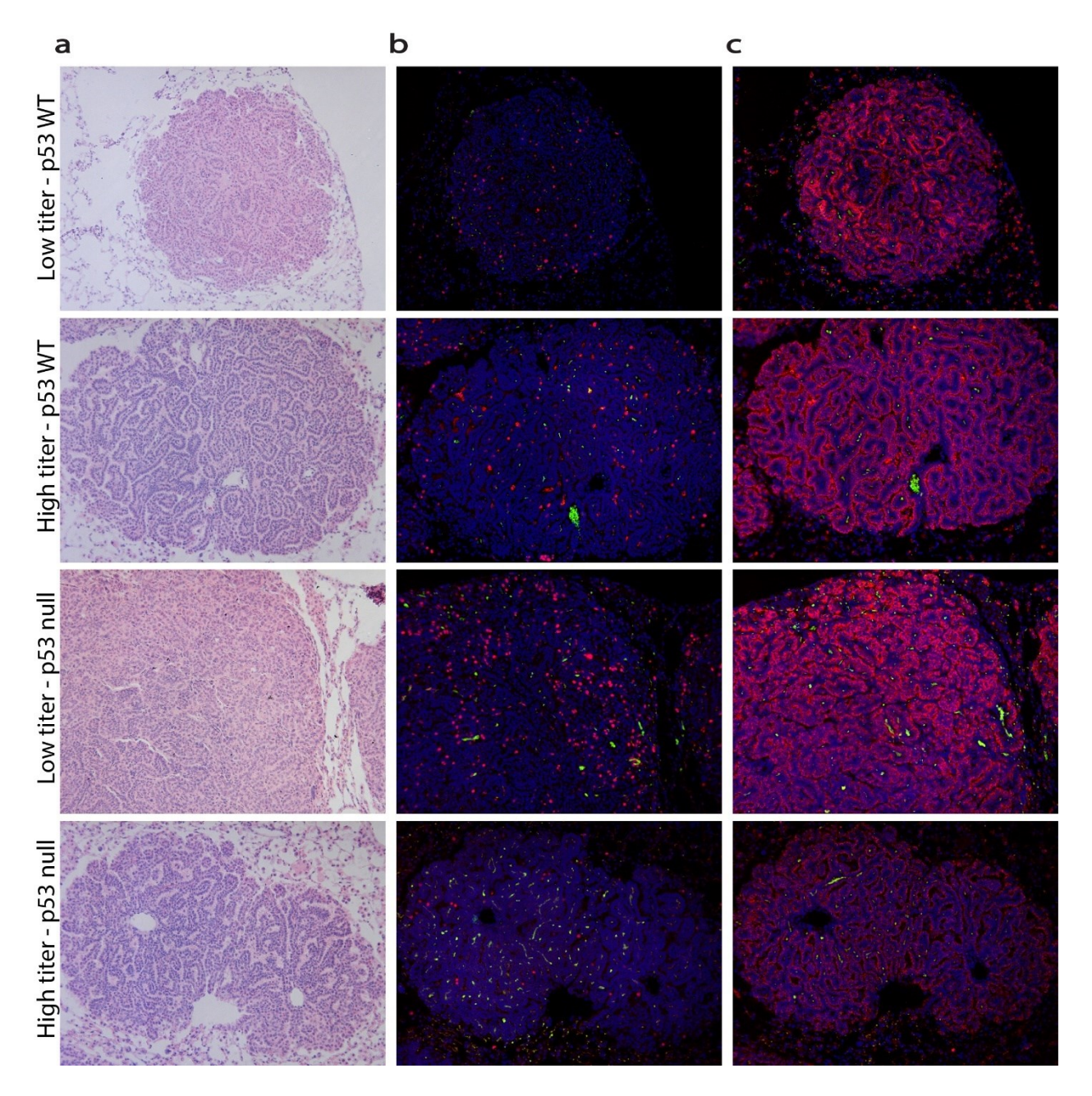


Figure 3-7. Histological and immunofluorescence staining of tumors 24-weeks post \textit{Braf}^{V600E}

induction. (a) H&E staining of tumor sections from low and high titer *p53* WT and *p53* null groups. (b) Immunofluorescence staining for Ki67 (red) and F4/80 (green), with DAPI (blue) marking nuclei. (c) Immunofluorescence staining for Surfactant Protein C (red) and CD45 (green), with DAPI marking nuclei.

3.2.3 Quantification Analysis

For each experimental group, ten tumors per mouse were analyzed. Fluorescent signals were quantified with Fiji ImageJ to compare immune infiltrations using markers like CD45 for leukocytes, F4/80 for macrophages, and Ki67 for cell proliferation, along structural markers such as DAPI and SPC (Figure 3-8).

Previous data generated by Garnett *et al.* demonstrate that active p53 tumors produced by low titers mostly consisted of low-grade (less than 3) adenomas across all groups, suggesting that OIS effectively represses malignant progression (Garnett, 2019). In contrast, the loss of p53 resulted in a higher incidence of Grade 3+ tumors, particularly in later groups, indicating that progression toward adenocarcinomas is pursued in the absence of p53.

To evaluate immune infiltration across all four groups (low and high titers, WT or null p53), immune cells were quantified using the CD45 marker as a proportion of DAPI-stained nuclei within tumors (Figure 3-8a). Important variations in immune infiltration emerged in each group. High titer p53 WT tumors exhibited a marked reduction in immune infiltrates compared to its low-titer counterpart, whereas high titer p53 null tumors appeared more immunogenic than the WT group. Overall, tumors generated from low viral titers and p53 ablation had the highest level of immune infiltration, which aligns with Garnett $et\ al$.'s findings, and suggests that advanced tumors also elicit the strongest immune response.

Macrophage infiltration was normalized to the number of nuclei within tumors (Figure 3-8b). Quantitative analysis revealed lower macrophage recruitment in the high titer *p53* WT group, reflecting senescence and SASP modulation, which may suppress macrophage migration and activity. In contrast, tumors formed under high viral titers and with *p53* ablation demonstrated a significant increase in macrophage infiltration, possibility due to a shift in the TME toward a proinflammatory SASP in the absence of *p53*-mediated tumor suppression. Additionally, high density tumors display opposite trends based on *p53* status, suggesting that the suppression of senescence and the promotion of an inflammatory phenotype may differentially regulate macrophage recruitment.

Next, cells positive for both F4/80 and Ki67 were counted to assess macrophage proliferation in all tumor groups (Figure 3-8c). Less proliferating macrophages appeared in *p53* WT tumors and high titer *p53* null conditions. High density tumors in *p53* WT conditions could be associated with enhanced OIS and SASP activity. High titer *p53* null tumors exhibited the largest population of double-positive cells, which might correlate with a pro-inflammatory environment that promotes the M2 phenotype and contribute to tumor remodeling. Within the macrophage population, the proportion of proliferating macrophages follows the same trend (Figure 3-8d).

These results demonstrate that the loss of p53 at 24-weeks post $Braf^{V600E}$ induction increases immune infiltration more remarkably in high density settings and underscores how the SASP can modulate the TME toward a pro-senescent or inflammatory phenotype, ultimately shaping immune infiltration patterns.

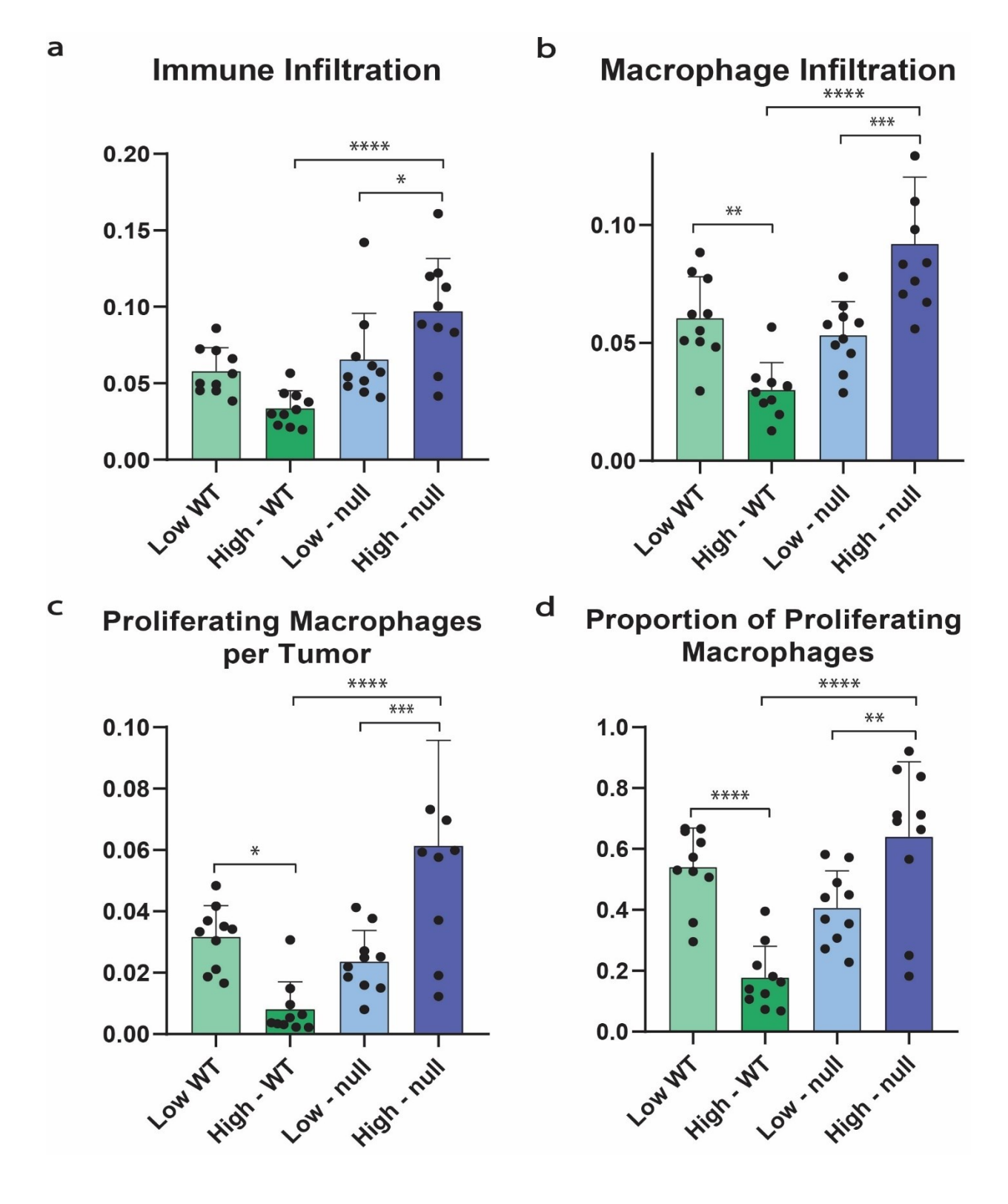


Figure 3-8. Immune infiltrates quantification and characterization in sparse or dense p53
WT or null tumors. (a) Leukocyte quantification according to CD45 staining of tumors

demonstrates elevated immune recruitment in low titer groups. (b) Macrophage quantification according to F4/80 staining of tumors displays a marked increase in high titer conditions. Proliferating macrophages were quantified and normalized according to tumor nuclei (c) or in proportion to total macrophages (d). High titer *p53* null tumors display the highest proliferative activity.

Chapter 4: Discussion

4.1 A MOB3A BRER Tissue Culture Model to Provide Insights into Senescence Bypass

MOB3A BRER cells were designed as a model to investigate the role of MOB3A in OIS bypass in the context of MAPK pathway hyperactivation. Previous iterations appeared to drift for reasons we can only begin to hypothesize, notably continuous cell replication, which may have led clones to accumulate undesired mutations. Interestingly, the cells generated by Dutchak *et al.* express MOB3A detectable by western blot, but their expression levels do not appear sufficient to enable proliferation in the presence of 4OHT, as observed in growth curve and washout experiments (Figure 3-1). Mutations may have arisen within the MOB3A gene, impairing its functional activity by preventing interactions with binding factors within the Hippo pathway. Replicating this model in two different fibroblast lines provides additional opportunities to investigate the molecular characteristics of MOB3A-mediated OIS bypass in a flexible and easily modulable manner.

The MOB3A BRER IMR90 cells (I-MBCs) and MOB3A BRER HF E1T cells (H-MBCs) completely rescued the senescent phenotype displayed by their respective BRER cells, confirming that MOB3A does indeed facilitate the bypass of cell cycle arrest, as previously demonstrated by Dutchak *et al.* (Dutchak et al., 2022). BRER cells enter senescence once exposed to 4OHT because the drug binds to the ER HBD, inducing a conformational change that activates the BRAF kinase domain. This activation mimics the oncogenic BRAF^{V600E} mutation and results in hyperactivation of the MAPK pathway (Innes and Gil, 2019). Such excessive mitogenic signaling is perceived by the cell as stress, triggering OIS. In response, cell cycle inhibitors such as p16^{INK4A} and p21^{CIP} halt proliferation and induce cell cycle arrest (Vizioli et al., 2014). Negative cell cycle regulators, such

as RB and P53, are activated and the DNA damage response is initiated (Lallet-Daher et al., 2013). Additionally, the secretion of the SASP reinforces the senescent state and modulates the surrounding microenvironment (Innes and Gil, 2019). In the absence of 4OHT, the ΔBRAF:ER remains inactive, as the HBD prevents constitutive activation of the kinase domain.

Considering the EGFP controls for both fibroblast cell lines exhibit the same susceptibility to 4OHT treatment as their corresponding BRER cells (Figure 3-3, Figure 3-5), the insertion of the plasmid does not seem to influence proliferation outcomes independently of 4OHT exposure. Indeed, both IMR90 and HF E1T cell lines maintained their splitting intervals and did not require adjustments to their culture media following MOB3A or EGFP introduction. Based on these observations, we conclude that MOB3A BRER cells differ from control solely by their MOB3A expression. This specificity makes them an excellent model for studying OIS bypass, as any observed differences can confidently be attributed to MO3A-mediated bypass. Interestingly, EGFP BRER IMR90 cells (I-EBCs) display a more polarized response to 4OHT compared to EGFP BRER HF E1T cells (H-EBCs), but this variation was anticipated given that it was already evident between the original BRER cell lines (Figure 3-3).

When exposed to 4OHT, MOB3A cells appear to shift their morphology toward one resembling senescent cells, but without compromising their proliferation (Dutchak et al., 2022). Further experiments are necessary to fully characterize how MOB3A expression affects the cell cycle and to elucidate the mechanism behind OIS bypass. Although all clones were subjected to identical treatment and express MOB3A, the protein's expression levels do not appear consistent across all cells. Such variability is expected following repeated clonal selection (Roberfroid et al., 2016; Brenière-Letuffe et al., 2018). Each selection round, whether it be for drugs or a particular cell response, applies stress to the population, potentially leading to diverse epigenetic modifications,

spontaneous mutations or genetic drift, especially after multiple passages in culture. In this study, cells were regularly frozen to ensure that the passage number remained below 20. Still, each clonal selection and subsequent expansion generates a new clonal population, each with unique genomic alterations that may or may not be related to MOB3A-mediated OIS bypass but could influence cellular responses under experimental conditions. This could possibly explain the drift observed with the previous iterations of the model (Masramon et al., 2006; Ben-David et al., 2019). I-EBCs currently exhibit a more polarized response to 4OHT compared to H-EBCs, but additional clonal selection could help normalize the responses of both cell lines.

Although drug susceptibility assays indicated that both puromycin and hygromycin resistance genes were suitable candidates for BRER IMR90 cells, hygromycin was ultimately selected, because HF E1Ts cells already presented innate resistance to this antibiotic (Figure 3-2). Puromycin is a potent antibiotic that requires only a few days to achieve thorough selection. Thus, preserving puromycin susceptibility in both I-MBCs and H-MBCs maintains the flexibility for future selections using this antibiotic. This is particularly important if additional oncogenic modifications are introduced, and subsequent rounds of selection become necessary.

Ultimately, OIS remains a poorly understood mechanism. Although results obtained from cell culture experiments may not directly translate to *in vivo* tumors, the generation of I-MBCs and H-MBCs provides valuable new opportunities to study MOB3A-mediated OIS bypass. Future experiments could involve analyzing senescence markers and SASP factors, as well as performing RNA sequencing to profile gene expression differences between MOB3A-expressing cells and EGFP controls under 4OHT treatment. These studies would help elucidate how interactions with tumor suppressors such as p53 and RB enable continued proliferation despite constitutive MAPK activation. The development of these MOB3A BRER cell lines paves the way for deeper

exploration of mechanisms underlying senescence bypass and creates opportunities for future research into MAPK signaling, checkpoint regulation, and potential therapeutic targets that exploit senescence pathways in cancer cells.

4.2 Immune Profiles are Modulated by Tumor Density, Senescence and P53 Status

Consistent with previous work performed in $Braf^{FA}$ mice, we observed that sparse tumors induced by a viral load of $5x10^5$ PFUs led to aggressive histological phenotypes characterized by loss of glandular structure and disorganized growth, especially upon p53 deletion. Aggressive and disorganised growth are histological features characteristic of concurrent Braf mutations and p53 inactivation, often described in melanoma studies (Yu et al., 2009; McFadden et al., 2014; Page et al., 2016). High density tumors generated from the high viral load of $5x10^6$ PFUs mostly remained low-grade adenomas, retaining their glandular architecture even after p53 ablation (Figure 3-7).

We suspect that this difference arises because the composition of the TME is influenced by cell density, resulting in variations in cytokine responses and senescence modulation depending on p53 status (Fedorov et al., 2003; Mijit et al., 2020). Adenomas represent early stages of tumor development and generally remain benign. We believe that OIS is the driving force preventing tumor progression, with the SASP playing a critical role in reinforcing senescence within the TME. Conversely, loss of p53 enables adenocarcinomas to progress by fostering a pro-inflammatory environment that facilitates immune evasion, angiogenesis, and TME remodeling (Coppé et al., 2014).

Although p53 deletion occurs 24 weeks $Braf^{V600E}$ induction, we observed that OIS is still bypassed, leading to adenocarcinoma formation as tumor cells continue to proliferate. This effect

is especially noticeable in low titer samples, which generate fewer, more isolated tumors. Such low tumor density reduces SASP signaling and immune cell recruitment, especially following *p53* ablation, diminishing tumor clearance and further compromising the proliferative barrier imposed by OIS, ultimately facilitating progression to adenocarcinoma (Dong et al., 2024).

The TME significantly influences immune cell recruitment. Indeed, the SASP within adenomas favours an inflammatory phenotype, characterized by the secretion of cytokines such as IL-6 and chemokines that recruit immune cells, notably macrophages (Coppé et al. 2014; Yue et al., 2022). Because OIS is maintained in adenomas, immune infiltrate primarily focuses on clearing senescent cells that could otherwise support a pro-tumorigenic environment. However, persistent SASP signaling can create chronic inflammation that bolsters the presence of M2 macrophages, fibrosis and eventually OIS bypass (Elder and Emmerson, 2020; Dyachkova et al. 2023). This scenario is particularly evident in adenocarcinomas, where continuous inflammation leads to increased immune infiltration and macrophage proliferation within the TME. Dense tumors also appear to promote this phenotype. Althought OIS might still prevent malignancy, a high proportion of senescent cells may amplify SASP secretion, intensifying immune cell recruitment, which, in turn, could either reinforce senescence, and limit progression to adenocarcinomas, or conversely, precipitate tumor growth (Prieto and Baker, 2020; Dong et al., 2024).

Although high density tumors form dense adenoma clusters that exhibit features of OIS, we observe a significant duality dependent on the status of p53. Under WT conditions, high density tumors undergo senescence and present minimal immune infiltration, whereas p53 deletion induces remarkable macrophage proliferation within the tumors. One possibility is that the extensive senescence observed in dense tumors with functional p53 may limit macrophage recruitment and proliferation or that clearance of senescent cells under these conditions requires

less immune cell involvement. Alternatively, macrophages themselves might become senescent in response to SASP factors (Prieto and Baker, 2020; Behmoaras and Gil, 2020). Additionally, the combined effect of density and p53 loss could alter the SASP composition and steeply increase macrophage recruitment relative to other conditions because senescence was disabled in favor of an inflammatory TME (Coppé et al., 2014). Within tumors, proliferating macrophages might adopt a tolerant phenotype, supporting tumor growth, angiogenesis and fibrosis by secreting growth factors. Further characterization of the precise activation state (M1 or M2) of proliferating macrophages within the TME under WT or p53-null conditions could provide valuable insights into whether their proliferation reflects a pro-inflammatory response aiming to clear senescent cells or instead supports a tumorigenic milieu (Boutilier and Elsawa, 2021; Hsiao et al., 2025).

Importantly, CD45 is a pan-leukocyte marker expressed by a large variety of immune cells including T cells, B cells, NK cell and APCs. Since macrophages are a subset of CD45-positive cells, the proportion of F4/80 positive cells will always be lower. Here, that result is relative since quantification of both markers was performed on consecutive slides, which may not have contained the same immune components per section. In some cases, other immune cells, such as T cells, may be preferentially recruited instead of macrophages. Additionally, although macrophages respond to the SASP, differences in responsiveness of other immune cell types to SASP factors or alternative signals could alter the CD45 to F4/80 ratio. Indeed, tumor density, senescence and cytokine production could selectively favor certain immune populations over others (Elder and Emmerson, 2020; Marin et al., 2023).

Limitations of this study include the method of $Braf^{V600E}$ induction, as intranasal delivery of adenoviral vectors is prone to inconsistencies in terms of infection efficiency, contributing to variability in tumor number, size and density. However, large sample values can help mitigate these

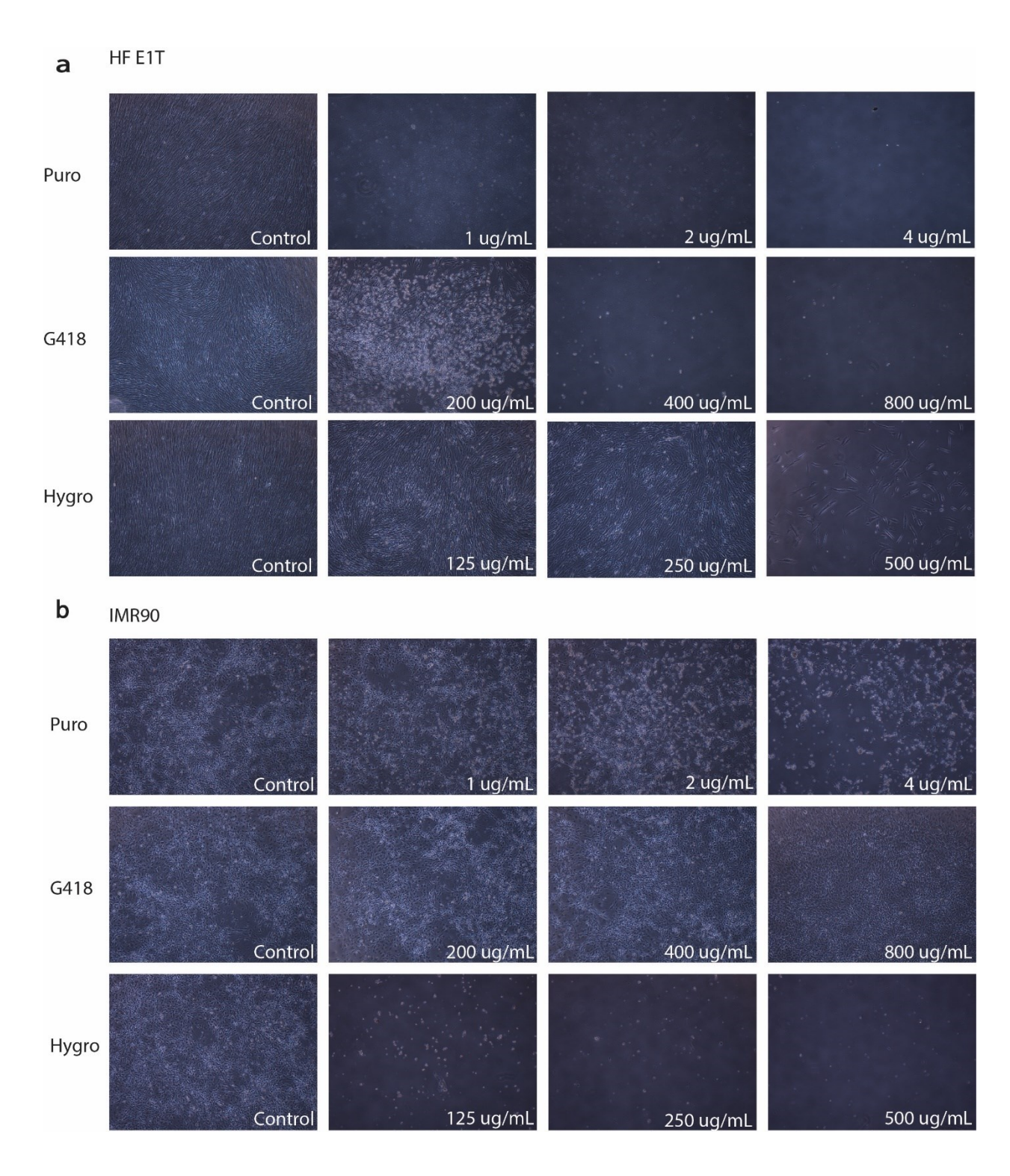
inconsistencies. It could also be argued that adenoviral delivery itself might provoke an immune response, potentially influencing tumor development. However, since high density tumors consistently displayed low immunogenicity in the presence of WT *p53*, this possibility seems unlikely in our context. Furthermore, the current experiment relies on CD45 and F4/80 as immune markers, limiting insights into the role of lymphocytes and their ability to modulate the TME. Finally, this study focuses on a single time point, which may provide a snapshot view of immune dynamics, rather than a continuous characterization of infiltration patterns.

Overall, this study highlights the interplay between *p53*, OIS, the SASP and immune infiltration within lung adenomas and adenocarcinomas. Going forward, a detailed time-course study involving the characterization of other immune components through flow cytometry could give further insight into the mechanism of immunogenicity within tumor progression.

Appendix

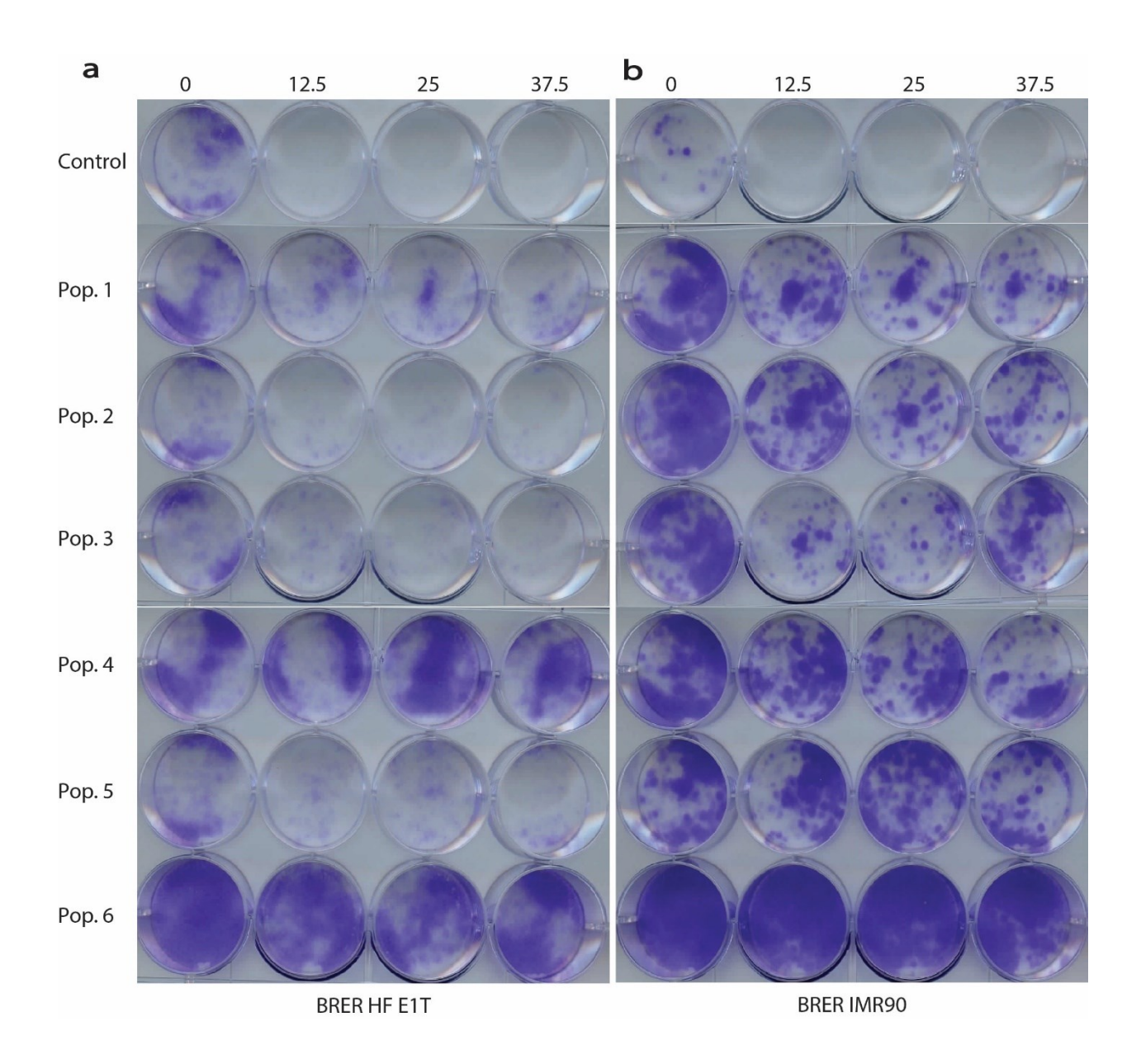
Table 1. Antibodies and reagents used in immunofluorescence and western blot.

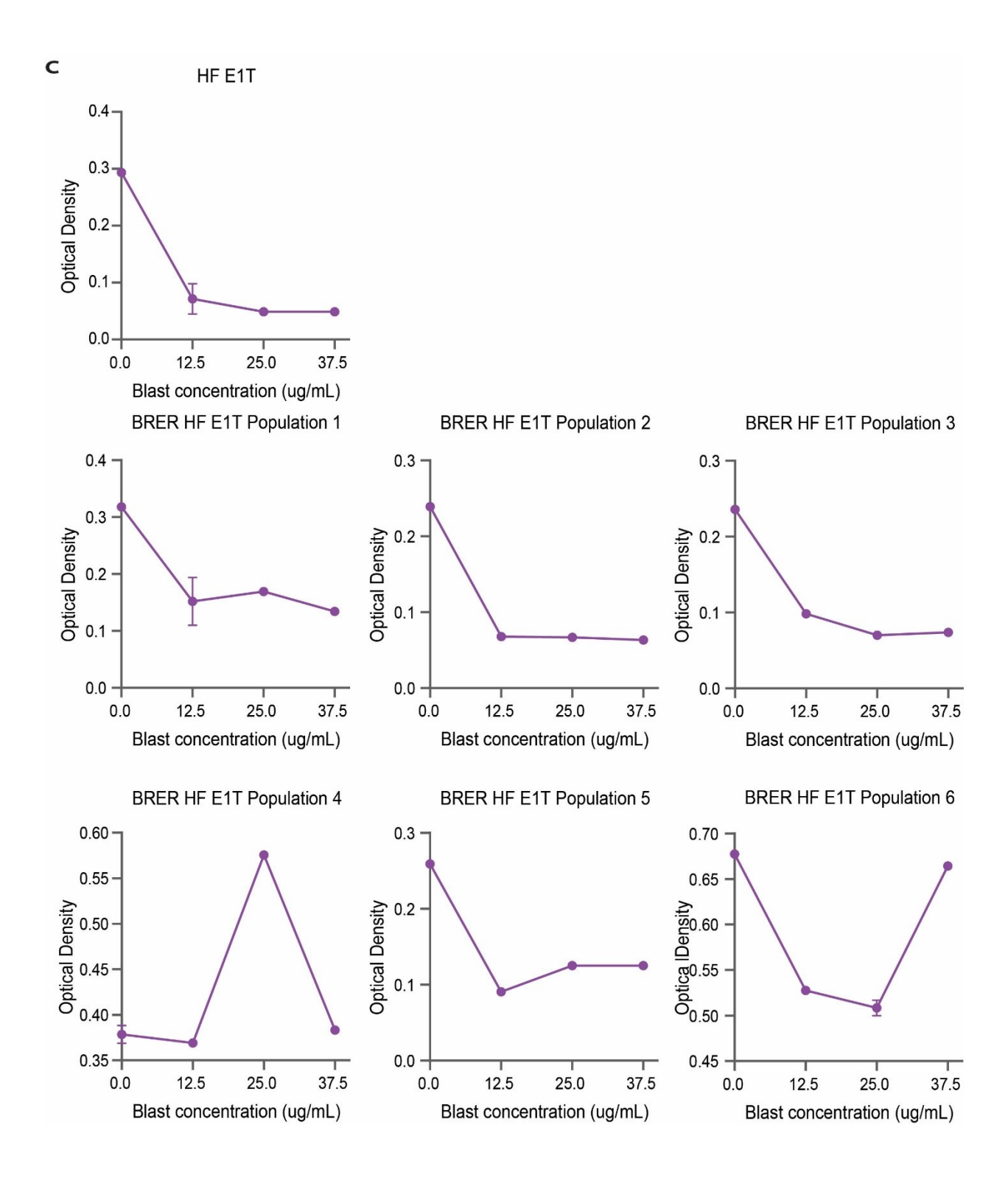
Target	Dilution	Supplier	Catalog
			No.
α-tubulin	1:1000	Santa Cruz Biotechnology	sc-32293
CD45	1:500	BD Biosciences	553078
DAPI	1:1000	Sigma-Aldrich	D9542-1MG
ERα	1:200	Santa Cruz Biotechnology	sc-543
Flag tag	1:700	Sigma	F74252MG
F4/80	1:500	Invitrogen	2488480
Ki67	1:500	Abcam	ab15580
MOB3A	1:1000	Proteintech	16942-1-AP
SPC	1:500	Santa Cruz Biotechnology	sc-7706
Alexa Fluor 555 AffiniPure Donkey	1:250	Jackson ImmunoResearch	705-565-147
Anti-Goat IgG			
Alexa Fluor 555 AffiniPure Donkey	1:250	Jackson ImmunoResearch	711-565-152
Anti-Rabbit IgG			
Biotin-SP-conjugated AffiniPure	1:250	Jackson ImmunoResearch	712-065-150
Donkey Anti-Rat IgG			
Alexa Fluor 488 Streptavidin	1:250	Jackson ImmunoResearch	016-540-084
Anti-rabbit IgG HRP-linked	1: 10 000	Cell Signaling Technology	7074S
Antibody			
Anti-mouse IgG HRP-linked	1: 10 000	Cell Signaling Technology	7076S
Antibody			

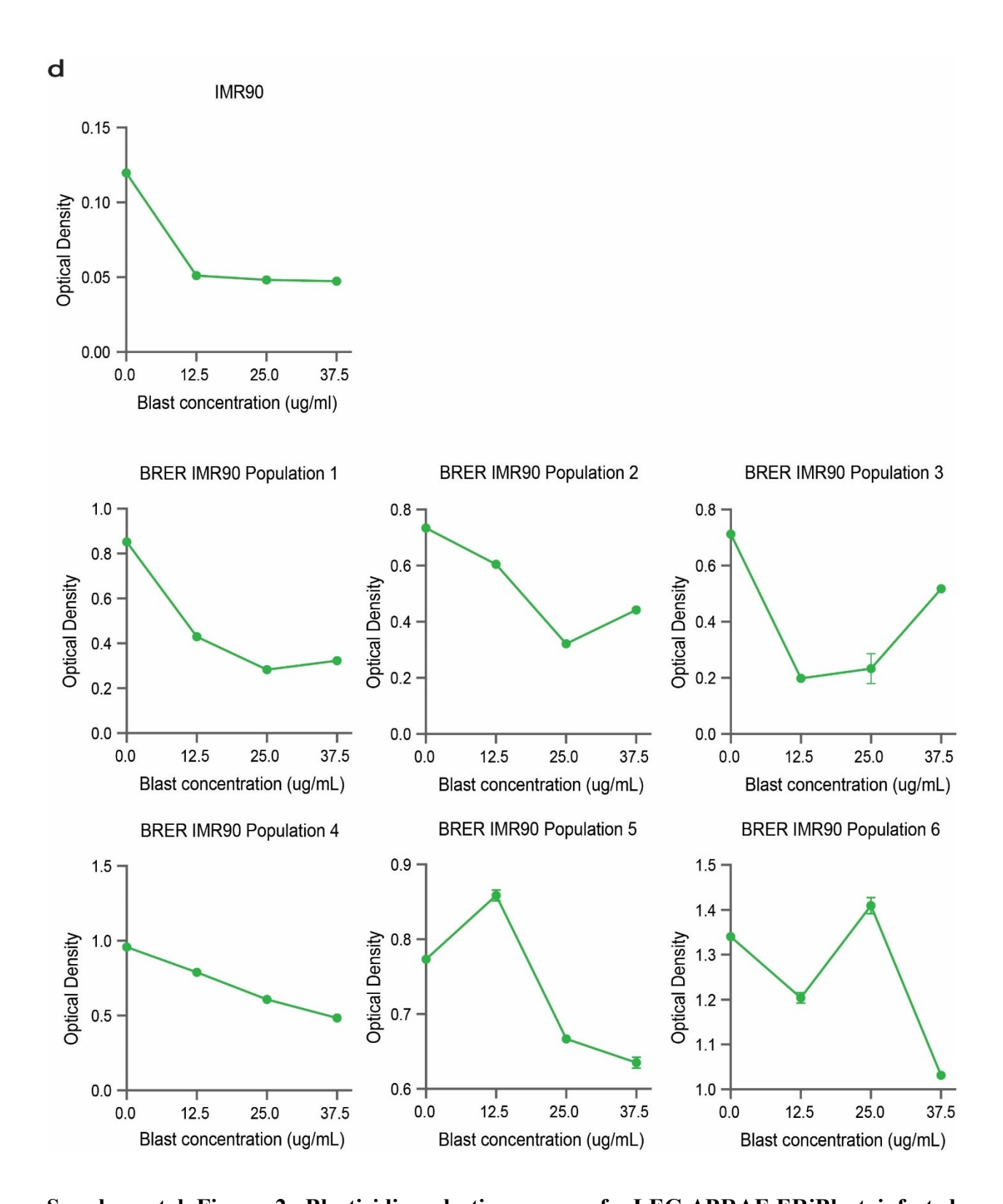


Supplemental Figure 1. Drug susceptibility profiles of HF E1T and IMR90 cell lines. HF E1T **(a)** and IMR90 **(b)** cells were treated with increasing concentrations of puromycin (none, 1 ug/mL, 2 ug/mL, 4 ug/mL), G418 (none, 200 ug/ml, 400 ug/ml and 800 ug/ml) and hygromycin (none,

125 ug/ml, 250 ug/ml and 500 ug/ml) over two weeks. HF E1T cells were found to be susceptible to G418 and puromycin but resistant to hygromycin, whereas IMR90 cells were susceptible to puromycin and hygromycin but resistant to G418.

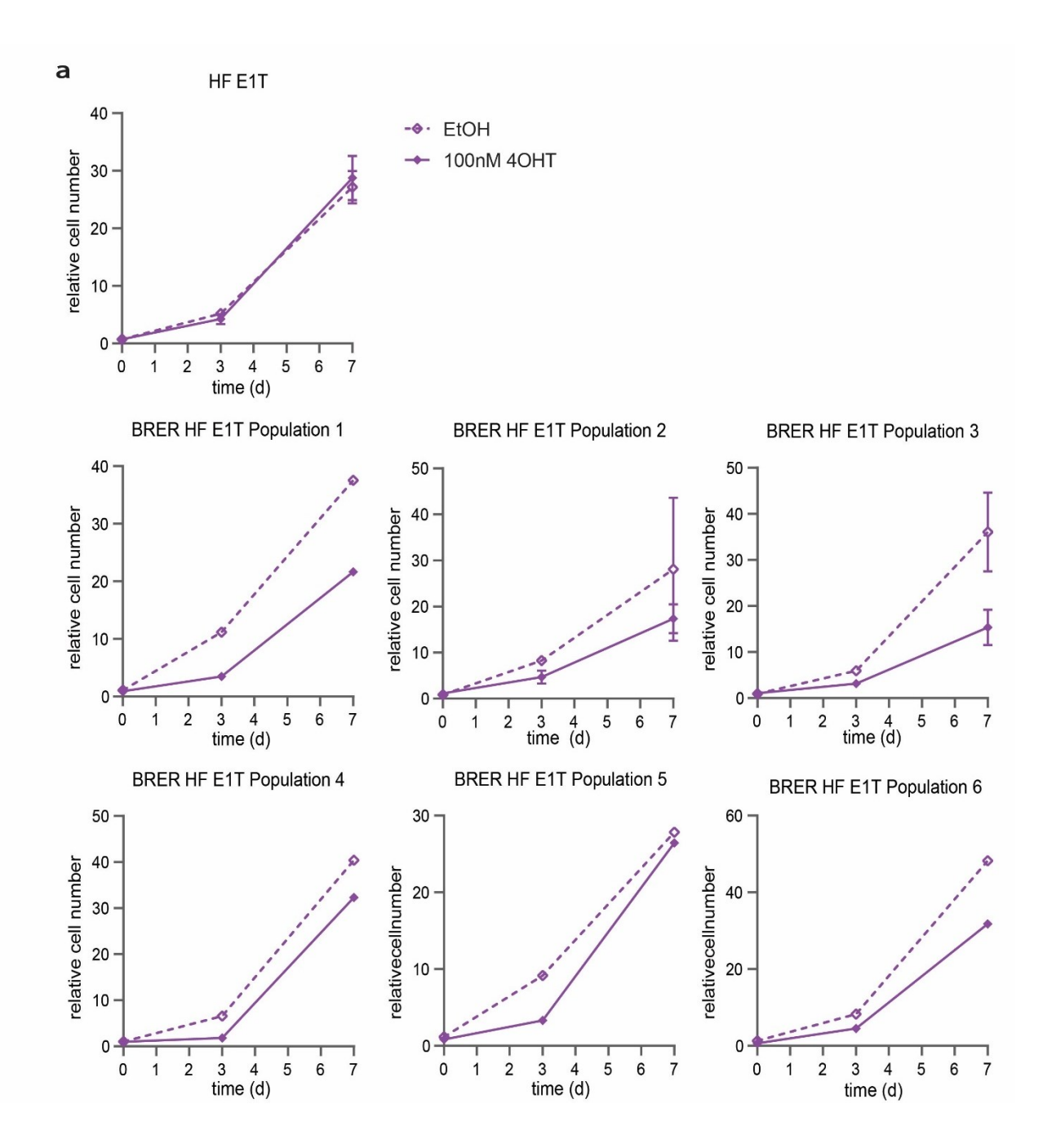


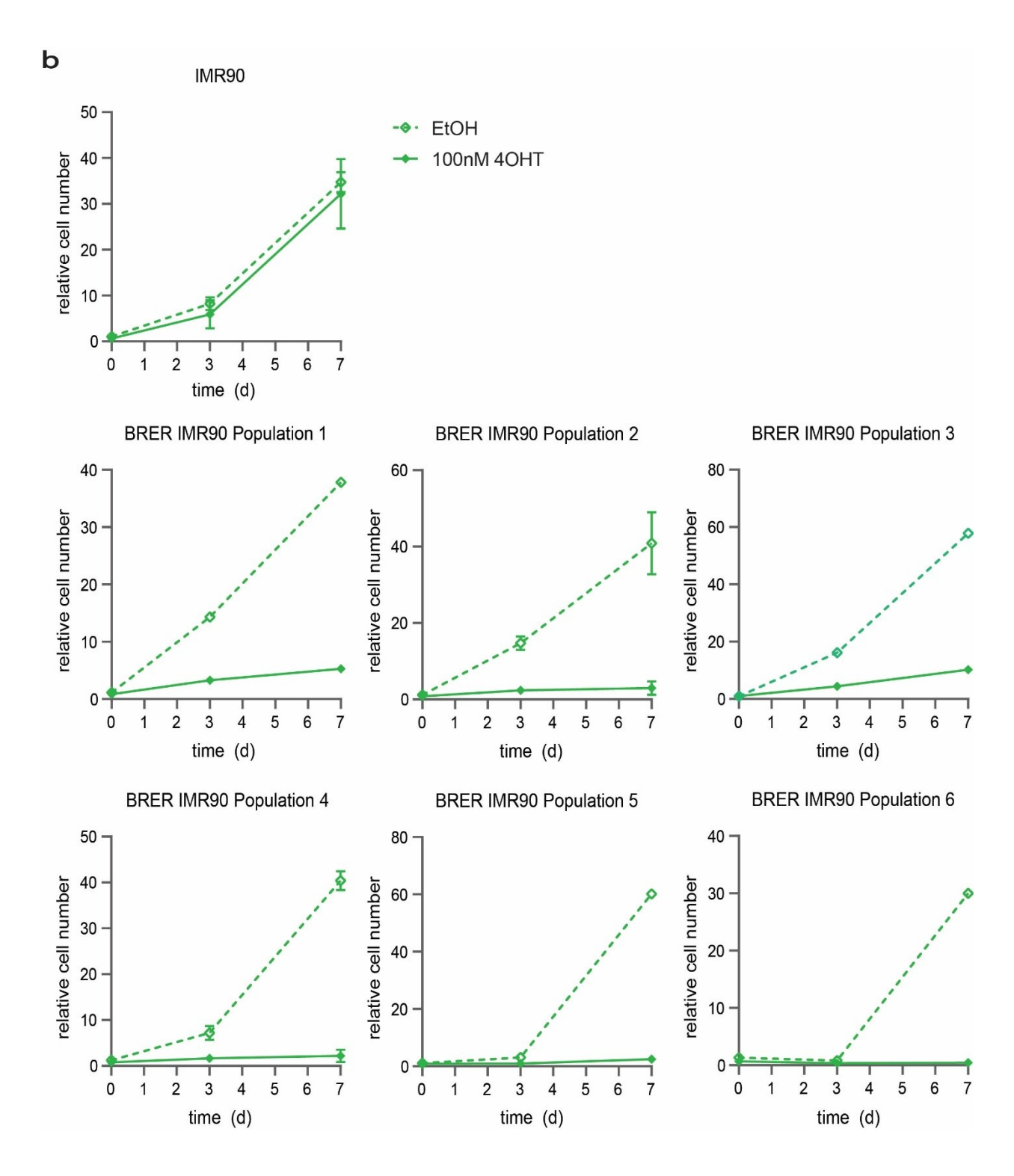




Supplemental Figure 2. Blasticidin selection assay of pLEG-ΔBRAF-ERiBlast-infected human fibroblasts. HF E1T (a) and IMR90 (b) parental fibroblast cell lines were infected with a

pLEG pLEG-ΔBRAF-ERiBlast lentivirus to introduce the ΔBRAF:ER construct. The cells were selected with blasticidin at increasing concentrations (none, 12.5 ug/mL, 25 ug/mL and 37.5 ug/mL) for three days. The amount of crystal violet stain relative to controls represents surviving cells and is a reflection of the antibiotic resistance conferred by the lentiviral integration. Solubilization of the crystal violet led to the measurement of optical densities plotted in (c) and (d).





E1T and IMR90 fibroblast cell lines exposed to 100 4OHT or EtOH. Cells were seeded at an initial density of 15,000 cells/well, and counted on days 0, 3, and 7. (a) HF E1T and IMR90 control

cells showed no significant proliferative differences between 4OHT and EtOH treatments. **(b)** BRER-infected populations displayed reduced proliferation in the presence of 4OHT. IMR90 populations 2 and 4 demonstrated the most polarized response to 4OHT compared to HF E1T populations.

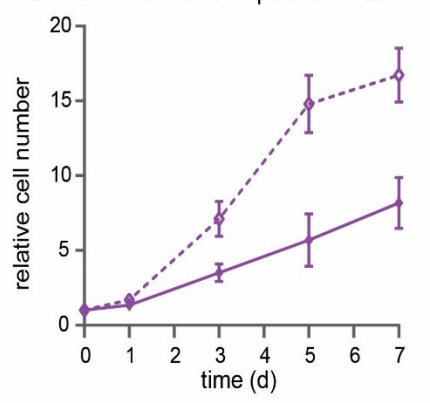
Cell Line	Clone	Control	4OHT	Fold-change	
BRER HF E1T	Clone 12	2.380	1.348	0.566	
Population 2	Clone 6	0.948	0.537	0.567	
	Clone 5	2.026	1.297	0.640	
	Clone 8	1.970	1.517	0.770	
	Clone 2	2.221	1.832	0.825	
	Clone 3	1.996	1.660	0.832	
	Clone 9	1.702	1.447	0.850	
	Clone 10	1.873	1.921	1.025	
	Clone 11	2.269	2.359	1.040	
	Clone 4	1.772	1.870	1.056	
	Clone 7	1.635	1.883	1.152	
	Clone 1	1.663	2.200	1.323	
BRER HF E1T	Clone 8	0.704	0.054	0.077	
Population 3	Clone 2	1.462	0.138	0.094	
•	Clone 6	1.814	0.252	0.139	
	Clone 7	1.245	0.190	0.153	
	Clone 4	1.489	0.371	0.249	
	Clone 12	1.882	0.875	0.465	
	Clone 11	1.680	1.101	0.656	
	Clone 5	1.876	1.256	0.670	
	Clone 10	1.292	1.029	0.797	
	Clone 3	2.229	1.843	0.827	
	Clone 1	1.160	1.130	0.974	
	Clone 9	1.414	1.843	1.304	
Cell Line	Clone	Control	4OHT	Fold-change	
BRER IMR90	Clone 11	0.946	0.022	0.023	
Population 2	Clone 10	1.021	0.045	0.045	
	Clone 5	0.818	0.039	0.048	
	Clone 2	0.756	0.043	0.056	
BRER IMR90	Clone 5	0.615	0.010	0.016	
Population 4	Clone 12	0.987	0.019	0.019	
	Clone 2	0.715	0.019	0.026	
	Clone 7	0.579	0.016	0.028	
	Clone 6	0.909	0.027	0.029	
	Clone 10	0.813	0.024	0.030	
	Clone 9	1.000	0.034	0.032	
	Clone 4	0.887	0.035	0.040	
	Clone 11	0.798	0.034	0.042	
	Clone 8	0.857	0.062	0.072	
Supplemental Table 1. Assessment of AOHT responsiveness in RDED HE F1T and					

Supplemental Table 1. Assessment of 4OHT responsiveness in BRER HF E1T and

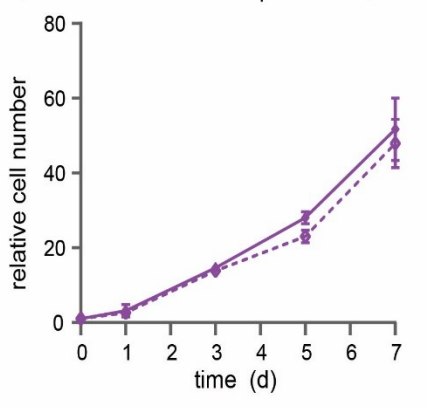
BRER IMR90 clones. Clones from BRER HF E1T and BRER IMR90 populations that demonstrated growth arrest upon 4OHT treatment were selected and assessed for 4OHT responsiveness by crystal violet staining in triplicates in 24-well plates. Each clone was treated

with 100 nM 4OHT or ethanol (control), and differences in growth were quantified by OD. The table shows the average OD values for each clone under control and 4OHT conditions, as well as the fold-change in growth. Clones with the largest differences in growth were chosen for subsequent experiments involving MOB3A/EGFP retroviral infection.

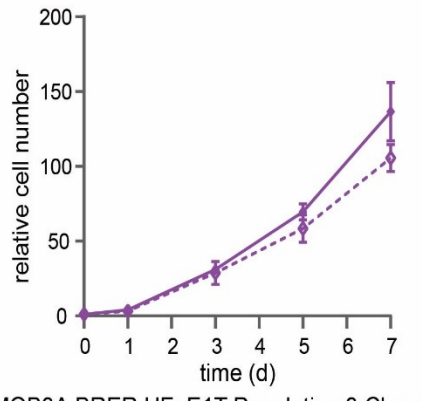




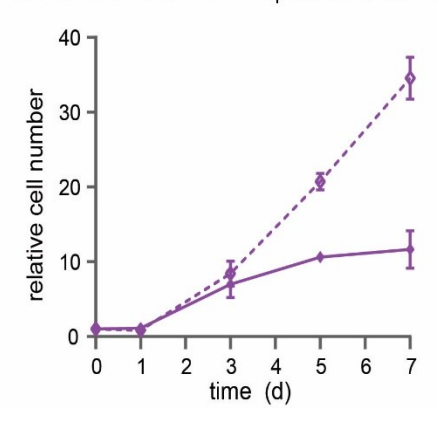
MOB3A BRER HF E1T Population 2 Clone 12-1



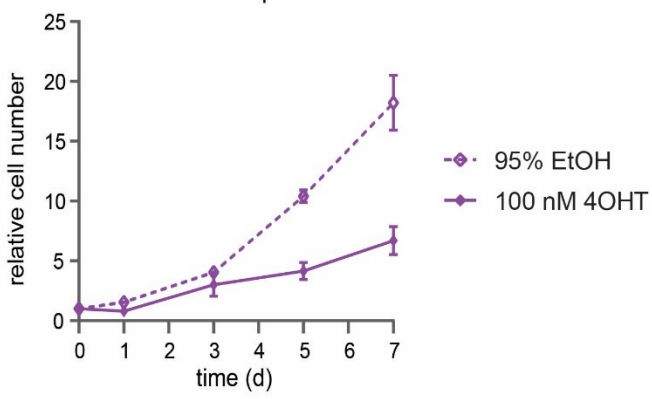
MOB3A BRER HF E1T Population 2 Clone 12-6



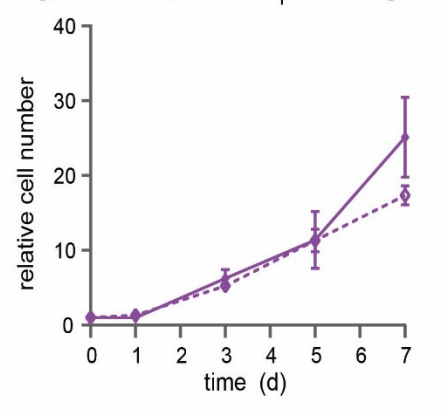
MOB3A BRER HF E1T Population 3 Clone 8-5



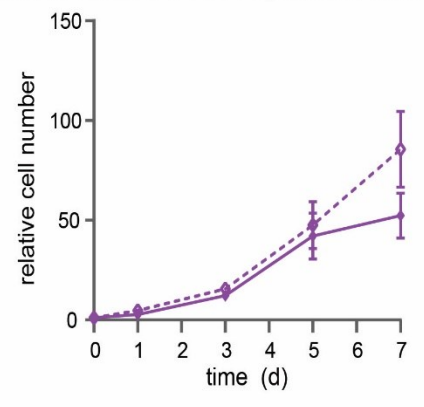
EGFP BRER HF E1T Population 3 Clone 8-5

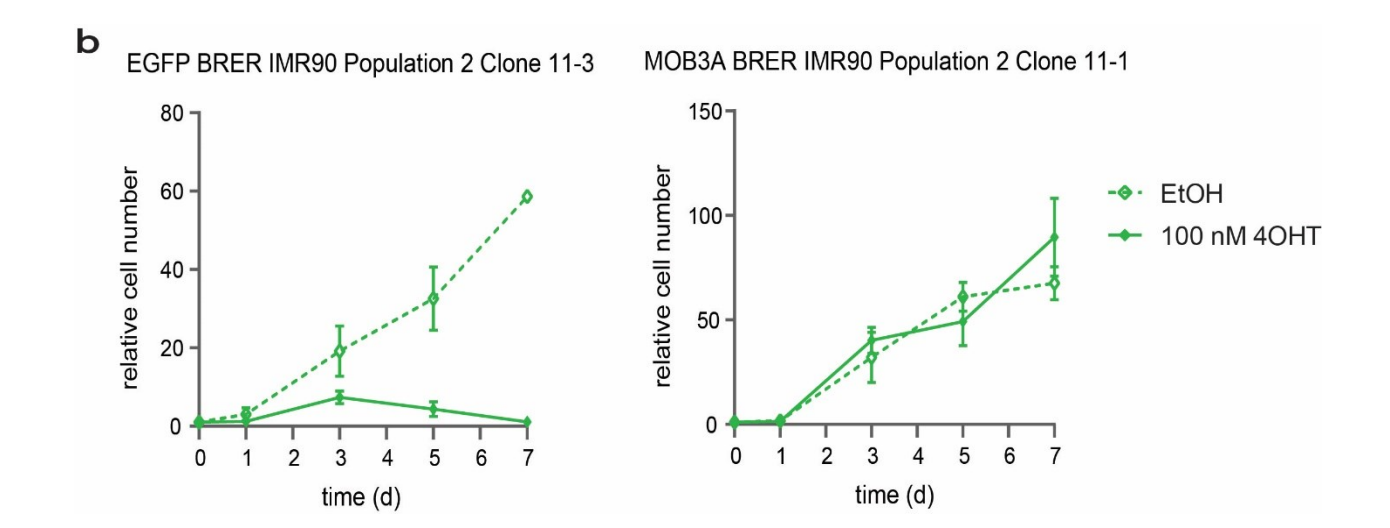


MOB3A BRER HF E1T Population 2 Clone 12-4



MOB3A BRER HF E1T Population 3 Clone 8-3





Supplemental Figure 6. MOB3A and EGFP BRER growth curves. Growth curves of MOB3A and EGFP BRER HF E1T (a) and BRER IMR90 (b) clones in the presence or absence of 100 nM 4OHT. 4OHT Treatment of EGFP BRER resulted in a significant reduction in proliferation while MOB3A-expressing BRER cells continued to proliferate despite 4OHT exposure.

References

- Ai, L., Xu, A., & Xu, J. (2020). Roles of PD-1/PD-L1 Pathway: Signaling, Cancer, and Beyond. In J. Xu (Ed.), *Regulation of Cancer Immune Checkpoints: Molecular and Cellular Mechanisms and Therapy* (pp. 33-59). Singapore: Springer Singapore.
- Alberts B, Johnson A, Lewis J, et al. Molecular Biology of the Cell. 4th edition. New York: Garland Science; 2002. Chapter 24, The Adaptive Immune System. Available from: https://www.ncbi.nlm.nih.gov/books/NBK21070/
- Aliyu, M., Zohora, F. T., Anka, A. U., Ali, K., Maleknia, S., Saffarioun, M., & Azizi, G. (2022). Interleukin-6 cytokine: An overview of the immune regulation, immune dysregulation, and therapeutic approach. *International Immunopharmacology, 111*, 109130. doi:https://doi.org/10.1016/j.intimp.2022.109130
- American Cancer Society. (2023, January 12). Lung Cancer Statistics | How Common is Lung Cancer? Www.cancer.org. https://www.cancer.org/cancer/types/lung-cancer/about/key-statistics.html
- Anderson, N. M., & Simon, M. C. (2020). The tumor microenvironment. Curr Biol, 30(16), R921-r925. doi:10.1016/j.cub.2020.06.081
- Ando, N., Tanaka, K., Otsubo, K., Toyokawa, G., Ikematsu, Y., Ide, M., . . . Okamoto, I. (2020). Association of Mps one binder kinase activator 1 (MOB1) expression with poor disease-free survival in individuals with non-small cell lung cancer. Thorac Cancer, 11(10), 2830-2839. doi:10.1111/1759-7714.13608
- Appella, E., & Anderson, C. W. (2001). Post-translational modifications and activation of P53 by genotoxic stresses. European Journal of Biochemistry, 268(10), 2764-2772. doi:https://doi.org/10.1046/j.1432-1327.2001.02225.x
- Aristizábal B, González Á. Innate immune system. In: Anaya JM, Shoenfeld Y, Rojas-Villarraga A, et al., editors. Autoimmunity: From Bench to Bedside [Internet]. Bogota (Colombia): El Rosario University Press; 2013 Jul 18. Chapter 2. Available from: https://www.ncbi.nlm.nih.gov/books/NBK459455/
- Ascierto, P. A., Kirkwood, J. M., Grob, J.-J., Simeone, E., Grimaldi, A. M., Maio, M., . . . Mozzillo, N. (2012). The role of BRAF V600 mutation in melanoma. Journal of Translational Medicine, 10(1), 85. doi:10.1186/1479-5876-10-85
- Assimakopoulos, S. F., Triantos, C., Maroulis, I., & Gogos, C. (2018). The Role of the Gut Barrier Function in Health and Disease. Gastroenterology Res, 11(4), 261-263. doi:10.14740/gr1053w
- Bamford, S., Dawson, E., Forbes, S., Clements, J., Pettett, R., Dogan, A., . . . Wooster, R. (2004). The COSMIC (Catalogue of Somatic Mutations in Cancer) database and website. Br J Cancer, 91(2), 355-358. doi:10.1038/sj.bjc.6601894
- Barnes, P. J., & Rennard, S. I. (2009). Chapter 34 Pathophysiology of COPD. In P. J. Barnes, J. M. Drazen, S. I. Rennard, & N. C. Thomson (Eds.), Asthma and COPD (Second Edition) (pp. 425-442). Oxford: Academic Press.

- Basisty, N., Kale, A., Jeon, O. H., Kuehnemann, C., Payne, T., Rao, C., . . . Schilling, B. (2020). A proteomic atlas of senescence-associated secretomes for aging biomarker development. PLoS Biol, 18(1), e3000599. doi:10.1371/journal.pbio.3000599
- Bates, S., Phillips, A. C., Clark, P. A., Stott, F., Peters, G., Ludwig, R. L., & Vousden, K. H. (1998). p14ARF links the tumour suppressors RB and P53. Nature, 395(6698), 124-125. doi:10.1038/25867
- Behmoaras, J., & Gil, J. (2021). Similarities and interplay between senescent cells and macrophages. J Cell Biol, 220(2). doi:10.1083/jcb.202010162
- Ben-David, U., Beroukhim, R., & Golub, T. R. (2019). Genomic evolution of cancer models: perils and opportunities. Nat Rev Cancer, 19(2), 97-109. doi:10.1038/s41568-018-0095-3
- Bieging, K. T., Mello, S. S., & Attardi, L. D. (2014). Unravelling mechanisms of P53-mediated tumour suppression. Nature Reviews Cancer, 14(5), 359-370. doi:10.1038/nrc3711
- Bichsel, S. J., Tamaskovic, R., Stegert, M. R., & Hemmings, B. A. (2004). Mechanism of activation of NDR (nuclear Dbf2-related) protein kinase by the hMOB1 protein. J Biol Chem, 279(34), 35228-35235. doi:10.1074/jbc.M404542200
- Biswas, S. K., Allavena, P., & Mantovani, A. (2013). Tumor-associated macrophages: functional diversity, clinical significance, and open questions. Seminars in Immunopathology, 35(5), 585-600. doi:10.1007/s00281-013-0367-7
- Bodnar, A. G., Ouellette, M., Frolkis, M., Holt, S. E., Chiu, C. P., Morin, G. B., . . . Wright, W. E. (1998). Extension of life-span by introduction of telomerase into normal human cells. Science, 279(5349), 349-352. doi:10.1126/science.279.5349.349
- Boehm, J. S., Zhao, J. J., Yao, J., Kim, S. Y., Firestein, R., Dunn, I. F., . . . Hahn, W. C. (2007). Integrative genomic approaches identify IKBKE as a breast cancer oncogene. Cell, 129(6), 1065-1079. doi:10.1016/j.cell.2007.03.052
- Boggiano, J. C., Vanderzalm, P. J., & Fehon, R. G. (2011). Tao-1 phosphorylates Hippo/MST kinases to regulate the Hippo-Salvador-Warts tumor suppressor pathway. Dev Cell, 21(5), 888-895. doi:10.1016/j.devcel.2011.08.028
- Bonilla, F. A., & Oettgen, H. C. (2010). Adaptive immunity. Journal of Allergy and Clinical Immunology, 125(2), S33-S40. doi:10.1016/j.jaci.2009.09.017
- Boopathy, G. T. K., & Hong, W. (2019). Role of Hippo Pathway-YAP/TAZ Signaling in Angiogenesis. Frontiers in Cell and Developmental Biology, 7. doi:10.3389/fcell.2019.00049
- Borgdorff, V., Lleonart, M., Bishop, C., Fessart, D., Bergin, A. H., Overhoff, M., & Beach, D. (2010). Multiple microRNAs rescue from Ras-induced senescence by inhibiting p21(Waf1/Cip1). Oncogene, 29, 2262-2271. doi:10.1038/onc.2009.497
- Botos, I., Segal, D. M., & Davies, D. R. (2011). The structural biology of Toll-like receptors. Structure, 19(4), 447-459. doi:10.1016/j.str.2011.02.004

- Boutilier, A. J., & Elsawa, S. F. (2021). Macrophage Polarization States in the Tumor Microenvironment. Int J Mol Sci, 22(13). doi:10.3390/ijms22136995
- Bradley, L. M., Dalton, D. K., & Croft, M. (1996). A direct role for IFN-gamma in regulation of Th1 cell development. J Immunol, 157(4), 1350-1358.
- Braig, M., Lee, S., Loddenkemper, C., Rudolph, C., Peters, A. H., Schlegelberger, B., . . . Schmitt, C. A. (2005). Oncogene-induced senescence as an initial barrier in lymphoma development. Nature, 436(7051), 660-665. doi:10.1038/nature03841
- Braig, M., & Schmitt, C. A. (2006). Oncogene-induced senescence: putting the brakes on tumor development. Cancer Res, 66(6), 2881-2884. doi:10.1158/0008-5472.Can-05-4006
- Brandstadter, J. D., & Yang, Y. (2011). Natural killer cell responses to viral infection. J Innate Immun, 3(3), 274-279. doi:10.1159/000324176
- Brenière-Letuffe, D., Domke-Shibamiya, A., Hansen, A., Eschenhagen, T., Fehse, B., Riecken, K., & Stenzig, J. (2018). Clonal dynamics studied in cultured induced pluripotent stem cells reveal major growth imbalances within a few weeks. Stem Cell Research & Therapy, 9(1), 165. doi:10.1186/s13287-018-0893-2
- Brenner, D. R., Gillis, J., Demers, A. A., Ellison, L. F., Billette, J.-M., Zhang, S. X., . . . Turner, D. (2024). Projected estimates of cancer in Canada in 2024. Canadian Medical Association Journal, 196(18), E615. doi:10.1503/cmaj.240095
- Brubaker, S. W., Bonham, K. S., Zanoni, I., & Kagan, J. C. (2015). Innate immune pattern recognition: a cell biological perspective. Annu Rev Immunol, 33, 257-290. doi:10.1146/annurev-immunol-032414-112240
- Cargnello, M., & Roux, P. P. (2011). Activation and function of the MAPKs and their substrates, the MAPK-activated protein kinases. Microbiol Mol Biol Rev, 75(1), 50-83. doi:10.1128/mmbr.00031-10
- Cenerenti, M., Saillard, M., Romero, P., & Jandus, C. (2022). The Era of Cytotoxic CD4 T Cells. Frontiers in Immunology, 13. doi:10.3389/fimmu.2022.867189
- Chandeck, C., & Mooi, W. J. (2010). Oncogene-induced Cellular Senescence. Advances in Anatomic Pathology, 17(1), 42-48. doi:10.1097/PAP.0b013e3181c66f4e
- Chaplin, D. D. (2010). Overview of the immune response. J Allergy Clin Immunol, 125(2 Suppl 2), S3-23. doi:10.1016/j.jaci.2009.12.980
- Chardin, L., & Leary, A. (2021). Immunotherapy in Ovarian Cancer: Thinking Beyond PD-1/PD-L1. Front Oncol, 11, 795547. doi:10.3389/fonc.2021.795547
- Chen, H. A., Ho, Y. J., Mezzadra, R., Adrover, J. M., Smolkin, R., Zhu, C., . . . Lowe, S. W. (2023). Senescence Rewires Microenvironment Sensing to Facilitate Antitumor Immunity. Cancer Discov, 13(2), 432-453. doi:10.1158/2159-8290.Cd-22-0528
- Chen, J. H., Hales, C. N., & Ozanne, S. E. (2007). DNA damage, cellular senescence and organismal ageing: causal or correlative? Nucleic Acids Res, 35(22), 7417-7428. doi:10.1093/nar/gkm681

- Chien, Y., Scuoppo, C., Wang, X., Fang, X., Balgley, B., Bolden, J. E., . . . Lowe, S. W. (2011). Control of the senescence-associated secretory phenotype by NF-κB promotes senescence and enhances chemosensitivity. Genes Dev, 25(20), 2125-2136. doi:10.1101/gad.17276711
- Chin, K. V., Ueda, K., Pastan, I., & Gottesman, M. M. (1992). Modulation of activity of the promoter of the human MDR1 gene by Ras and P53. Science, 255(5043), 459-462. doi:10.1126/science.1346476
- Christoffersen, N. R., Shalgi, R., Frankel, L. B., Leucci, E., Lees, M., Klausen, M., . . . Lund, A. H. (2010). P53-independent upregulation of miR-34a during oncogene-induced senescence represses MYC. Cell Death & Differentiation, 17(2), 236-245. doi:10.1038/cdd.2009.109
- Ciupka, B. (2020, November 4). Small Cell Lung Cancer vs. Non-small Cell Lung Cancer: What's the Difference? [Review of Small Cell Lung Cancer vs. Non-small Cell Lung Cancer: What's the Difference?]. National Foundation for Cancer Research. https://www.nfcr.org/blog/small-cell-lung-cancer-vs-non-small-cell-lung-cancer-whats-the-difference/
- Collado, M., Gil, J., Efeyan, A., Guerra, C., Schuhmacher, A. J., Barradas, M., . . . Serrano, M. (2005). Senescence in premalignant tumours. Nature, 436(7051), 642-642. doi:10.1038/436642a
- Collisson, E. A., Campbell, J. D., Brooks, A. N., Berger, A. H., Lee, W., Chmielecki, J., . . . John Flynn, H. (2014). Comprehensive molecular profiling of lung adenocarcinoma. Nature, 511(7511), 543-550. doi:10.1038/nature13385
- Colman, M. S., Afshari, C. A., & Barrett, J. C. (2000). Regulation of P53 stability and activity in response to genotoxic stress. Mutat Res, 462(2-3), 179-188. doi:10.1016/s1383-5742(00)00035-1
- Coppé, J. P., Patil, C. K., Rodier, F., Sun, Y., Muñoz, D. P., Goldstein, J., . . . Campisi, J. (2008). Senescence-associated secretory phenotypes reveal cell-nonautonomous functions of oncogenic RAS and the P53 tumor suppressor. PLoS Biol, 6(12), 2853-2868. doi:10.1371/journal.pbio.0060301
- Coppé, J. P., Desprez, P. Y., Krtolica, A., & Campisi, J. (2010). The senescence-associated secretory phenotype: the dark side of tumor suppression. Annu Rev Pathol, 5, 99-118. doi:10.1146/annurev-pathol-121808-102144
- Cortez-Retamozo, V., Etzrodt, M., Newton, A., Rauch, P. J., Chudnovskiy, A., Berger, C., . . . Pittet, M. J. (2012). Origins of tumor-associated macrophages and neutrophils. Proc Natl Acad Sci U S A, 109(7), 2491-2496. doi:10.1073/pnas.1113744109
- Courtois-Cox, S., Jones, S. L., & Cichowski, K. (2008). Many roads lead to oncogene-induced senescence. Oncogene, 27(20), 2801-2809. doi:10.1038/sj.onc.1210950
- Couzens, A. L., Knight, J. D. R., Kean, M. J., Teo, G., Weiss, A., Dunham, W. H., . . . Gingras, A.-C. (2013). Protein Interaction Network of the Mammalian Hippo Pathway Reveals Mechanisms of Kinase-Phosphatase Interactions. Science Signaling, 6(302), rs15-rs15. doi:doi:10.1126/scisignal.2004712
- Cristofalo, V. J., & Pignolo, R. J. (1996). Molecular markers of senescence in fibroblast-like cultures. Experimental Gerontology, 31(1), 111-123. doi:https://doi.org/10.1016/0531-5565(95)02018-7
- Damsky, W., Micevic, G., Meeth, K., Muthusamy, V., Curley, David P., Santhanakrishnan, M., . . . Bosenberg, M. (2015). mTORC1 Activation Blocks BrafV600E-Induced Growth Arrest but Is Insufficient for Melanoma Formation. *Cancer Cell*, 27(1), 41-56. doi:https://doi.org/10.1016/j.ccell.2014.11.014

- Dankort, D., Filenova, E., Collado, M., Serrano, M., Jones, K., & McMahon, M. (2007). A new mouse model to explore the initiation, progression, and therapy of BRAFV600E-induced lung tumors. Genes Dev, 21(4), 379-384. doi:10.1101/gad.1516407
- Dankort, D., Curley, D. P., Cartlidge, R. A., Nelson, B., Karnezis, A. N., Damsky, W. E., Jr., . . . Bosenberg, M. (2009). Braf(V600E) cooperates with Pten loss to induce metastatic melanoma. Nat Genet, 41(5), 544-552. doi:10.1038/ng.356
- Davies, H., Bignell, G. R., Cox, C., Stephens, P., Edkins, S., Clegg, S., . . . Futreal, P. A. (2002). Mutations of the BRAF gene in human cancer. Nature, 417(6892), 949-954. doi:10.1038/nature00766
- Demaria, M., Ohtani, N., Youssef, S. A., Rodier, F., Toussaint, W., Mitchell, J. R., . . . Campisi, J. (2014). An essential role for senescent cells in optimal wound healing through secretion of PDGF-AA. Dev Cell, 31(6), 722-733. doi:10.1016/j.devcel.2014.11.012
- Deng, Y., Chan, S. S., & Chang, S. (2008). Telomere dysfunction and tumour suppression: the senescence connection. Nat Rev Cancer, 8(6), 450-458. doi:10.1038/nrc2393
- Devarakonda, S., Morgensztern, D., & Govindan, R. (2015). Genomic alterations in lung adenocarcinoma. The Lancet Oncology, 16(7), e342-e351. doi:https://doi.org/10.1016/S1470-2045(15)00077-7
- Di Agostino, S., Strano, S., Emiliozzi, V., Zerbini, V., Mottolese, M., Sacchi, A., . . . Piaggio, G. (2006). Gain of function of mutant P53: the mutant P53/NF-Y protein complex reveals an aberrant transcriptional mechanism of cell cycle regulation. Cancer Cell, 10(3), 191-202. doi:10.1016/j.ccr.2006.08.013
- Di Micco, R., Fumagalli, M., Cicalese, A., Piccinin, S., Gasparini, P., Luise, C., . . . d'Adda di Fagagna, F. (2006). Oncogene-induced senescence is a DNA damage response triggered by DNA hyper-replication. Nature, 444(7119), 638-642. doi:10.1038/nature05327
- Dittmer, D., Pati, S., Zambetti, G., Chu, S., Teresky, A. K., Moore, M., . . . Levine, A. J. (1993). Gain of function mutations in P53. Nat Genet, 4(1), 42-46. doi:10.1038/ng0593-42
- Dobrzanski, M. J. (2013). Expanding roles for CD4 T cells and their subpopulations in tumor immunity and therapy. Front Oncol, 3, 63. doi:10.3389/fonc.2013.00063
- Dong, Z., Luo, Y., Yuan, Z., Tian, Y., Jin, T., & Xu, F. (2024). Cellular senescence and SASP in tumor progression and therapeutic opportunities. Molecular Cancer, 23(1), 181. doi:10.1186/s12943-024-02096-7
- Drosten, M., Guerra, C., & Barbacid, M. (2018). Genetically Engineered Mouse Models of K-Ras-Driven Lung and Pancreatic Tumors: Validation of Therapeutic Targets. Cold Spring Harb Perspect Med, 8(5). doi:10.1101/cshperspect.a031542
- Duhart, J. C., & Raftery, L. A. (2020). Mob Family Proteins: Regulatory Partners in Hippo and Hippo-Like Intracellular Signaling Pathways. Frontiers in Cell and Developmental Biology, 8. doi:10.3389/fcell.2020.00161

- DuPage, M., Dooley, A. L., & Jacks, T. (2009). Conditional mouse lung cancer models using adenoviral or lentiviral delivery of Cre recombinase. Nature Protocols, 4(7), 1064-1072. doi:10.1038/nprot.2009.95
- Dutchak, K., Garnett, S., Nicoll, M., de Bruyns, A., & Dankort, D. (2022). MOB3A Bypasses BRAF and RAS Oncogene-Induced Senescence by Engaging the Hippo Pathway. Molecular Cancer Research, 20(5), 770-781. doi:10.1158/1541-7786.Mcr-21-0767
- Dyachkova, U., Vigovskiy, M., Basalova, N., Efimenko, A., & Grigorieva, O. (2023). M2-Macrophage-Induced Chronic Inflammation Promotes Reversible Mesenchymal Stromal Cell Senescence and Reduces Their Anti-Fibrotic Properties. Int J Mol Sci, 24(23). doi:10.3390/ijms242317089
- Egea, L., Hirata, Y., & Kagnoff, M. F. (2010). GM-CSF: a role in immune and inflammatory reactions in the intestine. Expert Rev Gastroenterol Hepatol, 4(6), 723-731. doi:10.1586/egh.10.73
- Elder, S. S., & Emmerson, E. (2020). Senescent cells and macrophages: key players for regeneration? Open Biology, 10(12), 200309. doi:doi:10.1098/rsob.200309
- Fanale, D., Dimino, A., Pedone, E., Brando, C., Corsini, L. R., Filorizzo, C., . . . Bazan, V. (2022). Prognostic and Predictive Role of Tumor-Infiltrating Lymphocytes (TILs) in Ovarian Cancer. Cancers (Basel), 14(18). doi:10.3390/cancers14184344
- Fasbender, A., Lee, J. H., Walters, R. W., Moninger, T. O., Zabner, J., & Welsh, M. J. (1998). Incorporation of adenovirus in calcium phosphate precipitates enhances gene transfer to airway epithelia in vitro and in vivo. J Clin Invest, 102(1), 184-193. doi:10.1172/jci2732
- Fedorov, L. M., Papadopoulos, T., Tyrsin, O. Y., Twardzik, T., Götz, R., & Rapp, U. R. (2003). Loss of P53 in craf-induced transgenic lung adenoma leads to tumor acceleration and phenotypic switch. Cancer Res, 63(9), 2268-2277.
- Fujita, K. (2019). P53 Isoforms in Cellular Senescence- and Ageing-Associated Biological and Physiological Functions. International Journal of Molecular Sciences, 20(23), 6023. Retrieved from https://www.mdpi.com/1422-0067/20/23/6023
- Garnett, M. J., & Marais, R. (2004). Guilty as charged: B-RAF is a human oncogene. Cancer Cell, 6(4), 313-319. doi:https://doi.org/10.1016/j.ccr.2004.09.022
- Garnett, S., Dutchak, K. L., McDonough, R. V., & Dankort, D. (2017). P53 loss does not permit escape from BrafV600E-induced senescence in a mouse model of lung cancer. Oncogene, 36(45), 6325-6335. doi:10.1038/onc.2017.235
- Garnett, S. (2019). Mechanisms of oncogene-induced senescence in MAPK-driven cancer development (Doctoral dissertation). McGill University, Montreal, Canada. Retrieved from [https://escholarship.mcgill.ca/concern/theses/k35698612].
- Garnett, S., de Bruyns, A., Provencher-Tom, V., Dutchak, K., Shu, R., & Dankort, D. (2021). Metabolic Regulator IAPP (Amylin) Is Required for BRAF and RAS Oncogene-Induced Senescence. Mol Cancer Res, 19(5), 874-885. doi:10.1158/1541-7786.Mcr-20-0879
- Geiling, B., Vandal, G., Posner, A. R., de Bruyns, A., Dutchak, K. L., Garnett, S., & Dankort, D. (2013). A Modular Lentiviral and Retroviral Construction System to Rapidly Generate Vectors for Gene

- Expression and Gene Knockdown In Vitro and In Vivo. PLOS ONE, 8(10), e76279. doi:10.1371/journal.pone.0076279
- Greulich, H. (2010). The genomics of lung adenocarcinoma: opportunities for targeted therapies. Genes Cancer, 1(12), 1200-1210. doi:10.1177/1947601911407324
- Griffith, J. D., Comeau, L., Rosenfield, S., Stansel, R. M., Bianchi, A., Moss, H., & de Lange, T. (1999). Mammalian telomeres end in a large duplex loop. Cell, 97(4), 503-514. doi:10.1016/s0092-8674(00)80760-6
- Gutschner, T., & Diederichs, S. (2012). The hallmarks of cancer: a long non-coding RNA point of view. RNA Biol, 9(6), 703-719. doi:10.4161/rna.20481
- Harley, C. B., Futcher, A. B., & Greider, C. W. (1990). Telomeres shorten during ageing of human fibroblasts. Nature, 345(6274), 458-460. doi:10.1038/345458a0
- Harris, S. L., & Levine, A. J. (2005). The P53 pathway: positive and negative feedback loops. Oncogene, 24(17), 2899-2908. doi:10.1038/sj.onc.1208615
- Hayflick, L., & Moorhead, P. S. (1961). The serial cultivation of human diploid cell strains. Experimental Cell Research, 25(3), 585-621. doi:https://doi.org/10.1016/0014-4827(61)90192-6
- Hergovich, A., Schmitz, D., & Hemmings, B. A. (2006). The human tumour suppressor LATS1 is activated by human MOB1 at the membrane. Biochem Biophys Res Commun, 345(1), 50-58. doi:10.1016/j.bbrc.2006.03.244
- Hergovich, A. (2016). The Roles of NDR Protein Kinases in Hippo Signalling. Genes (Basel), 7(5). doi:10.3390/genes7050021
- Hernandez-Segura, A., de Jong, T. V., Melov, S., Guryev, V., Campisi, J., & Demaria, M. (2017). Unmasking Transcriptional Heterogeneity in Senescent Cells. Curr Biol, 27(17), 2652-2660.e2654. doi:10.1016/j.cub.2017.07.033
- Higashimoto, Y., Asanomi, Y., Takakusagi, S., Lewis, M. S., Uosaki, K., Durell, S. R., . . . Sakaguchi, K. (2006). Unfolding, Aggregation, and Amyloid Formation by the Tetramerization Domain from Mutant P53 Associated with Lung Cancer. Biochemistry, 45(6), 1608-1619. doi:10.1021/bi051192j
- Hinshaw, D. C., & Shevde, L. A. (2019). The Tumor Microenvironment Innately Modulates Cancer Progression. Cancer Res, 79(18), 4557-4566. doi:10.1158/0008-5472.Can-18-3962
- Hong, A. W., Meng, Z., Plouffe, S. W., Lin, Z., Zhang, M., & Guan, K. L. (2020). Critical roles of phosphoinositides and NF2 in Hippo pathway regulation. Genes Dev, 34(7-8), 511-525. doi:10.1101/gad.333435.119
- Hmitou, I., Druillennec, S., Valluet, A., Peyssonnaux, C., & Eychène, A. (2007). Differential regulation of B-raf isoforms by phosphorylation and autoinhibitory mechanisms. Mol Cell Biol, 27(1), 31-43. doi:10.1128/mcb.01265-06
- Hsiao, Y.-J., Hsieh, M.-S., Chang, G.-C., Hsu, Y.-C., Wang, C.-Y., Chen, Y.-M., . . . Yu, S.-L. (2025). TP53 determines the spatial dynamics of M1/M2 tumor-associated macrophages and M1-driven tumoricidal effects. Cell Death & Disease, 16(1), 38. doi:10.1038/s41419-025-07346-0

- Hu, Y., Dong, Z., & Liu, K. (2024). Unraveling the complexity of STAT3 in cancer: molecular understanding and drug discovery. Journal of Experimental & Clinical Cancer Research, 43(1), 23. doi:10.1186/s13046-024-02949-5
- Hubackova, S., Krejcikova, K., Bartek, J., & Hodny, Z. (2012). IL1- and TGFβ-Nox4 signaling, oxidative stress and DNA damage response are shared features of replicative, oncogene-induced, and drug-induced paracrine 'Bystander senescence'. Aging, 4(12), 932-951. doi:10.18632/aging.100520
- Innes, A. J., & Gil, J. (2019). IMR90 ER:RAS: A Cell Model of Oncogene-Induced Senescence. Methods Mol Biol, 1896, 83-92. doi:10.1007/978-1-4939-8931-7 9
- Jacks, T., Remington, L., Williams, B. O., Schmitt, E. M., Halachmi, S., Bronson, R. T., & Weinberg, R. A. (1994). Tumor spectrum analysis in *P53*-mutant mice. Current Biology, 4(1), 1-7. doi:10.1016/S0960-9822(00)00002-6
- Jackson, E. L., Willis, N., Mercer, K., Bronson, R. T., Crowley, D., Montoya, R., . . . Tuveson, D. A. (2001). Analysis of lung tumor initiation and progression using conditional expression of oncogenic K-ras. Genes Dev, 15(24), 3243-3248. doi:10.1101/gad.943001
- Jamieson, T., Clarke, M., Steele, C. W., Samuel, M. S., Neumann, J., Jung, A., . . . Sansom, O. J. (2012). Inhibition of CXCR2 profoundly suppresses inflammation-driven and spontaneous tumorigenesis. The Journal of Clinical Investigation, 122(9), 3127-3144. doi:10.1172/JCI61067
- Justice, R. W., Zilian, O., Woods, D. F., Noll, M., & Bryant, P. J. (1995). The Drosophila tumor suppressor gene warts encodes a homolog of human myotonic dystrophy kinase and is required for the control of cell shape and proliferation. Genes Dev, 9(5), 534-546. doi:10.1101/gad.9.5.534
- Johnson, L., Mercer, K., Greenbaum, D., Bronson, R. T., Crowley, D., Tuveson, D. A., & Jacks, T. (2001). Somatic activation of the K-ras oncogene causes early onset lung cancer in mice. Nature, 410(6832), 1111-1116. doi:10.1038/35074129
- Kaech, S. M., & Wherry, E. J. (2007). Heterogeneity and cell-fate decisions in effector and memory CD8+ T cell differentiation during viral infection. Immunity, 27(3), 393-405. doi:10.1016/j.immuni.2007.08.007
- Kang, C., Xu, Q., Martin, T. D., Li, M. Z., Demaria, M., Aron, L., . . . Elledge, S. J. (2015). The DNA damage response induces inflammation and senescence by inhibiting autophagy of GATA4. Science, 349(6255), aaa5612. doi:doi:10.1126/science.aaa5612
- Kieser, A., Weich, H. A., Brandner, G., Marmé, D., & Kolch, W. (1994). Mutant P53 potentiates protein kinase C induction of vascular endothelial growth factor expression. Oncogene, 9(3), 963-969.
- Koh, T. J., & DiPietro, L. A. (2011). Inflammation and wound healing: the role of the macrophage. Expert Rev Mol Med, 13, e23. doi:10.1017/s1462399411001943
- Kohler, R. S., Schmitz, D., Cornils, H., Hemmings, B. A., & Hergovich, A. (2010). Differential NDR/LATS interactions with the human MOB family reveal a negative role for human MOB2 in the regulation of human NDR kinases. Mol Cell Biol, 30(18), 4507-4520. doi:10.1128/mcb.00150-10

- Krtolica, A., Parrinello, S., Lockett, S., Desprez, P.-Y., & Campisi, J. (2001). Senescent fibroblasts promote epithelial cell growth and tumorigenesis: A link between cancer and aging. Proceedings of the National Academy of Sciences, 98(21), 12072-12077. doi:doi:10.1073/pnas.211053698
- Kruse, J. P., & Gu, W. (2009). Modes of P53 regulation. Cell, 137(4), 609-622. doi:10.1016/j.cell.2009.04.050
- Kuilman, T., Michaloglou, C., Vredeveld, L. C., Douma, S., van Doorn, R., Desmet, C. J., . . . Peeper, D. S. (2008). Oncogene-induced senescence relayed by an interleukin-dependent inflammatory network. Cell, 133(6), 1019-1031. doi:10.1016/j.cell.2008.03.039
- Kumari, R., & Jat, P. (2021). Mechanisms of Cellular Senescence: Cell Cycle Arrest and Senescence Associated Secretory Phenotype. Frontiers in Cell and Developmental Biology, 9. doi:10.3389/fcell.2021.645593
- Lai, Z. C., Wei, X., Shimizu, T., Ramos, E., Rohrbaugh, M., Nikolaidis, N., . . . Li, Y. (2005). Control of cell proliferation and apoptosis by mob as tumor suppressor, mats. Cell, 120(5), 675-685. doi:10.1016/j.cell.2004.12.036
- Lallet-Daher, H., Wiel, C., Gitenay, D., Navaratnam, N., Augert, A., Le Calvé, B., . . . Bernard, D. (2013). Potassium Channel KCNA1 Modulates Oncogene-Induced Senescence and Transformation. Cancer Research, 73(16), 5253-5265. doi:10.1158/0008-5472.Can-12-3690
 - Lane, D. P. (1992). P53, guardian of the genome. Nature, 358(6381), 15-16. doi:10.1038/358015a0
- Larsson, L.-G. (2011). Oncogene- and tumor suppressor gene-mediated suppression of cellular senescence. Seminars in Cancer Biology, 21(6), 367-376. doi:https://doi.org/10.1016/j.semcancer.2011.10.005
- Lavoie, H., & Therrien, M. (2015). Regulation of RAF protein kinases in ERK signalling. Nature Reviews Molecular Cell Biology, 16(5), 281-298. doi:10.1038/nrm3979
- Le, L., Tokumaru, Y., Oshi, M., Asaoka, M., Yan, L., Endo, I., . . . Takabe, K. (2021). Th2 cell infiltrations predict neoadjuvant chemotherapy response of estrogen receptor-positive breast cancer. Gland Surg, 10(1), 154-165. doi:10.21037/gs-20-571
- Lee, S. (2020). Cancer statistics at a glance. Canadian Cancer Society. https://cancer.ca/en/research/cancer-statistics/cancer-statistics-at-a-glance
- Lei, X., Lei, Y., Li, J.-K., Du, W.-X., Li, R.-G., Yang, J., . . . Tan, H.-B. (2020). Immune cells within the tumor microenvironment: Biological functions and roles in cancer immunotherapy. Cancer Letters, 470, 126-133. doi:https://doi.org/10.1016/j.canlet.2019.11.009
- Lin, A. W., Barradas, M., Stone, J. C., van Aelst, L., Serrano, M., & Lowe, S. W. (1998). Premature senescence involving P53 and p16 is activated in response to constitutive MEK/MAPK mitogenic signaling. Genes Dev, 12(19), 3008-3019. doi:10.1101/gad.12.19.3008
- Liu, X.-l., Ding, J., & Meng, L.-h. (2018). Oncogene-induced senescence: a double edged sword in cancer. Acta Pharmacologica Sinica, 39(10), 1553-1558. doi:10.1038/aps.2017.198

- Luckheeram, R. V., Zhou, R., Verma, A. D., & Xia, B. (2012). CD4⁺T cells: differentiation and functions. Clin Dev Immunol, 2012, 925135. doi:10.1155/2012/925135
- Mallette, F. A., Gaumont-Leclerc, M.-F., Huot, G., & Ferbeyre, G. (2007). Myc Down-regulation as a Mechanism to Activate the Rb Pathway in STAT5A-induced Senescence. Journal of Biological Chemistry, 282(48), 34938-34944. doi:10.1074/jbc.M707074200
- Malumbres, M., & Barbacid, M. (2005). Mammalian cyclin-dependent kinases. Trends Biochem Sci, 30(11), 630-641. doi:10.1016/j.tibs.2005.09.005
- Marin, I., Serrano, M., & Pietrocola, F. (2023). Recent insights into the crosstalk between senescent cells and CD8 T lymphocytes. npj Aging, 9(1), 8. doi:10.1038/s41514-023-00105-5
- Marshall, J. S., Warrington, R., Watson, W., & Kim, H. L. (2018). An introduction to immunology and immunopathology. Allergy, Asthma & Clinical Immunology, 14(2), 49. doi:10.1186/s13223-018-0278-1
- Masramon, L., Vendrell, E., Tarafa, G., Capellà, G., Miró, R., Ribas, M., & Peinado, M. A. (2006). Genetic instability and divergence of clonal populations in colon cancer cells in vitro. Journal of Cell Science, 119(8), 1477-1482. doi:10.1242/jcs.02871
- Matallanas, D., Birtwistle, M., Romano, D., Zebisch, A., Rauch, J., von Kriegsheim, A., & Kolch, W. (2011). Raf family kinases: old dogs have learned new tricks. Genes Cancer, 2(3), 232-260. doi:10.1177/1947601911407323
- McCain, J. (2013). The MAPK (ERK) Pathway: Investigational Combinations for the Treatment Of BRAF-Mutated Metastatic Melanoma. Pt, 38(2), 96-108.
- McClure, R., & Massari, P. (2014). TLR-Dependent Human Mucosal Epithelial Cell Responses to Microbial Pathogens. Front Immunol, 5, 386. doi:10.3389/fimmu.2014.00386
- McFadden, D. G., Vernon, A., Santiago, P. M., Martinez-McFaline, R., Bhutkar, A., Crowley, D. M., . . . Jacks, T. (2014). P53 constrains progression to anaplastic thyroid carcinoma in a *Braf*-mutant mouse model of papillary thyroid cancer. Proceedings of the National Academy of Sciences, 111(16), E1600-E1609. doi:doi:10.1073/pnas.1404357111
- Meng, Z., Moroishi, T., & Guan, K. L. (2016). Mechanisms of Hippo pathway regulation. Genes Dev, 30(1), 1-17. doi:10.1101/gad.274027.115
- Michaloglou, C., Vredeveld, L. C., Soengas, M. S., Denoyelle, C., Kuilman, T., van der Horst, C. M., . . . Peeper, D. S. (2005). BRAFE600-associated senescence-like cell cycle arrest of human naevi. Nature, 436(7051), 720-724. doi:10.1038/nature03890
- Mijit, M., Caracciolo, V., Melillo, A., Amicarelli, F., & Giordano, A. (2020). Role of P53 in the Regulation of Cellular Senescence. Biomolecules, 10(3). doi:10.3390/biom10030420
- Molina, J. R., Yang, P., Cassivi, S. D., Schild, S. E., & Adjei, A. A. (2008). Non-small cell lung cancer: epidemiology, risk factors, treatment, and survivorship. Mayo Clin Proc, 83(5), 584-594. doi:10.4065/83.5.584

- Muraille, E., Leo, O., & Moser, M. (2014). TH1/TH2 paradigm extended: macrophage polarization as an unappreciated pathogen-driven escape mechanism? Front Immunol, 5, 603. doi:10.3389/fimmu.2014.00603
- Nag, S., Qin, J., Srivenugopal, K. S., Wang, M., & Zhang, R. (2013). The MDM2-P53 pathway revisited. J Biomed Res, 27(4), 254-271. doi:10.7555/jbr.27.20130030
- Navalkar, A., Paul, A., Sakunthala, A., Pandey, S., Dey, A. K., Saha, S., . . . Maji, S. K. (2022). Oncogenic gain of function due to P53 amyloids occurs through aberrant alteration of cell cycle and proliferation. J Cell Sci, 135(15). doi:10.1242/jcs.259500
- Narita, M., Nũnez, S., Heard, E., Narita, M., Lin, A. W., Hearn, S. A., . . . Lowe, S. W. (2003). Rb-mediated heterochromatin formation and silencing of E2F target genes during cellular senescence. Cell, 113(6), 703-716. doi:10.1016/s0092-8674(03)00401-x
- National Cancer Institute. (2019, May 14). Small Cell Lung Cancer Treatment (PDQ®)-Patient Version. National Cancer Institute; Cancer.gov. https://www.cancer.gov/types/lung/patient/small-cell-lung-treatment-pdq
- National Cancer Institute. (2023, October 11). Non-Small Cell Lung Cancer Treatment. National Cancer Institute; Cancer.gov. https://www.cancer.gov/types/lung/patient/non-small-cell-lung-treatment-pdq
- Ni, L., Zheng, Y., Hara, M., Pan, D., & Luo, X. (2015). Structural basis for Mob1-dependent activation of the core Mst-Lats kinase cascade in Hippo signaling. Genes Dev, 29(13), 1416-1431. doi:10.1101/gad.264929.115
- Nishimura, T., Iwakabe, K., Sekimoto, M., Ohmi, Y., Yahata, T., Nakui, M., . . . Ohta, A. (1999). Distinct role of antigen-specific T helper type 1 (Th1) and Th2 cells in tumor eradication in vivo. J Exp Med, 190(5), 617-627. doi:10.1084/jem.190.5.617
- Oh, D. Y., & Fong, L. (2021). Cytotoxic CD4(+) T cells in cancer: Expanding the immune effector toolbox. Immunity, 54(12), 2701-2711. doi:10.1016/j.immuni.2021.11.015
- Orjalo, A. V., Bhaumik, D., Gengler, B. K., Scott, G. K., & Campisi, J. (2009). Cell surface-bound IL-lalpha is an upstream regulator of the senescence-associated IL-6/IL-8 cytokine network. Proc Natl Acad Sci U S A, 106(40), 17031-17036. doi:10.1073/pnas.0905299106
- Page, A., Navarro, M., Suarez-Cabrera, C., Alameda, J. P., Casanova, M. L., Paramio, J. M., . . . Ramirez, A. (2016). Protective role of P53 in skin cancer: Carcinogenesis studies in mice lacking epidermal P53. Oncotarget, 7(15), 20902-20918. doi:10.18632/oncotarget.7897
- Pan, D. (2010). The hippo signaling pathway in development and cancer. Dev Cell, 19(4), 491-505. doi:10.1016/j.devcel.2010.09.011
- Paul, S., & Lal, G. (2017). The Molecular Mechanism of Natural Killer Cells Function and Its Importance in Cancer Immunotherapy. Front Immunol, 8, 1124. doi:10.3389/fimmu.2017.01124
- Pérez-Mancera, P. A., Young, A. R., & Narita, M. (2014). Inside and out: the activities of senescence in cancer. Nat Rev Cancer, 14(8), 547-558. doi:10.1038/nrc3773

- Pfister, N. T., & Prives, C. (2017). Transcriptional Regulation by Wild-Type and Cancer-Related Mutant Forms of P53. Cold Spring Harb Perspect Med, 7(2). doi:10.1101/cshperspect.a026054
- Prieto, L. I., & Baker, D. J. (2019). Cellular Senescence and the Immune System in Cancer. Gerontology, 65(5), 505-512. doi:10.1159/000500683
- Pixley, F. J., & Stanley, E. R. (2010). Chapter 319 Cytokines and Cytokine Receptors Regulating Cell Survival, Proliferation, and Differentiation in Hematopoiesis. In R. A. Bradshaw & E. A. Dennis (Eds.), Handbook of Cell Signaling (Second Edition) (pp. 2733-2742). San Diego: Academic Press.
- Plitas, G., & Rudensky, A. Y. (2016). Regulatory T Cells: Differentiation and Function. Cancer Immunol Res, 4(9), 721-725. doi:10.1158/2326-6066.Cir-16-0193
- Pollock, P. M., Harper, U. L., Hansen, K. S., Yudt, L. M., Stark, M., Robbins, C. M., . . . Meltzer, P. S. (2003). High frequency of BRAF mutations in nevi. Nat Genet, 33(1), 19-20. doi:10.1038/ng1054
- Pritchard, C. A., Samuels, M. L., Bosch, E., & McMahon, M. (1995). Conditionally oncogenic forms of the A-Raf and B-Raf protein kinases display different biological and biochemical properties in NIH 3T3 cells. Mol Cell Biol, 15(11), 6430-6442. doi:10.1128/mcb.15.11.6430
- Pritchard, C., Carragher, L., Aldridge, V., Giblett, S., Jin, H., Foster, C., . . . Kamata, T. (2007). Mouse models for BRAF-induced cancers. Biochem Soc Trans, 35(Pt 5), 1329-1333. doi:10.1042/bst0351329
- Qazi, B. S., Tang, K., & Qazi, A. (2011). Recent advances in underlying pathologies provide insight into interleukin-8 expression-mediated inflammation and angiogenesis. Int J Inflam, 2011, 908468. doi:10.4061/2011/908468
- Riudavets, M., Cascetta, P., & Planchard, D. (2022). Targeting BRAF-mutant non-small cell lung cancer: Current status and future directions. Lung Cancer, 169, 102-114. doi:https://doi.org/10.1016/j.lungcan.2022.05.014
- Roberfroid, S., Vanderleyden, J., & Steenackers, H. (2016). Gene expression variability in clonal populations: Causes and consequences. Crit Rev Microbiol, 42(6), 969-984. doi:10.3109/1040841x.2015.1122571
- Saito, A., Horie, M., Micke, P., & Nagase, T. (2018). The Role of TGF-β Signaling in Lung Cancer Associated with Idiopathic Pulmonary Fibrosis. *Int J Mol Sci*, 19(11). doi:10.3390/ijms19113611
- Schmitt, C. A., Wang, B., & Demaria, M. (2022). Senescence and cancer role and therapeutic opportunities. Nature Reviews Clinical Oncology, 19(10), 619-636. doi:10.1038/s41571-022-00668-4
- Seidel, J. A., Otsuka, A., & Kabashima, K. (2018). Anti-PD-1 and Anti-CTLA-4 Therapies in Cancer: Mechanisms of Action, Efficacy, and Limitations. Front Oncol, 8, 86. doi:10.3389/fonc.2018.00086
- Serrano, M., Lee, H.-W., Chin, L., Cordon-Cardo, C., Beach, D., & DePinho, R. A. (1996). Role of the *INK4a* Locus in Tumor Suppression and Cell Mortality. Cell, 85(1), 27-37. doi:10.1016/S0092-8674(00)81079-X
- Serrano, M., Lin, A. W., McCurrach, M. E., Beach, D., & Lowe, S. W. (1997). Oncogenic ras Provokes Premature Cell Senescence Associated with Accumulation of P53 and p16INK4a. Cell, 88(5), 593-602. doi:https://doi.org/10.1016/S0092-8674(00)81902-9

- Shi, D., & Gu, W. (2012). Dual Roles of MDM2 in the Regulation of P53: Ubiquitination Dependent and Ubiquitination Independent Mechanisms of MDM2 Repression of P53 Activity. Genes Cancer, 3(3-4), 240-248. doi:10.1177/1947601912455199
- Shiloh, Y. (2003). ATM and related protein kinases: safeguarding genome integrity. Nature Reviews Cancer, 3(3), 155-168. doi:10.1038/nrc1011
- Spinner, C. A., & Lazarevic, V. (2021). Transcriptional regulation of adaptive and innate lymphoid lineage specification. Immunol Rev, 300(1), 65-81. doi:10.1111/imr.12935
- Stefani, C., Miricescu, D., Stanescu, S., II, Nica, R. I., Greabu, M., Totan, A. R., & Jinga, M. (2021). Growth Factors, PI3K/AKT/mTOR and MAPK Signaling Pathways in Colorectal Cancer Pathogenesis: Where Are We Now? Int J Mol Sci, 22(19). doi:10.3390/ijms221910260
- Stein, Y., Aloni-Grinstein, R., & Rotter, V. (2019). Mutant P53-a potential player in shaping the tumor-stroma crosstalk. J Mol Cell Biol, 11(7), 600-604. doi:10.1093/jmcb/mjz071
- Sun, L., Su, Y., Jiao, A., Wang, X., & Zhang, B. (2023). T cells in health and disease. Signal Transduction and Targeted Therapy, 8(1), 235. doi:10.1038/s41392-023-01471-y
- Tanaka, N., Ishihara, M., Kitagawa, M., Harada, H., Kimura, T., Matsuyama, T., . . . Taniguchi, T. (1994). Cellular commitment to oncogene-induced transformation or apoptosis is dependent on the transcription factor IRF-1. Cell, 77(6), 829-839. doi:10.1016/0092-8674(94)90132-5
- Tanaka, T., Narazaki, M., & Kishimoto, T. (2014). IL-6 in inflammation, immunity, and disease. Cold Spring Harb Perspect Biol, 6(10), a016295. doi:10.1101/cshperspect.a016295
- Tanel, A., Fonseca, S. G., Yassine-Diab, B., Bordi, R., Zeidan, J., Shi, Y., . . . Sékaly, R. P. (2009). Cellular and molecular mechanisms of memory T-cell survival. Expert Rev Vaccines, 8(3), 299-312. doi:10.1586/14760584.8.3.299
- Tapon, N., Harvey, K. F., Bell, D. W., Wahrer, D. C., Schiripo, T. A., Haber, D., & Hariharan, I. K. (2002). salvador Promotes both cell cycle exit and apoptosis in Drosophila and is mutated in human cancer cell lines. Cell, 110(4), 467-478. doi:10.1016/s0092-8674(02)00824-3
- Tasdemir, N., Banito, A., Roe, J. S., Alonso-Curbelo, D., Camiolo, M., Tschaharganeh, D. F., . . . Lowe, S. W. (2016). BRD4 Connects Enhancer Remodeling to Senescence Immune Surveillance. Cancer Discov, 6(6), 612-629. doi:10.1158/2159-8290.Cd-16-0217
- Teh, H. S., Kisielow, P., Scott, B., Kishi, H., Uematsu, Y., Blüthmann, H., & von Boehmer, H. (1988). Thymic major histocompatibility complex antigens and the alpha beta T-cell receptor determine the CD4/CD8 phenotype of T cells. Nature, 335(6187), 229-233. doi:10.1038/335229a0
- Truett, G. E., Heeger, P., Mynatt, R. L., Truett, A. A., Walker, J. A., & Warman, M. L. (2000). Preparation of PCR-quality mouse genomic DNA with hot sodium hydroxide and tris (HotSHOT). Biotechniques, 29(1), 52, 54. doi:10.2144/00291bm09
- van Deursen, J. M. (2014). The role of senescent cells in ageing. Nature, 509(7501), 439-446. doi:10.1038/nature13193

- Victorelli, S., & Passos, J. F. (2017). Telomeres and Cell Senescence Size Matters Not. EBioMedicine, 21, 14-20. doi:10.1016/j.ebiom.2017.03.027
- Vizioli, M. G., Santos, J., Pilotti, S., Mazzoni, M., Anania, M. C., Miranda, C., . . . Greco, A. (2014). Oncogenic RAS-induced senescence in human primary thyrocytes: molecular effectors and inflammatory secretome involved. Oncotarget, 5(18), 8270-8283. doi:10.18632/oncotarget.2013
- Vitale, I., Manic, G., Coussens, L. M., Kroemer, G., & Galluzzi, L. (2019). Macrophages and Metabolism in the Tumor Microenvironment. Cell Metabolism, 30(1), 36-50. doi:https://doi.org/10.1016/j.cmet.2019.06.001
- Wajapeyee, N., Serra, R. W., Zhu, X., Mahalingam, M., & Green, M. R. (2008). Oncogenic BRAF Induces Senescence and Apoptosis through Pathways Mediated by the Secreted Protein IGFBP7. Cell, 132(3), 363-374. doi:10.1016/j.cell.2007.12.032
- Walker, J. A., & McKenzie, A. N. J. (2018). TH2 cell development and function. Nature Reviews Immunology, 18(2), 121-133. doi:10.1038/nri.2017.118
- Wan, P. T., Garnett, M. J., Roe, S. M., Lee, S., Niculescu-Duvaz, D., Good, V. M., . . . Marais, R. (2004). Mechanism of activation of the RAF-ERK signaling pathway by oncogenic mutations of B-RAF. Cell, 116(6), 855-867. doi:10.1016/s0092-8674(04)00215-6
- Wei, X., Shimizu, T., & Lai, Z. C. (2007). Mob as tumor suppressor is activated by Hippo kinase for growth inhibition in *Drosophila*. The EMBO Journal, 26(7), 1772-1781-1781. doi:https://doi.org/10.1038/sj.emboj.7601630
- Wellbrock, C., Rana, S., Paterson, H., Pickersgill, H., Brummelkamp, T., & Marais, R. (2008). Oncogenic BRAF Regulates Melanoma Proliferation through the Lineage Specific Factor MITF. PLOS ONE, 3(7), e2734. doi:10.1371/journal.pone.0002734
- Wooster, R., Futreal, A. P., & Stratton, M. R. (2006). Sequencing Analysis of BRAF Mutations in Human Cancers. In Methods in Enzymology (Vol. 407, pp. 218-224): Academic Press.
- Wu, S., Huang, J., Dong, J., & Pan, D. (2003). hippo encodes a Ste-20 family protein kinase that restricts cell proliferation and promotes apoptosis in conjunction with salvador and warts. Cell, 114(4), 445-456. doi:10.1016/s0092-8674(03)00549-x
- Xiao, L., Chen, Y., Ji, M., & Dong, J. (2011). KIBRA regulates Hippo signaling activity via interactions with large tumor suppressor kinases. J Biol Chem, 286(10), 7788-7796. doi:10.1074/jbc.M110.173468
- Xie, N., Shen, G., Gao, W., Huang, Z., Huang, C., & Fu, L. (2023). Neoantigens: promising targets for cancer therapy. Signal Transduction and Targeted Therapy, 8(1), 9. doi:10.1038/s41392-022-01270-x
- Yin, F., Yu, J., Zheng, Y., Chen, Q., Zhang, N., & Pan, D. (2013). Spatial organization of Hippo signaling at the plasma membrane mediated by the tumor suppressor Merlin/NF2. Cell, 154(6), 1342-1355. doi:10.1016/j.cell.2013.08.025

- Yu, H., McDaid, R., Lee, J., Possik, P., Li, L., Kumar, S. M., . . . Xu, X. (2009). The role of BRAF mutation and P53 inactivation during transformation of a subpopulation of primary human melanocytes. Am J Pathol, 174(6), 2367-2377. doi:10.2353/ajpath.2009.081057
- Yue, X., Zhao, Y., Xu, Y., Zheng, M., Feng, Z., & Hu, W. (2017). Mutant P53 in Cancer: Accumulation, Gain-of-Function, and Therapy. J Mol Biol, 429(11), 1595-1606. doi:10.1016/j.jmb.2017.03.030
- Yue, Z., Nie, L., Zhao, P., Ji, N., Liao, G., & Wang, Q. (2022). Senescence-associated secretory phenotype and its impact on oral immune homeostasis. Front Immunol, 13, 1019313. doi:10.3389/fimmu.2022.1019313
- Zitvogel, L., & Kroemer, G. (2012). Targeting PD-1/PD-L1 interactions for cancer immunotherapy. Oncoimmunology, 1(8), 1223-1225. doi:10.4161/onci.21335
- Zhang, A., Xu, M., & Mo, Y. Y. (2014). Role of the lncRNA-P53 regulatory network in cancer. J Mol Cell Biol, 6(3), 181-191. doi:10.1093/jmcb/mju013
- Zhang, C., Liu, J., Xu, D., Zhang, T., Hu, W., & Feng, Z. (2020). Gain-of-function mutant P53 in cancer progression and therapy. Journal of Molecular Cell Biology, 12(9), 674-687. doi:10.1093/jmcb/mjaa040
- Zhang, J. M., & An, J. (2007). Cytokines, inflammation, and pain. Int Anesthesiol Clin, 45(2), 27-37. doi:10.1097/AIA.0b013e318034194e
- Zhao, B., Wei, X., Li, W., Udan, R. S., Yang, Q., Kim, J., . . . Guan, K. L. (2007). Inactivation of YAP oncoprotein by the Hippo pathway is involved in cell contact inhibition and tissue growth control. Genes Dev, 21(21), 2747-2761. doi:10.1101/gad.1602907